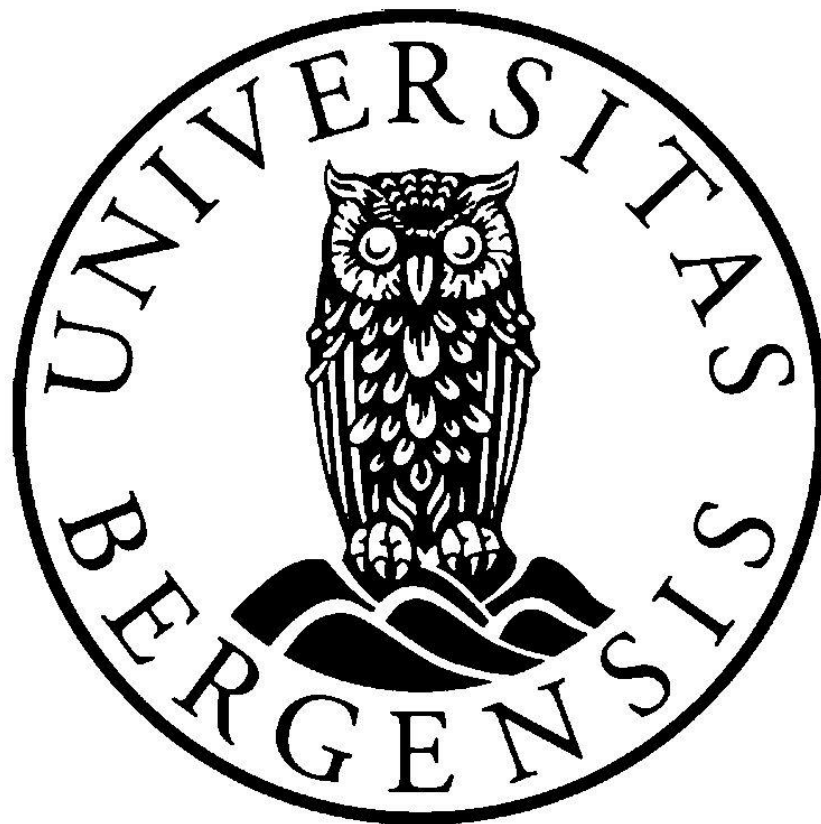


An Experimental Study of Tertiary CO₂ Injection Strategies in Fractured Limestone Rocks



Master Thesis in Reservoir Physics

by

Tomas Nordeide Hjartnes

Department of Physics and Technology

University of Bergen

June 2015

ABSTRACT

The experimental work within this thesis is a continued investigation of tertiary recovery by injection of supercritical CO₂ and CO₂-foam under miscible conditions for enhanced oil recovery in fractured limestone. Secondary recovery methods in heterogeneous and fractured reservoirs can leave two-thirds of the oil behind, drawing attention to alternative injection schemes. CO₂ injection is a widely established technique within the oil industry, and has been in use for over 40 years. When CO₂ achieves a supercritical state, it has the properties of a gas but behaves similar to a liquid. Above the minimum miscibility pressure, interfacial tension between CO₂ and the oil is eliminated, making the phases miscible. Since CO₂ has much lower viscosity than water and oil, the gas-oil mobility ratio becomes unfavorable. Fingering and channeling of gas through the oil is a direct result of this, and is often considered a major problem for fractured reservoirs.

Combining CO₂ with water in a water-alternating-gas (WAG) process can significantly reduce mobility of CO₂ and delay CO₂ breakthrough. Further reduction in gas mobility may be achieved through implementation of foam. This can be done in two ways: 1) simultaneous injection of CO₂ and surfactant, called co-injection. 2) surfactant-alternating-gas (SAG).

A total of 13 experiments were conducted as tertiary injection methods on outcrop limestone cores in this thesis. Single CO₂ and co-injection of CO₂ and surfactant tests were conducted in both whole and fractured cores. One of these was a tertiary injection with integrated CO₂ and CO₂-foam on the same core. Tertiary WAG and SAG injections, mostly integrated on the same core, were performed to evaluate its effect on oil recovery. Injection methods were studied for both whole and fractured cores to observe the impact of fractures on different injection strategies. Experimental setups were designed to maintain conditions (90 bar and 35 °C) such that the CO₂ would become supercritical and miscible with n-Decane.

Results from experiments showed that pure CO₂ injection had the same final recovery in whole and fractured cores, while co-injection in whole cores recovered less than in fractured cores. No significant difference was found between recovery in tertiary WAG and SAG, with 13.4 % of OOIP and 12.5 % of OOIP, respectively. The two most promising tertiary injection methods were integrated WAG and SAG with 32.4 % of OOIP, as well as integrated CO₂ and co-injection with 36.2 % of OOIP.

The experimental work in this thesis shows that by combining several injection strategies, in integrated EOR, more residual oil can potentially become mobilized that may not have been possible through utilization of each method individually. The timing of switching from CO₂ to CO₂-foam proved to be crucial at CO₂ breakthrough to maximize ultimate recovery.

ACKNOWLEDGEMENTS

I would like to thank my supervisor Associate Professor Martin Fernø at the Department of Physics and Technology, University of Bergen, for offering guidance and support with the material within this thesis.

I would also like to thank Professor Arne Graue for the opportunity to study reservoir physics at the Department of Physics and Technology, and for the financial support in regards to lab equipment that has made it possible for me to conduct experiments.

Thanks to PhD Bergit Brattekås and PhD Candidate Marianne Steinsbø for guidance and advice with laboratory work and data analysis. I also want to thank the mechanical workshop that provided me with necessary lab equipment.

Special thanks my fellow lab associate Henriette Horjen for good teamwork in the laboratory. And thanks to fellow master students for keeping the office environment in high spirits.

Finally, I would like to express my gratitude to my parents for motivation and support throughout my years as a student at UiB.

June 1., 2015

Tomas Nordeide Hjartnes

CONTENTS

ABSTRACT	II
ACKNOWLEDGEMENTS	IV
INTRODUCTION	IX
1 CARBONATE RESERVOIRS AND PRODUCTION	12
1.1 CARBONATE RESERVOIRS	12
1.2 PRODUCTION IN FRACTURED RESERVOIRS	13
2 ENHANCED OIL RECOVERY (EOR).....	14
2.1 PRIMARY RECOVERY	14
2.2 SECONDARY RECOVERY.....	14
2.3 TERTIARY RECOVERY	15
2.4 CO₂.....	16
2.4.1 PHYSICAL AND CHEMICAL PROPERTIES.....	16
2.4.2 CO₂ INJECTION IN FRACTURED RESERVOIRS.....	19
2.4.3 CO₂-FOAM.....	22
2.5 FOAM.....	23
2.5.1 DEFINITION	23
2.5.2 ADVANTAGES.....	24
2.5.3 FOAM STATES	25
2.5.4 GENERATION MECHANISMS.....	26
2.5.5 STABILITY	27
2.5.6 FLOW BEHAVIOR	29
2.6 WATER-ALTERNATING-GAS (WAG).....	31
2.6.1 GENERAL DESCRIPTION	31
2.6.2 WAG DESIGN	31
2.6.3 FACTORS INFLUENCING INJECTIVITY	33
2.6.4 OPERATIONAL CHALLENGES	36
2.7 SURFACTANT-ALTERNATING-GAS (SAG)	36
2.7.1 GENERAL DESCRIPTION	36
2.7.2 RESPONSES FROM SAG	37
2.7.3 SAG DESIGN.....	38
2.7.4 FOAM SELECTION AND RESERVOIR CONDITIONS	42
3 LITERATURE SURVEY	43

3.1 EOR ON FIELD SCALE.....	43
3.1.1 MISCIBLE CO ₂ -FLOODING	43
3.1.2 WAG INJECTION	44
3.1.3 FOAM: CO-INJECTION AND SAG.....	45
3.2 EOR ON CORE SCALE.....	46
3.2.1 WAG	46
3.2.2 FOAM.....	47
4 EXPERIMENTAL SETUP AND PROCEDURES.....	49
4.1 FLUID PROPERTIES AND ROCK MATERIAL.....	49
4.1.1 FLUIDS.....	49
4.1.2 EDWARD LIMESTONE.....	50
4.1.3 PREPARATION AND FRACTURING OF CORES	51
4.2 SETUP AND PROCEDURES.....	56
4.2.1 SETUP.....	56
4.2.2 EQUIPMENT.....	57
4.2.3 PROCEDURES	57
5 RESULTS AND DISCUSSION	60
5.1 CORE PROPERTIES	60
5.2 INJECTION METHODS.....	62
5.3 TERTIARY WAG AND SAG INJECTION WITH SUPERCRITICAL CO ₂	65
5.3.1 BASELINE: WAG AND SAG COMBINED IN WHOLE CORES.....	65
5.3.2 WAG AND SAG COMBINED IN FRACTURED CORES	68
5.3.3 COMPARISON: WHOLE AND FRACTURED CORES	71
5.3.4 TERTIARY WAG VS. TERTIARY SAG IN FRACTURED CORES	74
5.4 TERTIARY CO-INJECTION OF SUPERCRITICAL CO ₂ AND SURFACTANT	76
5.4.1 BASELINE: CO ₂ AND CO ₂ -FOAM IN WHOLE CORES	76
5.4.2 CO ₂ AND CO ₂ -FOAM IN FRACTURED CORES.....	80
5.4.3 COMPARISON: WHOLE AND FRACTURED CORES	82
5.4.4 INTEGRATED EOR: CO ₂ AND CO ₂ -FOAM IN FRACTURED CORES	84
5.5 COMPARISON OF SUPERCRITICAL CO ₂ EOR INJECTION STRATEGIES	87
5.6 UNCERTAINTIES AND CALCULATIONS	90
6 CONCLUSION AND FUTURE WORK	95
6.1 CONCLUSION.....	95
6.2 FUTURE WORK.....	96

7 | **ABBREVIATIONS AND NOMENCLATURE** 97

8 | **REFERENCES** 100

INTRODUCTION

The rate of replacement, by new discoveries, to the already produced reserves has been steadily declining these past few decades (Manrique, et al., 2010). Meeting energy demands in coming years requires focused efforts on recovering remaining oil resources from known reservoirs. Fractured reservoirs pose problems during production of oil through conventional recovery methods, such as water injection and pressure depletion, leaving more than half of the original oil in place behind. Therefore, more advanced methods are required to mobilize the oil from reservoirs that have already been subjected to secondary recovery methods.

Enhanced oil recovery (EOR) in declining oil fields, by the use of CO₂, pioneered in West Texas in 1974. CO₂ was considered the best choice as an injection fluid because of its ability to mix with the oil and extract more of the oil from the reservoir (Chordia & Trivedi, 2010). After its success, this production mechanism has become a major contributor to the increased oil production and economic gain in the United States to this day. By 2012, approximately 65 million tons of CO₂ was purchased by the industry for EOR purposes (NEORI, 2012). There were more than 100 CO₂ injection projects producing over 250,000 barrels of oil per day in the U.S. CO₂ is also the largest source of U.S. greenhouse gas emissions. By injecting CO₂ and producing oil, storage of CO₂ for reduced gas emissions will benefit the environment (Lee & Kam, 2013).

Many CO₂ EOR projects implement continuous CO₂ injection, yielding additional recoveries between 5-10 % OOIP for immiscible floods and 10-20 % OOIP for miscible floods (NETL, 2011). Large amounts of CO₂ must be recycled in the production wells due to the large mobility of CO₂ adding to the costs.

Continuous CO₂ injection has a higher utilization factor in comparison to water-alternating-gas (WAG). For this reason, many fields would convert from continuous CO₂ injection to WAG in order to cut back on the use of CO₂ (Zhou, et al., 2012). More than 90 % of projects existing in the U.S. implement WAG. Another reason for switching from CO₂ to WAG is because a more stable displacement front occurs during WAG since the CO₂ is much lighter than oil and water (Christensen, et al., 2001).

The process of CO₂ and WAG injection has attracted more attention over the years. Although these methods have proven themselves as profitable, critical problems occur with insufficient displacement of oil (Salehi, et al., 2014). Notable advantages in WAG become impaired by gravity segregation as a result of density differences in gas and oil. Throughout the years, chemical EOR methods have emerged.

The use of foam for mobility control of CO₂ has been implemented in several fields (Turta & Singhal, 2002). The difference from continuous CO₂ and WAG was that a foaming agent would be injected together with the CO₂. Most notably, foam-assisted WAG was successfully completed in the North Sea, Snorre Field in 1994 (Aarra, et al., 2002). Foam was intended to propagate through the reservoir formation and improve sweep efficiency. There are challenges within the utilization of EOR techniques, especially considering low oil prices combined with relatively constant chemical cost. Such factors directly influence whether or not a certain injection scheme should be implemented (NETL, 2011). A large number of lab-scale research projects have been conducted as well as pilot test on CO₂ foams. Much of this indicates that there is a large potential within mobility reduction of CO₂ by chemical additive.

The work within this thesis will focus on investigating enhanced oil recovery methods that have been widely used in the field, namely miscible CO₂ and WAG injection, and compare or combine these with emerging injection strategies that involve in situ foam generation. Since a large percentage of the world's hydrocarbon reserves are found in carbonates, especially in the U. S. and Middle East (Ahr, 2008), experiments are performed in limestone cores, a type of carbonate rock. In the field, this rock contains natural fractures as a result of overburden sediments and geo-mechanical stress. Therefore, the cores have been cut to resemble the presence of fractures.

Most reservoirs have undergone secondary waterflooding, therefore all experiments in this thesis are conducted as tertiary injections. Results from experiments are divided into two sections where the first one looks at miscible WAG and SAG as integrated enhanced oil recovery. Water can reduce mobility of CO₂ and delay breakthrough for a limited period of time. The aim of adding a SAG injection at the end is to see if foam can counteract the main challenges of WAG, such as gravity segregation, by further reducing CO₂ mobility. The second section of results compares pure CO₂ injection with CO₂-foam through co-injecting CO₂ and surfactant. These two methods are then combined as integrated enhanced oil recovery to directly test the potential of foam by switching from CO₂ to CO₂-foam during the experiment. Finally, all injection strategies are compared in terms of their tertiary recovery. The aim is to evaluate the performance of different injection strategies and determine best suited method based on highest ultimate recovery and lowest amount of pore volume injected to achieve this recovery.

1 | CARBONATE RESERVOIRS AND PRODUCTION

1.1 | CARBONATE RESERVOIRS

Carbonate is a mutual term referring to rock types made from calcite and dolomite minerals. Limestone (consisting of calcite) and dolostone (consisting of dolomite) make up 90 % of all carbonate reservoirs worldwide (Ahr, 2008). Carbonates hold more than half of the world's oil and gas reserves. The Middle East, for instance, has most of their hydrocarbons within carbonates (Schlumberger, 2014). Shallow shelf carbonates hold 22 % of the OOIP in the United States (Manrique, et al., 2007).

Porosity is the void space or the fraction of pores that occupies a rock. *Permeability* is a measure of how effectively fluids are transported through the pore network for a rock. Combined, these properties give an indication of whether or not the reservoir has the ability to store and produce hydrocarbons (Zolotukhin & Ursin, 2000). Porosity and permeability measurements can be reliable for small sandstone plugs, but carbonate plugs may need to be larger in magnitude to achieve results that can be representative of a field (Ahr, 2008).

Carbonate fields are naturally fractured with heterogeneous porosity and permeability distributions (Manrique, et al., 2007). *Fractures* are naturally occurring discontinuities in a rock, owing to deformation or physical diagenesis. Fractures are also produced by mechanical stresses after the rocks have been lithified and may be associated with features such as folds and faults. A reservoir develops several generations of fractures with most of them closed through cementation or compaction. Closed fractures can impede flow through certain parts of the reservoir. Some fractures will remain open, specifically the ones that have a parallel orientation to maximum stress conditions. These are also the ones that will have the greatest impact on reservoir properties as permeability increases. Dolomitic rocks tend to fracture more easily than limestone, and fine-grained rocks fracture more easily than coarse-grained rocks. Thin beds are more prone to fracturing than thick beds (Ahr, 2008). Once fractures are introduced, the displacement process no longer depends on fluid properties alone (Uleberg & Høier, 2002). In a fractured reservoir, total porosity and permeability consist of both matrix and fracture components. It is necessary to determine relative contributions from both in order to assess reservoir performance (Ahr, 2008).

There are four important petrophysical parameters that need to be accounted for in fractured reservoirs. These are (a) *fracture permeability*, (b) *fracture porosity*, (c) *fluid saturations* (in fractures) and (d) *recovery factor* (expected). Fracture permeability and fracture width decrease

exponentially with depth and confining pressure. Fracture porosity is a small percentage of total reservoir porosity, but due to connected fractures, the small fracture volume can contribute significantly to total permeability (Ahr, 2008).

A carbonate field with low porosity and permeability, initially, may have its permeability increased by fracturing. Injected fluids tend to flow through the fracture network and bypass the oil in the matrix. For this reason, a more porous carbonate reservoir rock, containing a fracture network, could become swept unevenly. This leads to an early breakthrough of injected fluids in the producing wells, resulting in low recovery factors. It is apparent that fracturing is of major importance to reservoir properties if present (Manrique, et al., 2007).

Formation *wettability* is a crucial factor that controls fluid distribution in the reservoir. Whether a reservoir has a water-wet or oil-wet preference could significantly influence production performance. Most carbonate reservoirs have wettabilities ranging from mixed-wet to oil-wet (Alotaibi, et al., 2010).

1.2 | PRODUCTION IN FRACTURED RESERVOIRS

Reservoirs with low matrix permeability cannot be produced economically without the presence of fractures. Production characteristics in fractured reservoirs are different from conventional reservoirs. Because of this, production strategy and reservoir performance will vary (Allan & Sun, 2003).

- I. Fracture networks have high *transmissivity*, which refers to the transport of fluids between matrix blocks across fractures (Frampton, 2014). This causes a very low pressure drop around the producing well. In contrast to un-fractured reservoirs, pressure drop becomes insignificant in the production process.
- II. Fluid expansion, gravity drainage and imbibition are processes that will continue to transport oil from matrix blocks into the fractures while producing.
- III. Gas-to-oil ratio is lower in fractured reservoirs during the production because the oil liberates gas, which will follow the fracture pathways upwards instead of horizontally. The consequence is an extended gas cap or a secondary gas cap on top of the reservoir.
- IV. Water production is only a function of production rate, and independent of the reservoir rock characteristics and fluid properties.
- V. The bubble point does not vary in a fractured reservoir as PVT properties change throughout production.

2 | ENHANCED OIL RECOVERY (EOR)

2.1 | PRIMARY RECOVERY

Reservoirs contain natural pressures caused by various forces, such as: (1) Expanding natural gas, (2) gravitational force, (3) buoyancy force from surrounding water, and (4) forces from compaction of reservoir rocks (Donaldson, et al., 1989). When a well is drilled for production or exploration, oil will flow through the porous media and into the wells. Sufficient pressures make the oil rise towards the surface, but if initial pressures are too low or fall during production, artificial lifting methods such as pumping are applied. Utilizing natural or artificial pressures as means of producing oil is referred to as primary recovery (Brown, 2002), and generally produces less than 30 % of the oil in a reservoir (Kokal & Al-Kaabi, 2010).

There are different mechanisms of primary recovery. One type is the *solution gas drive*; occurring as pressures are lowered during production and gas is liberated from the oil. The expanding bubbles of gas push the oil towards the producing well. Another is the *gas cap drive*; taking place when a reservoir has a gas cap on top, and expands as oil is being produced. In this way, it acts as an additional driving force. Lastly, there is the *water drive*, where pressures in an aquifer, connected to the reservoir, may be sufficient to drive the oil out during production (Brown, 2002).

2.2 | SECONDARY RECOVERY

After reservoir pressure has been reduced until it no longer induces movement of hydrocarbons, other measures must be considered. Primary recovery has a tendency to leave much of the oil behind. Therefore, secondary recovery methods are used in most fields (Brown, 2002). These methods include flooding the reservoir with water or gas. A variety of different gases could be used: natural gas, CO₂, nitrogen and air (Skarestad, 2012). Oil produced after secondary recovery is normally 30-50 % of original oil in place (Kokal & Al-Kaabi, 2010). Waterflooding has been in use for decades with the purpose of displacing oil into producing wells and to maintain reservoir pressure. There are especially two negative aspects of waterflooding. One is that water does not sweep oil from the reservoir efficiently as it moves through the pores. The performance of waterflooding is often dependent on the formation wettability. A water-wet reservoir has water coating the pore walls. During waterflooding, water enters the pores along the coated walls as it displaces the oil in a *spontaneous imbibition* process (Alotaibi, et al., 2010). Imbibition refers to displacement of the non-wetting phase (oil) by the wetting phase (water). Immiscibility between water and oil leads to snap-off of oil

droplets which become trapped by capillary forces in the center of the pores. Another issue is that water can bypass certain parts of the reservoir due to heterogeneity (such as fractures) that inhibit flow. With large parts of the reservoir remaining un-swept, recovery becomes inefficient (Shehata, et al., 2014).

The pressure decrease following primary recovery may be partially restored by injecting gas. In this instance, gas from the production wells are recompressed and injected into selected wells for pressure support. The most beneficial application of the natural gas is the gas drive method. Gas is injected into the reservoir under pressure and sweeps the oil from injector to producer continuously. Injection of gas is favorable if the reservoir has a gas cap. In this way, the gas cap expands as more gas is injected, expelling the oil (Donaldson, et al., 1989). However, the low viscosity of gas leads to a high mobility ratio between gas and oil. This results in an early breakthrough of gas in the production well and makes volumetric sweep efficiency less favorable compared to that of waterfloods. This is mainly caused by channeling of gas through preferred pathways and gas fingering through the oil. However, injecting gas into a dipping reservoir may counteract these problems and improve the sweep by gravity stable displacement (Skarestad, 2012).

2.3 | TERTIARY RECOVERY

When secondary recovery methods have been exhausted to a point where they are no longer economical, supplementary energy is required (Stosur, et al., 2003). Enhanced oil recovery is defined as processes that seek to improve recovery of hydrocarbon from a reservoir after the primary production phase. That implies that both secondary and tertiary recovery processes belong in enhanced oil recovery (Terry & Rogers, 2014). Tertiary recovery processes generally refers to injection strategies involving miscible flooding, chemical flooding and thermal flooding processes.

The challenge lies in mobilizing oil trapped in pores already swept and reaching un-swept parts of the reservoir. Mobilization of oil is controlled by viscous forces and interfacial tension in pores filled with water and oil. The fraction of oil recovered is a function of a dimensionless parameter called the *capillary number*, N_{vc} , which is a function of both viscous and capillary forces. Viscous forces depend on fluid viscosity, flow velocity and flow path length. Capillary forces depend on interfacial tension and pore geometry. So by altering any of these parameters, the residual oil saturation can be decreased (Fulcher, et al., 1985). A capillary number greater than 10^{-5} is generally required to mobilize oil droplets after a waterflood. Tertiary methods have been developed with the objective of either increasing the viscous force of injected fluid, or decreasing the interfacial tension between the fluid injected and the reservoir oil (Terry &

Rogers, 2014). With oil still remaining after primary and secondary recovery methods, 70-75 % of the remaining oil is a considerable target for EOR processes.

2.4 | CO₂

2.4.1 | PHYSICAL AND CHEMICAL PROPERTIES

CO₂ is in the global spotlight because it is the largest source of U.S. greenhouse gas emissions. CO₂-driven EOR has provided an increase in hydrocarbon production, while capturing and storing CO₂ underground in geological structures. These are major reasons why the utilization of CO₂ in EOR processes has become more prevalent in recent years (Lee & Kam, 2013).

CO₂ is preferable to other gases because of its ability to become a supercritical phase at typical reservoir pressure and temperature conditions. This gas is also less expensive than other similarly miscible fluids (NETL, 2010). The density of CO₂ approaches that of liquid water, but behaves like a gas. By using supercritical CO₂ in an EOR project, the displacement front becomes more stable, thus naturally counteracting gravity segregation and viscous fingering to a greater extent, in contrast to other gases (Lee & Kam, 2013).

In Figure 2.4.1 (a), all the possible phases, within their respective temperature and pressure boundaries, can be observed. CO₂ exist as a gas at normal temperatures below the critical point. At low temperatures, and at pressures above the sublimation line, CO₂ takes the shape of a solid. It may transfer into vapor if the decrease in pressure is sufficient. At temperatures between -56.5 C° (triple point) and 31.1 C° (critical point) an increase in pressure can turn vapor into a liquid state.

The critical point is at 31.1 C° and 71.9 bar. When increasing both temperature and pressure beyond this point, CO₂ enters a supercritical state. The phase transitions solid-gas, solid-liquid and liquid-gas require a release or an adsorption of heat. Moving between phases such as supercritical- liquid or supercritical gas, heat release is not a necessity, making the use of CO₂ that much more advantageous (IPCC, 2005).

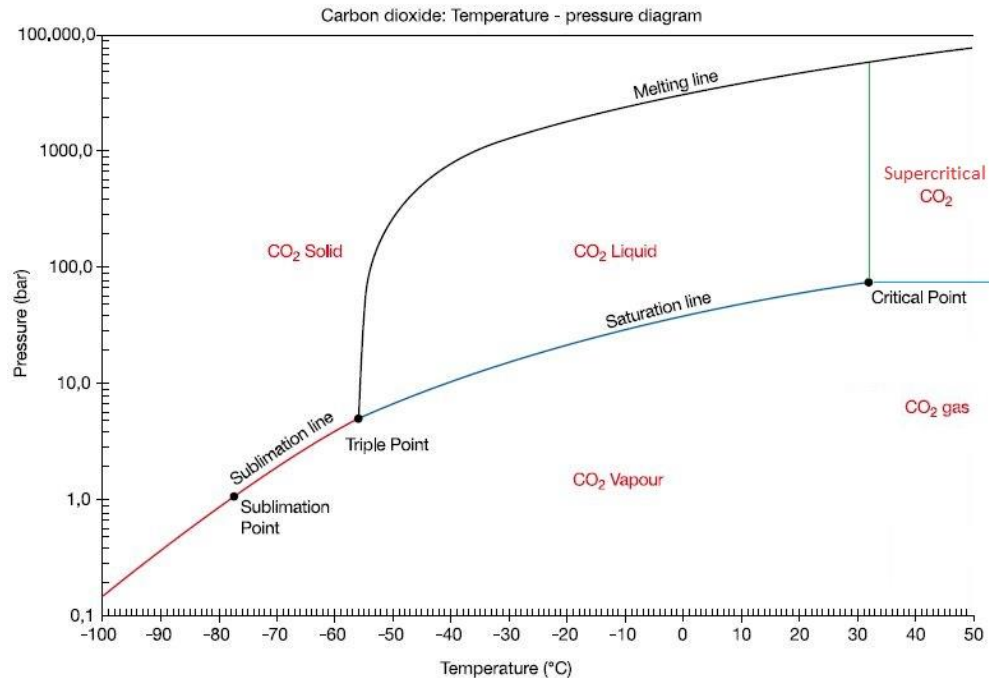


Figure 2.4.1(a): Pressure vs. temperature diagram for carbon dioxide. CO₂ can vary between solid, vapor, liquid, gas and supercritical phases (IPCC, 2005).

When CO₂ is injected into a reservoir, it becomes soluble with the residual crude oil because lighter hydrocarbons from the oil dissolve in the CO₂ while CO₂ also dissolves in the oil. However, this is mainly achieved with a high CO₂ density in addition to the oil containing many light components. Miscibility between CO₂ and oil can only occur above a certain pressure, which in turn depends on density of the fluids (NETL, 2010). Therefore, it is important to have an idea of how density of CO₂ varies with temperature and pressure, as displayed in the figures below.

The density of CO₂ within the supercritical region can be set as a function of temperature and pressure, as shown in figure 2.4.1 (b). Density decreases with increasing temperatures and falls more steeply with lower pressures. For high pressures the decline in density is almost a linear function. As the CO₂ crosses the supercritical boundary, the density declines more sharply with increasing temperatures.

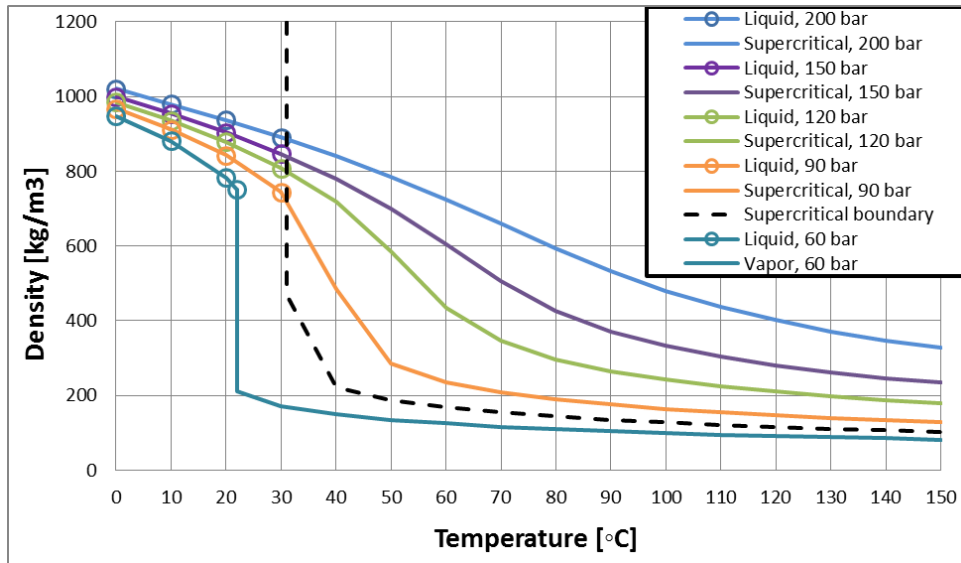


Figure 2.4.1 (b): Density vs. temperature diagram for carbon dioxide at fixed pressures (NIST, 2011).

In figure 2.4.1 (c), we can observe the density change with increasing pressure at a constant temperature. As CO₂ becomes more compressed under high pressures, density increases. This trend is slow at first but as phase transitions take place, density increases sharply.

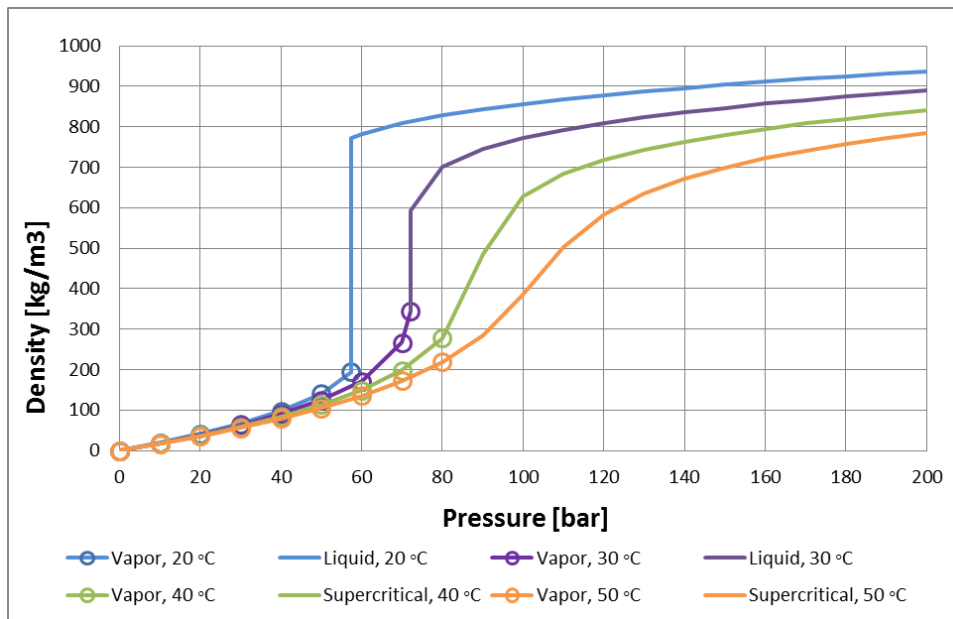


Figure 2.4.1 (c): Density vs. pressure for carbon dioxide at constant temperatures (NIST, 2011).

The dissolution of CO₂ in water is known to have a certain impact on the pH of water. Chemical reactions between CO₂ and water produce carbonic acid, which lowers the pH significantly. This is seen from the chemical reaction: $\text{CO}_2 (\text{aq}) + \text{H}_2\text{O} \leftrightarrow \text{H}_2\text{CO}_3 (\text{aq})$, where the product is known as carbonic acid (IPCC, 2005). Figure 2.4.1 (d) is presented below with pH as a function of CO₂ concentration in sea water. It shows how an increase in the weight percentage of CO₂ in water will lower pH in a steep linear curve.

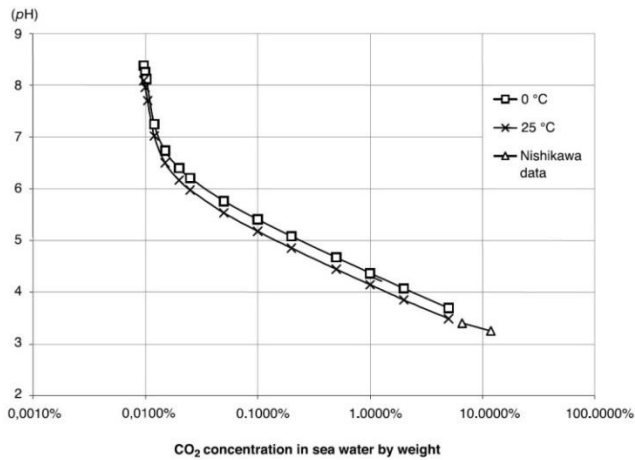


Figure 2.4.1 (d): pH vs. CO₂ concentration in sea water by weight (IPCC, 2005).

2.4.2 | CO₂ INJECTION IN FRACTURED RESERVOIRS

Both laboratory and field studies have established that CO₂ can be an efficient oil-displacing agent (Holm, 1974). The main recovery mechanisms known to occur during gas injection for naturally fractured reservoirs are listed below. Several factors determine the relative significance of each mechanism, including permeability of the matrix, level of fracturing, fluid properties, injection rate and reservoir conditions (Shojaei & Jessen, 2015).

Gravity Drainage: This is an important process in fractured reservoirs when recovering oil by gas injection from low permeability matrix blocks. The density difference between gas in the fracture and oil in the matrix results in oil drainage from the matrix. Gravitational forces would have to exceed the capillary forces in order for this to occur. Recovery has been found to increase with higher influence of gravitational forces. Increasing the injection rate results in higher pressures, which affects the viscous flow, leading to a less gravity dominated process (Chordia & Trivedi, 2010).

Molecular Diffusion: Under miscible or near-miscible conditions, diffusion is often considered to be the most important production mechanism in fractured reservoirs (Hoiteit & Firoozabadi, 2006). Diffusion is the process where molecules, ions or other small particles mix

spontaneously, moving from a region of high concentration to a region of lower concentration (Crussler, 2009). If CO₂ and oil are in contact, with a sharp interface between them, they will slowly diffuse into one another, causing the fluids to become a diffuse mixed zone (Perkins & Johnston, 1963). For small and low permeable matrix blocks, with high capillary pressure, gravity drainage becomes less effective, turning diffusion into the dominating process. The effects of diffusion are less predominant in large scale bypassing because of gravity segregation (Chordia & Trivedi, 2010). The impact of molecular diffusion plays a more significant role in fractured reservoirs, contrary to conventional reservoirs, because of the large fracture surface area available, increasing the characteristic time for diffusion to take place (Shojaei & Jessen, 2015).

Water-Shielding: High water saturation in a porous media is known to affect the diffusion process because of water barriers shielding the oil from the CO₂. This may limit the contact between CO₂ and the oil. In water-wet media, this phenomenon is especially severe (Eide, 2014).

Miscible Displacement: A CO₂ displacement may be *miscible* or *immiscible* (Skarestad, 2012). In a petroleum reservoir miscibility is the physical condition between fluids that allows them to mix in all proportions with no interface. If the interfacial tension between oil and gas is eliminated, all of the oil will be swept and residual oil saturation will be reduced to zero (Holm, 1986).

There are two types of miscible displacements: *first-contact* and *multi-contact* (Holm, 1986). These are illustrated in a ternary diagram, shown in Figure 2.4.2 (b) below. In each corner of the diagram components are at 100 % saturation. *First-contact* means that any amount of solvent (gas) injected will exist as a single phase with the oil in the reservoir (Holm, 1986). In the diagram this is represented by the dilution path from I₂-J₃ outside of the two-phase region. Miscibility can also occur by a *multi-contact* process, where gas and oil mix in repeated contacts. When the phase compositions formed in each contact move towards a critical point, miscibility can be achieved. This happens through processes called *vaporizing* and *condensing* gas drive. In figure 2.4.2 (b) this is illustrated by the dilution paths I₂-J₁ and I₁-J₂, respectively. (Johns & Dindoruk, 2013).

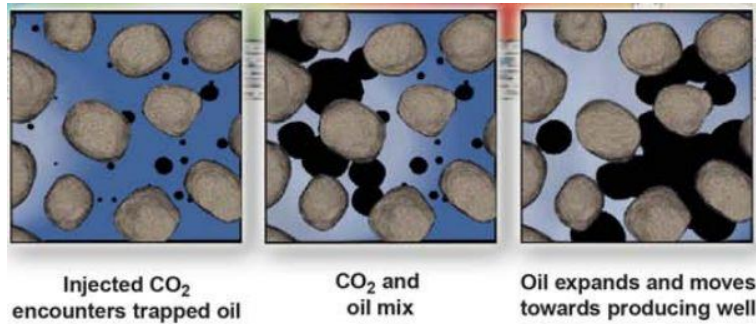


Figure 2.4.2 (a): Production of oil by miscible injection (NETL, 2010).

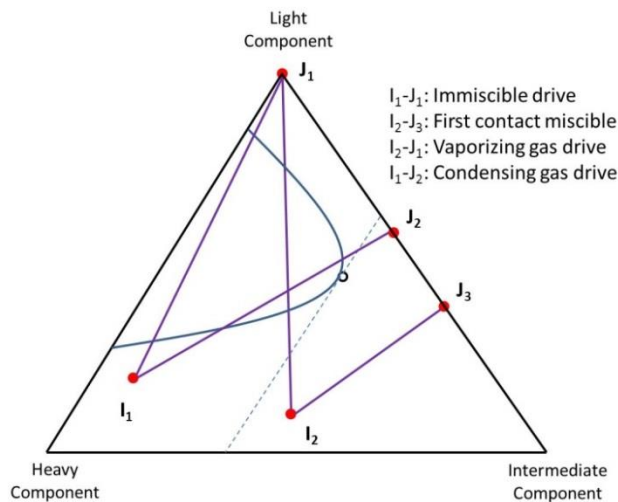


Figure 2.4.2 (b): Modified figure from (Mathiassen, 2003). Ternary diagram showing different dilution paths related to their respective displacement process.

A miscible displacement becomes effective in producing hydrocarbons because mechanisms such as mixing and reduced interfacial tension between gas and oil occur, as shown in Figure 2.4.2 (a). Through mixing, oil viscosity is reduced and, thereby, relative permeability of the oil is increased. When CO₂ contacts the oil, *swelling* occurs, causing the oil to expand and move towards the producing well. Observations suggest that when the oil and gas mix, drainage rates become higher in the oil zone, driving the excess oil towards the fractures (Chordia & Trivedi, 2010). Mixing during a miscible injection is due to *convection*, diffusion and *mechanical dispersion*. Uneven fluid flow or a concentration gradient will cause increased mixing, referred to as dispersion (Perkins & Johnston, 1963). A concentration gradient controls the diffusion process while velocity variations cause mechanical dispersion (Kamalipour, et al., 2014).

Immiscible Displacement: This type of displacement has a more limited degree of mass transfer between the gas and oil phases. Although gas will extract some components from the oil, true immiscibility is regarded as a limit where solubility of oil in the gas phase is negligible. An

immiscible gas flood is outperformed by a miscible one in terms of production because gas is less likely to bypass or finger through the oil. The displacement efficiency improves as the gas flood becomes more miscible (Johns & Dindoruk, 2013).

Minimum Miscibility Pressure (MMP): The lowest pressure required to reach miscibility between two phases is known as the Minimum Miscibility Pressure (MMP). The two phase region is dependent on pressure. A displacement that is immiscible at a specific pressure may become miscible at a higher pressure (Skarestad, 2012). The slim tube experiment provides a measurement of MMP. The experimental setup consist of a long tubes of small radiuses packed with unconsolidated sand. This tube is saturated with oil at reservoir conditions. Gas is then injected at a constant rate using a high pressure pump. Figure 2.4.2 (c) illustrates recovery of oil at 1.2 hydrocarbon pore volumes when injecting CO₂. As pressure increases the recovery starts to level off, which is defined as the point of minimum miscibility pressure. In the ternary diagrams, previously shown in Figure 2.4.2 (b), the MMP occurs where the critical tie line passes through the crude composition (Skarestad, 2012).

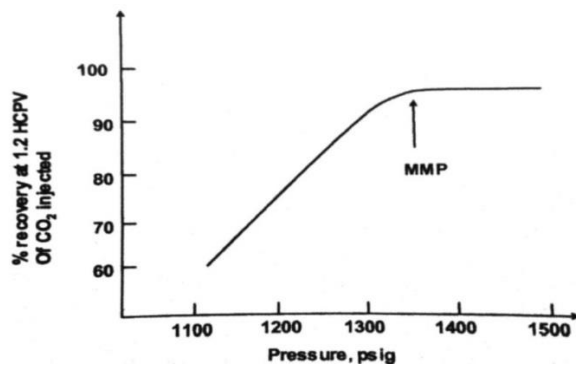


Figure 2.4.2 (c): Minimum Miscibility Pressure is achieved at the end point production in a slim-tube experiment (Skarestad, 2012).

2.4.3 | CO₂-FOAM

CO₂ Injection has been in use for over 40 years and has been considered an economically successful recovery technique. Even though CO₂ flooding is often used as a tertiary method, it still does not recover most of the oil from the reservoir. Typically, 10-20 % of the OOIP is swept by miscible CO₂ flood, while immiscible CO₂ floods have recoveries as low as 5 – 10 % of OOIP. Consequently, the remaining hydrocarbons lie in the range of 35-65 % of OOIP when the CO₂ flood is complete (NETL, 2011).

The low oil recoveries can be ascribed to two major reasons. (1) The density of pure CO₂ under high pressure is lower than oil, causing gravity override and early CO₂ breakthrough as a result.

This leads to large amounts of oil remaining un-swept in the lower regions. (2) The viscosity of supercritical CO₂ is also much lower than typical values for both oil and brine. Because of this, unfavorable mobility ratios can be expected to occur, thus promoting fingering of CO₂ through the oil. This has several important implications such as: early breakthrough, high CO₂ utilization, delayed CO₂ production, depressed oil production rates and low oil recovery efficiency (NETL, 2011).

Mobility control of CO₂ aims to reduce large differences in density and viscosity between CO₂ and other fluids. Injecting CO₂ as a supercritical phase together with a foaming agent, generating in situ foam, can be a very efficient recovery method (NETL, 2011). Another reason to inject CO₂ as foam is its ability to overcome subsurface heterogeneity. This is because foam is more sensitive to capillary pressure. A number of CO₂-foam field applications have showed that this method could delay the breakthrough of injected fluids while enhancing oil production dramatically (Lee & Kam, 2013)

2.5 | FOAM

2.5.1 | DEFINITION

Foam is comprised of a gas dispersed in a continuous liquid phase (Schramm, 2005). The liquid is generally water but could also be hydrocarbon-based fluids or acids. Foam can be generated as a result of liquid disturbance where the liquid contains a small amount of foaming agent, known as *surfactant*, while contacting a gas. A foaming agent is necessary to better generate foam and keep it stable. Without it, foams are unstable and quickly break down (Sheng, 2013). Pockets of trapped gas are packed tightly together at large gas fractions so that they form polyhedral rather than spherical cells. These cells are separated by thin films of surfactant-solubilized water, known as *lamellae*, as shown in Figure 2.5.1. The junction that connects three lamellae is referred to as a plateau border (NETL, 2011).

Characterization of foam is done through foam quality and bubble size. Foam quality is expressed as the percentage of gas volume present in the foam. Typical foam quality ranges from 75% to 90% (Lake, 1989). Bubble size refers to the average diameter and distribution of bubble sizes. There is a correlation between the quality of foam and its bubble size. As bubble sizes become larger, foams become less stable, resulting in a lower foam quality (Sheng, 2013).

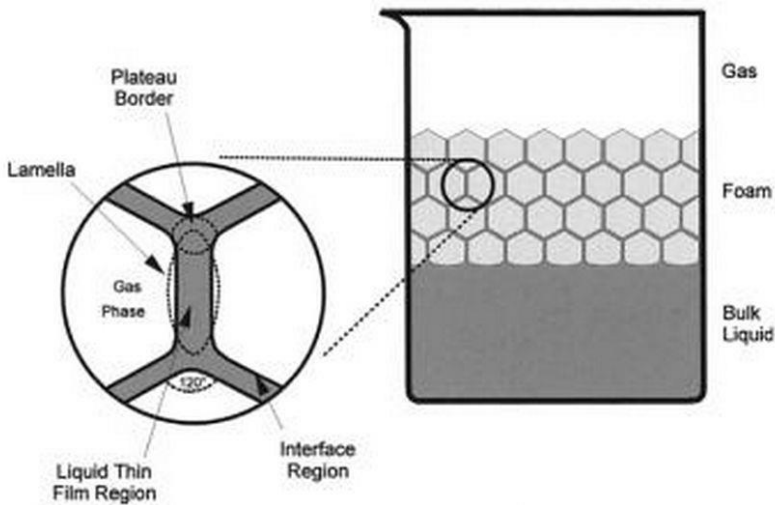


Figure 2.5.1: A container filled with gas and liquid, with surfactant solution, generates foam if mixed. Gas bubbles are separated by thin liquid films (lamellae) stabilized by surfactants (Schramm, 2005).

2.5.2 | ADVANTAGES

Foams can be injected into reservoirs to achieve mobility control or to block and divert flow (Schramm, 2005). Gas injected into a porous oil-saturated media, without the possibility of foam generation, can quickly flow to the producing well. This will leave a lot of the oil untouched. Foam addresses the issue regarding low viscosity of the gas, which renders a high mobility ratio between oil and gas. By creation of foam with the injected gas, the gas becomes more viscous which lowers its velocity. The addition of surfactants helps generate foam in situ, but also improves displacement efficiency (Sheng, 2013).

The advantage of foam is especially apparent in heterogeneous and fractured reservoirs, such as carbonates. Foams are stronger in high permeability layers because of lower capillary pressure, compared to layers with lower permeability where capillary pressure is higher (Yan, et al., 2006). Non-wetting gas will preferably stay in high permeability channels, which helps to divert flow into lower permeability layers. Decrease in gas mobility indirectly diminishes gravity segregation if the pressure in the injection well can be increase. Thus, foam will drive the gas to other parts of the porous media, naturally increasing the sweep efficiency (Sheng, 2013).

Selecting the proper surfactant for generating foam, under reservoir conditions, is considered a major challenge. The economic feasibility of foam flooding is largely determined by the amount of surfactant needed in order to generate and propagate foam. As a reservoir undergoes foam flooding, the amount of adsorbed surfactant can be of great importance. Therefore, selecting a

surfactant with acceptable adsorption levels, under reservoir conditions, is crucial (Schramm, 2005).

2.5.3 | FOAM STATES

Co-injection, of surfactant and gas, into a porous medium is subjected to mechanisms of in situ lamella creation. When foam flows through a porous media, three different situations may arise, as Figure 2.5.3 (a) shows. In the first situation (A) there are no foam films present, originally. This could be the case in a high capillary pressure formation, strongly oil-wet rock or highly oil saturated rock, where foams are destabilized and broken down. Consequently, two-phase flow of gas and liquid continues without foam. The formation is left with a high saturation of water as it fills the smaller pores (Lee & Kam, 2013).

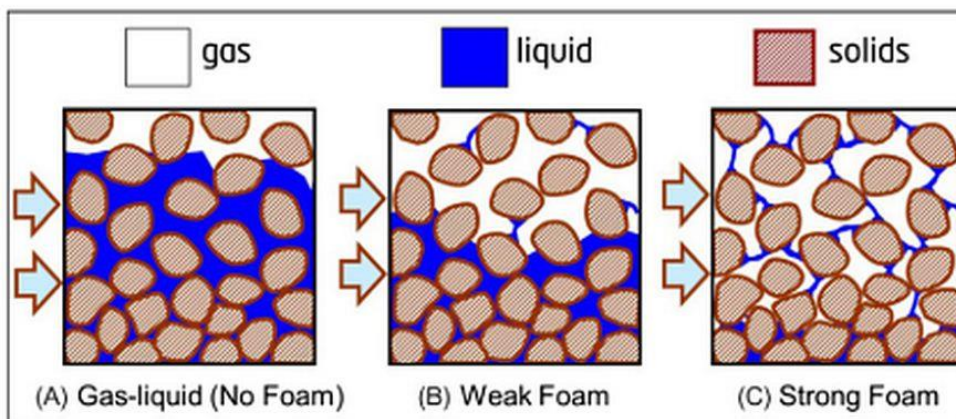


Figure 2.5.3 (a): Different foam regimes occur depending on the presence of foam films (Lee & Kam, 2013).

In the second instance (B), a moderate increase in foam viscosity, followed by a moderate increase in the pressure gradient, will result in the formation of weak foams. In the last situation (C), significant amounts of very fine-textured foams are present. These are referred to as strong foams and can increase the effective foam viscosity (or decrease mobility of gas) additionally once they have been generated. Strong foam can drastically increase the pressure gradient (Lee & Kam, 2013). In coreflood experiments, foam generation is defined by the transition between weak foam to strong foam. Figure 2.5.3 (b) illustrates the pressure vs. time (A) and pressure vs. injection rate (B) for a Berea sandstone core. Different injection rates have been used with a constant foam quality of 80 %. What stands out is how sudden the increase in pressure drop occurs once generation of foam starts. The figure also shows in what ranges of pressure drop the weak and strong foams occur.

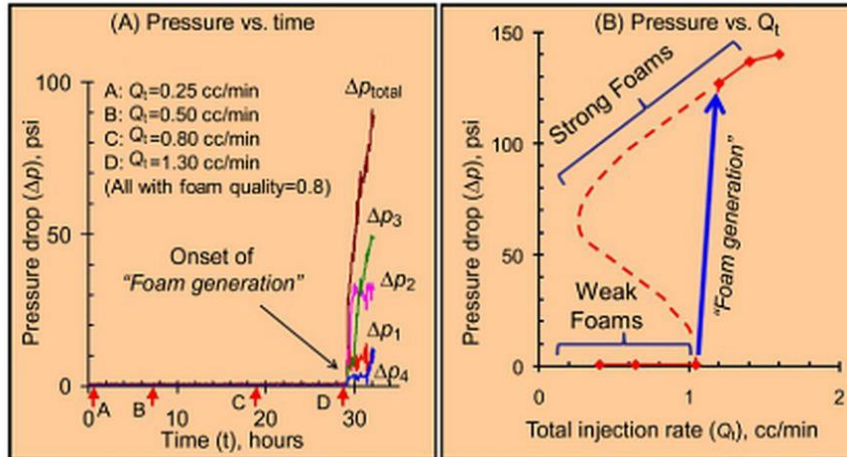


Figure 2.5.3 (b): (A) Pressure drop vs. time and (B) pressure drop vs. injection rate for a coreflood experiment where foam is generated (Lee & Kam, 2013).

2.5.4 | GENERATION MECHANISMS

Major lamella creation mechanisms include *snap-off*, *lamella division* and *leave behind* (Ransohoff & Radke, 1988). These concepts are displayed in Figure 2.5.4, where gas flows through a porous media, displacing a liquid.

Snap-off (a) occurs when gas intrudes through a pore space, resulting in a thinning by the narrow pore throat until it snaps into two. This mechanism occurs repeatedly at the same site, affecting a large portion of the flow field. Snap-off creates discontinuity in the gas phase as well as formation of lamella. The generated bubbles may block the pathway of gas behind it, naturally reducing the permeability of the gas. This is regarded as the most dominating foam generation mechanism (Liontas, et al., 2013).

Lamella division (b) is another mechanism where lamella (pre-generated foam) flows through a point, branching out, which will separate the lamella into two. This process also occurs repeatedly at the same site. At high flow velocities, both snap-off and lamella division occur simultaneously (Liontas, et al., 2013).

Leave-behind (c) happens when two gas menisci intrude saturated pores from different directions, effectively trapping liquid and leaving lamella behind. As the number of lamella increase, more pathways become blocked, thus reducing permeability of gas. This mechanism is especially relevant in low velocity regimes and generates weak foams. It has been concluded that foams generated entirely by leave-behind gave a fivefold reduction in gas permeability. On

the contrary, snap-off gave a hundred-fold reduction in gas permeability (Ransohoff & Radke, 1988).

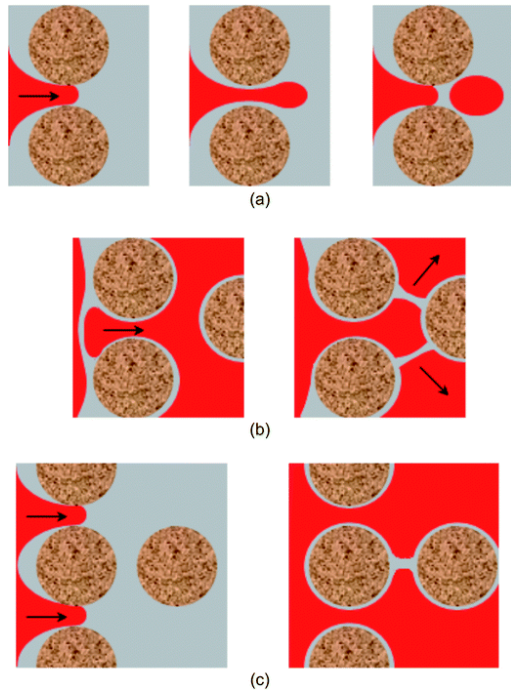


Figure 2.5.4: Schematics of mechanisms for foam generation including a) snap-off, b) lamella division and c) leave-behind (Liontas, et al., 2013).

2.5.5 | STABILITY

Foams are not thermodynamically stable, meaning that they eventually will collapse over time. Stability of foam is dependent on a number of factors presented by (Sheng, 2013), which will be discussed.

Effect of Oil: A major concern regarding foam injection in reservoirs is the stability of foam in the presence of oil. In order to achieve good mobility control, it is important that foam remains stable when contacting the oil (Simjoo, et al., 2013). As the oil spreads on the foam film, the film tends to break as the oil displaces the original liquid film. What is left behind is an unstable oil film which breaks easily. Foam destabilization by oil can happen in several ways: (1) Surfactants partitioning in the oil phase, reducing the surfactant concentration at the gas-water interface. (2) Oil spreads on the foam lamellae, displacing the interface originally stabilizing the foam (Farajzadeh, et al., 2012). (3) Oil generating emulsions which allows drops to break out and rapture the stabilizing interface. (4) Oil droplets blocking certain parts of the porous media where bubble snap-off is inhibited, thus preventing foam generation to occur. Lighter oils are known to destabilize foam the most. Foams with intermediate to low tolerance for oil may be adequate if injected into low oil saturation zones for mobility control (Schramm, 2005).

Surfactants: Stable foams are caused by the presence of a foaming agent at the gas-liquid surface. Surfactants will lower the interfacial energy at the liquid-gas interface once it is adsorbed. This will make it easier to form and maintain a large interfacial area constituted by many gas bubbles in a liquid. It also results in an increase in interfacial viscosity, which further substantiates stability. Foaming ability reaches its maximum at or above the critical micelle concentration of surfactants (Schramm, 2005).

Wettability: Foams are observed to be less stable when contacting crude oil in the presence of an oil-wet surface compared to the same crude oil in the presence of a water-wet surface (Suffridge, et al., 1989).

Disjoining Pressure: This is an additional pressure within a film which supports or stabilizes the film. It is denoted $\Pi(d)$ and depends on the film thickness, d , as shown in Figure 2.5.5 (b). There are attractive forces between oil-water and solid-water surfaces, as well as repulsive forces between oil-water and solid-water surfaces, as can be seen in Figure 2.5.5 (a) (Skauge, 2013).

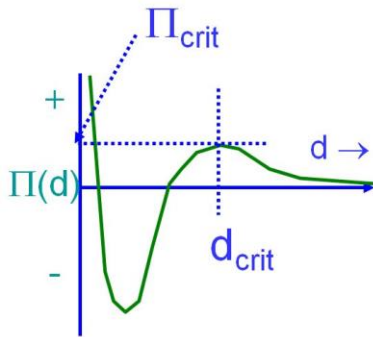


Figure 2.5.5 (a): Profile of the disjoining pressure with film thickness (Skauge, 2013).

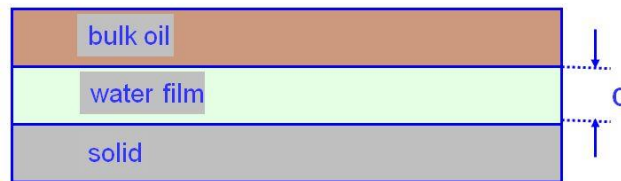


Figure 2.5.5 (b): Illustration of water film thickness between the oil phase and solid phase (Skauge, 2013).

Positive values of $\Pi(d)$ represent repulsive film forces, and negative values of $\Pi(d)$ imply attractive film forces. At a certain film thickness, referred to as the critical film thickness, d_{crit} , the film will become so unstable that it collapses (Skauge, 2013).

Liquid Drainage: After foam generation there is a tendency for the liquid, which constitutes the film, to drain as gravitational forces act upon it. This can be seen from Figure 2.5.5 (c). As liquid starts moving downwards, bubble shapes transition from approximately spherical to polyhedral shapes. At this stage, capillary forces compete with gravitational forces. Along the plateau borders, gas-liquid interfaces are more curved, generating a lower pressure. Higher pressures reside along the thin film region, and this pressure difference causes liquid to flow towards the

plateau borders. This results in a thinning of the films while generating a motion in the foam (Schramm, 2005).

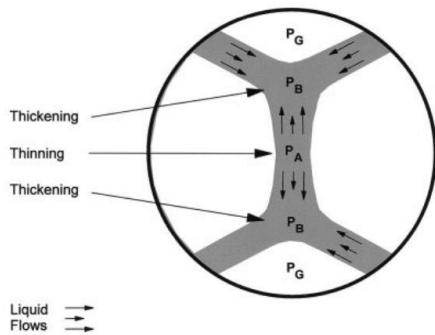


Figure 2.5.5 (c): Illustration of thickening and thinning of the films during a liquid drainage (Schramm, 2005).

Bubble Sizes and Diffusion: Foams are generally more stable if bubble sizes are uniformly distributed. Foam that has a bubble size distribution of mostly smaller sizes is representative of stable foam. Small gas bubbles have a higher pressure than larger bubbles. This pressure difference results in a chemical difference, causing gas to diffuse through liquid from small bubbles to larger bubbles. Consequently, bubbles will merge together (Sheng, 2013).

Pressure and Temperature: Higher pressure helps stabilize foams because this results in smaller bubbles. However, if a certain pressure is exceeded foams may collapse. Liquid films also become larger and thinner, which slows down liquid drainage. With increasing temperatures, surfactants become more soluble in the liquid phase. High temperatures increase liquid drainage of the films, meaning that foam becomes destabilized (Sheng, 2013).

Limiting Capillary Pressure: If the capillary pressure, in a porous media, surpasses a «limiting» value then the foam becomes unstable. This limiting capillary pressure is a strong function of the wetting phase and rock morphology. Foam coalescence occurring at this limit, in a porous media, has been found to be close to the rupture pressure of a foam film (Farajzadeh, et al., 2012).

2.5.6 | FLOW BEHAVIOR

There are several mathematical relations that can be used to describe the foam flow behavior, as presented by Bertin et al. (1998). These are foam viscosity, foam relative permeability and the mobility reduction factor.

Apparent Viscosity: The apparent viscosity of foam, μ_f , is a function of both bubble density (n_f) and real velocity of foam (v_f). It is calculated by a combination of gas permeability and Darcy's law. The expression is written as:

$$\mu_f = \mu_g + \frac{\alpha n_f}{v_f^c} \quad 2.5.1$$

Here, α is a proportional constant and a function of surfactant properties. And c is the empirical exponent with a theoretical value of 1/3. Viscosity of foam is known to be much higher than both water and gas (Bertin, et al., 1998).

Relative Permeability: Generated foam leads to reduced gas relative permeability as foams block flow paths of least resistance in a porous media. The following equation has been presented to describe relative permeability of foam, k_{rf} :

$$k_{rf} = k_{rg}^0 \bar{S}_f^{n_g} \quad 2.5.2$$

Here, k_{rg}^0 is the relative permeability of gas at connate water saturation, S_{wc} . The gas exponent is represented by n_g . The saturation of foam (S_f) in Equation 2.5.2 is expressed as:

$$\bar{S}_f = X_f(1 - \bar{S}_w) \quad 2.5.3$$

$X_f = S_f/S_g$ is the fraction (surfactant-to-gas) of the foam phase that is flowing. Water saturation in equation (2.5.3) is expressed as \bar{S}_w (Kovscek, et al., 1995).

Mobility Reduction Factor: In field scale application, the parameters related to surfactant concentration, oil saturation, water saturation and capillary number are considered to have the most significant effect on foam flow behavior. These can all be correlated through the mobility reduction factor, M_{rf} , (Kovscek, 1998), expressed as:

$$M_{rf} = \frac{1}{1 + M_r F_s F_w F_o F_c} \quad 2.5.4$$

Here, M_r is the reference mobility reduction factor. This means that the factor is calculated for a system with a reference values for surfactant concentration, water saturation, oil saturation and capillary number. F_s , F_w , F_o and F_c are mobility reduction factor components for surfactant concentration, water saturation, oil saturation and capillary number, respectively. The mobility reduction factor indicates to what extent mobility of gas has been reduced.

2.6 | WATER-ALTERNATING-GAS (WAG)

2.6.1 | GENERAL DESCRIPTION

Mobility control is also possible without the use of foams. WAG injection was introduced as a method to control the mobility of a gas injection by the use of water, thereby stabilizing the displacement front. Water and gas are injected in alternating slugs, displacing the oil in a reservoir. Microscopic displacement of oil by gas is usually more efficient than for a water injection. WAG becomes a better alternative because it combines improved displacement of the gas flooding with an improved macroscopic sweep of water injection. In addition to mobility control, the use of WAG is also environmentally favorable when it comes to reinjection of gas for storage purposes (Christensen, et al., 2001). Figure 2.6.1 illustrates the use of alternating water and gas slugs as an enhanced oil recovery process.

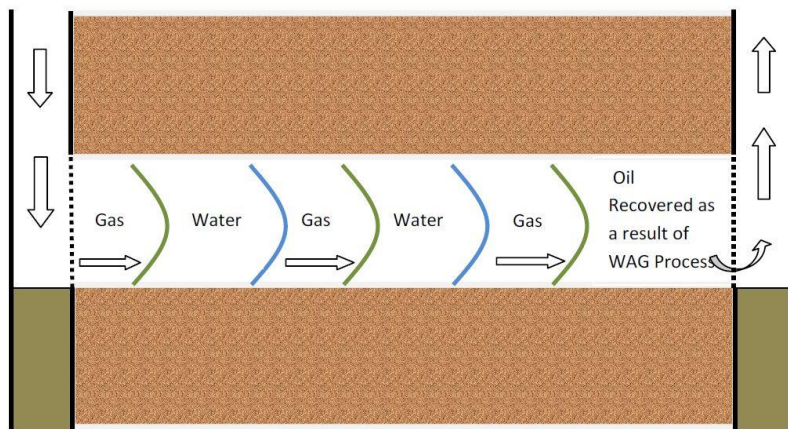


Figure 2.6.1: Schematics of a water-alternating-gas flood for enhanced oil recovery (Zahoor, et al., 2011).

2.6.2 | WAG DESIGN

WAG injection is normally applied as an enhanced oil recovery method in the late stages of field production, after primary and secondary recovery has been conducted. WAG has been utilized successfully in many field trials, most of which are in Canada and the U.S. (Christensen, et al., 2001).

Immiscible/miscible: The WAG process can either be immiscible or miscible. Deciding on which should be used is reportedly based on availability and economic considerations. From a total of 60 projects reviewed by Christensen (2001), 79 % were applying miscible WAG injection, mostly at onshore reservoirs. The majority of these projects were re-pressurized so that reservoir

pressure exceeds minimum miscibility pressure of the fluids. Immiscible WAG has been used where gravity-stable gas injection is inapplicable because of limited gas resources, unfavorable dipping angles or reservoir heterogeneity. The first gas slug in a WAG injection could potentially dissolve into the oil, causing a favorable change in the fluid viscosity/density relations at the displacement front. As a result of this, the displacement can become near-miscible (Christensen, et al., 2001).

Injection Gas: The gases used in a WAG are divided into groups: CO₂, hydrocarbons and non-hydrocarbons. Although it is an expensive gas, CO₂ possesses certain properties which make it eligible when aiming for a miscible process. Corrosion is often a negative aspect of applying CO₂, but nearly impossible to avoid. From the 60 projects reviewed by Christensen (2001), 28 were using CO₂ as the gas of choice in their WAG process. Due to the availability of hydrocarbon gas directly from production, all offshore projects use it in their WAG injections. It has been reported that 24 out of 60 reviewed fields were using hydrocarbon gas. Every WAG flood has its optimal amount of gas needed for injection, and exceeding this limit means gas will be recycled, gaining limited extra recovery. WAG with CO₂ in a miscible process shows an average improved oil recovery of 10% OOIP, whereas hydrocarbon and nitrogen gases in an immiscible process have improved recoveries of 8% OOIP (Christensen, et al., 2001).

Injection Pattern: The most utilized pattern for WAG onshore is the five-spot injection pattern. The same pattern is not necessarily applied offshore due to the expensive drilling and data collection that is required compared to onshore projects. Four injection wells are placed in a box-like shape, with the producing well in the center (Dai, et al., 2013), as can be seen from Figure 2.6.2.

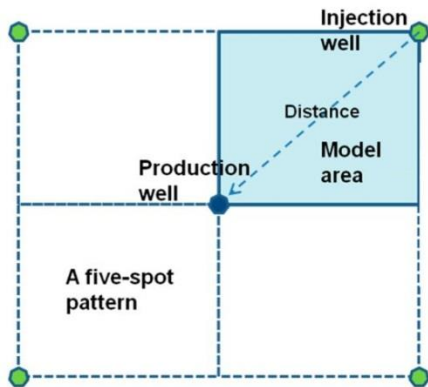


Figure 2.6.2: Schematics of a five-spot well pattern consisting of four injection wells and a production well in the center (Dai, et al., 2013).

WAG Ratio: It is crucial to find the optimum WAG ratio before beginning the injection process. In field applications, the most used WAG ratio is 1:1, meaning that the gas and water cycles are equal. It is influenced by the rock's wetting state (Zahoor, et al., 2011). Water-wet bead packs have shown optimum WAG ratio of 0:1 (gas injection), while oil-wet packs imply that 1:1 is the optimum WAG ratio (Rogers & Grigg, 2001). Typical cycle times range from months to a year (NETL, 2011). Recovery efficiency has been proven to be a function of both the injection rate and the WAG ratio (Al-Shuraiqi, et al., 2003). Injecting below the optimum WAG ratio (more gas than water) creates viscous instability. On the contrary, injecting above the optimum WAG ratio (more water than gas) has a tendency to stabilize the process, but lower the efficiency of displacement as production becomes prolonged (Rogers & Grigg, 2001).

2.6.3 | FACTORS INFLUENCING INJECTIVITY

Some simple relations will be presented that provides insight into the advantages of WAG injection.

Recovery Factor: There are three contributions to the oil recovery factor, R_f :

$$R_f = E_v * E_h * E_m \quad 2.6.1$$

Here, E_v is the vertical sweep, E_h the horizontal sweep and E_m the microscopic sweep. In literature, E_v and E_h is referred to as macroscopic sweep. Recovery can be enhanced by improving one or all of the three factors. The horizontal displacement efficiency is largely affected by the stability of the displacement front, which in turn depends on the mobility of the fluids (Christensen, et al., 2001).

Horizontal Displacement Efficiency: This displacement efficiency is largely affected by gas and oil, mobility ratio (Amin, et al., 2012) defined as:

$$M = \frac{k_{rg}/\mu_g}{k_{ro}/\mu_o} \quad 2.6.2$$

The equation involves relative permeabilities, k_{rg} and k_{ro} for gas and oil, respectively. It also includes viscosities, μ_g and μ_o of gas and oil, respectively. With a mobility ratio of $M > 1$, the displacement becomes unfavorable as the gas will finger or channel through the oil, leading to an early gas breakthrough. In addition to mobility ratio, heterogeneity, such as high permeable layers in the reservoir, may also cause the sweep to become inefficient.

Miscible gas injection has good microscopic sweep efficiency but poor macroscopic sweep efficiency because of viscous fingering and gravity over-ride (Al-Shuraiqi, et al., 2003). In addition, it is expensive to apply. On the contrary, water flooding is cheap and less prone to gravity segregation and unstable displacement fronts. The downside, however, is the large volumes of residual oil left behind, which makes it a less than optimal injection strategy.

Gravity Segregation: During a gas injection cycle, gas may tongue upwards and away from the wells, while water moves downwards during a water injection cycle. Fluids will segregate, like Figure 2.6.3 illustrates, once there is a significant vertical permeability and because of density differences between the respective fluids (Johns & Dindoruk, 2013).

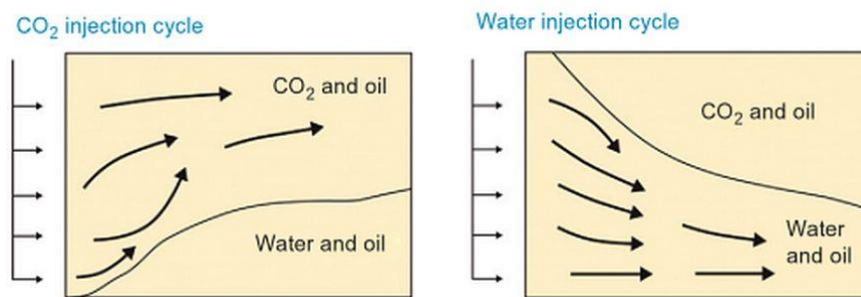


Figure 2.6.3: During a WAG, gas may move upwards and water may move downwards, owing to the nature of their densities (Johns & Dindoruk, 2013).

Vertical Sweep Efficiency: This depends on both viscous and gravitational forces, expressed by the viscous/gravity ratio (Christensen, et al., 2001):

$$R_{v/g} = \left(\frac{v\mu_o}{k_o g \Delta\rho} \right) \left(\frac{L}{h} \right) \quad 2.6.3$$

Here, v = Darcy velocity, μ_o = oil viscosity, L = distance between wells, k_o = oil permeability, g = gravitational force, $\Delta\rho$ = fluid density difference, h = height of displacement zone. This ratio of viscous to gravity forces is the prime variable when assessing the efficiency of WAG injection (Rogers & Grigg, 2001). Properties affecting vertical sweep include reservoir dip angle, permeability differences and porosity. Increasing porosity and permeability downwards is advantageous to WAG as it is favorable in stabilizing the front (Christensen, et al., 2001). Laboratory and simulation results have found that oil becomes trapped by water that would otherwise be contacted by CO₂ during the WAG injection. And water-wet cores have proven a higher degree of oil trapping than oil-wet cores (Jackson & Andrews, 1985). This causes gravity

forces dominate water-wet tertiary floods while viscous fingering controls oil-wet tertiary floods (Amin, et al., 2012).

Heterogeneous Permeability: Most reservoirs, especially carbonates, have non-uniform pore size distribution as well as variable interconnectivity. Due to the nature of these phenomena, a certain level of heterogeneous permeability is expected. This can severely affect the WAG injection process and, ultimately, the recovery efficiency. This effect worsens with an increasing vertical/horizontal permeability ratio, because gravity segregation becomes more dominant (Zahoor, et al., 2011).

Trapped-gas Saturation: This is one of the key parameters when assessing injectivity and displacement efficiency in a miscible WAG injection. There is entrapment of gas in high permeability layers, diverting water towards layers of lower permeability. Mobilization of residual oil is heavily dependent on the amount of gas trapping. Initial water saturation before water flooding, as well as wettability, will influence oil-saturation reduction and gas trapping (Rogers & Grigg, 2001).

Bypassing Mechanisms: A clear understanding of important bypassing mechanisms is needed to be able to interpret experimental results, as explained by Stern (1991). These include: 1) *dispersive* and (2) *capillary-induced bypassing*, as well as 3) *viscous fingering*

1) *Dispersive bypassing* occurs in single-phase flow, at the mixing zone between oil and solvent. If the viscosity ratio between oil and solvent is unfavorable, more extensive bypassing occurs. This mechanism is dependent on flow rate, but not on core length.

2) *Capillary-induced bypassing* is similar to dispersive bypassing, and occurs in tertiary displacements since the solvent has to first displace water to contact the oil. As the solvent enters the largest pores first in a water-wet system, preferred high conductivity paths will be developed during formation of the oil bank, which leads to pore-level bypassing of the oil. This mechanism is reduced if flow rate or viscosity of the solvent is increased.

3) *Viscous fingering* is a result of macroscopic heterogeneities as well as mobility contrasts between oil and solvent. Because of core-scale heterogeneities, the solvent finds a preferred path that most of the solvent flows through. The result is limited additional oil recovered. This bypassing mechanism can be counteracted through mixing between solvent and oil, reducing mobility contrast at the displacement front.

2.6.4 | OPERATIONAL CHALLENGES

WAG is more challenging than pure gas or water injection due to the constant alteration of fluids throughout the injection process. Some common problems from different fields will be discussed next. Several fields have experienced early gas breakthrough due to channeling or override. Another serious problem is the loss of miscibility, leading to lower recovery than expected. Reduced injectivity has been experienced, meaning a rapid pressure drop in the reservoir, which will influence production. Corrosion often occurs in WAG projects applied as tertiary recovery methods. This means that the production of a reservoir continues in older facilities, which it may not have been designed for in the first place. A WAG project was delayed on Ekofisk due to formation of hydrates, plugging the injector (Christensen, et al., 2001).

Water-alternating-gas is a proven recovery technique that normally renders better results compared to continuous CO₂ and water injection. However, WAG floods still leave behind approximately one-third to two-thirds of the oil that a waterflood does (NETL, 2011). From field experience, it is apparent that WAG is not an optimal strategy, and it is worth considering other alternatives for further improvements within enhanced oil recovery.

2.7 | SURFACTANT-ALTERNATING-GAS (SAG)

2.7.1 | GENERAL DESCRIPTION

Foam is formed on the contact of the gas with surfactant, and viscosity of the injected gas is reduced. Although foam can improve sweep efficiency, direct injection of pre-generated foam would not be practical because of its poor injectivity. Field experience suggests that injectivity can be improved through alternating slugs of gas and surfactant, resulting in foam creation inside the porous medium (Farajzadeh, et al., 2015). This is referred to as surfactant-alternating-gas (SAG), and is operationally similar to WAG. SAG injection is one of the methods commonly used to counter problems related to early breakthrough caused by override, fingering and channeling of gas (Salehi, et al., 2014).

SAG injection has several advantages over co-injection. For one, water and gas contact is reduced in surface facilities and pipes, preventing the corrosive effects of acidic gases (when contacting water) such as CO₂. SAG may promote foam formation in the near-well region. By displacing water from the near-well region, using gas, injectivity can improve as gas mobility rises. Loss of surfactant due to adsorption is a central factor when considering the economic feasibility of SAG injection. Thus, understanding the adsorption process is critical in evaluating transport of chemicals. SAG is a function of gas-to-surfactant ratio at certain temperature and

pressure. Before SAG can be optimized, the concentration of surfactant must be optimized (Salehi, et al., 2014).

2.7.2 | RESPONSES FROM SAG

Injection of gas and surfactant in repetitive cycles will cause the capillary pressure near the well to move up and down, which proves to be favorable for generating foam in situ. When gas is injected in the wellbore area, stable foams will be generated near the wellbore if surfactant has been pre-injected. During a continuous CO₂ and surfactant injection an exponential decrease of injection pressure occurs, suggesting that the CO₂ is displacing fine-textured foams. This will eventually dry out the region near the wellbore. Regions away from the wellbore ends up having stable foams, while the regions near the wellbore are without foams. For a SAG process, the opposite occurs: foams are stable in the wellbore region. This describes the basis of why SAG improves injectivity (Lee & Kam, 2013).

The gas-oil ratio (GOR) of a SAG process has been proven to be 10 times smaller than the GOR for a WAG process in the producing well (Lee & Kam, 2013). Figure 2.7.2 is from the EMU unit in Texas, comparing oil production rates for SAG, WAG and a waterflood. For the SAG injection, 13 cycles of CO₂ and surfactant were injected. Based on the decline curves, SAG has performs better than both WAG and waterflooding by improving sweep efficiency.

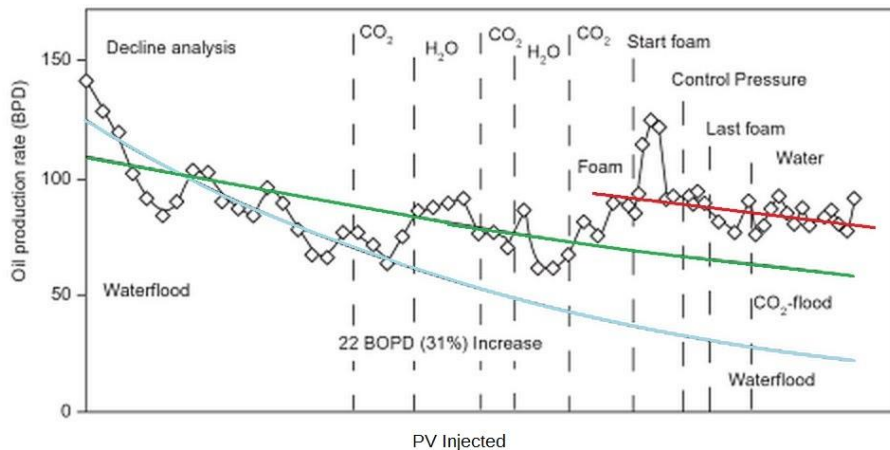


Figure 2.7.2: Oil production rate (BPD) vs. PV injected for SAG (red), WAG (green) and a waterflood (blue) from the EMU unit in Texas. Decline analysis curves have been drawn. Modified from (Lee & Kam, 2013).

2.7.3 | SAG DESIGN

It is necessary to consider certain factors before choosing the appropriate foam injection strategy. The options are surfactant-alternating-gas, co-injection or pre-formed foam. Operating fields often consider reservoir pressure, permeability and expected duration of surfactant injection as very important. SAG is mainly used in high pressure formations with low permeability ranging from medium to low surfactant concentrations (Turta & Singhal, 2002).

Injection Gas: In previous field pilots several injection gases have been utilized for surfactant-alternating-gas processes. Most fields in the U.S. have been applying CO₂ as this is the most available gas, but also due to the possibility of achieving miscibility with the oil. For fields in the North Sea, hydrocarbon miscible gas is most widely applied. Some field pilots in China (Shengli and Sabei) have successfully completed SAG using nitrogen. Flue gas (N₂, CO₂) was used at some point, but was essentially replaced by CO₂ by the 1980s. Implementation of miscible CO₂ in SAG projects, and EOR processes in general, has been increasing steadily over the past two decades (NETL, 2011).

Surfactant Optimization: Choosing the proper surfactant is critical in CO₂ foam flooding. The surfactant needs to be soluble in brine in order to have it stabilize CO₂-in-brine emulsions. As the temperature in a reservoir increases, the surfactant tends to become less soluble in brines, increasing the total amount of dissolved ions (NETL, 2011).

Different types of surfactants are used depending on the reservoir formation rock. This is to prevent large amounts of surfactants to adsorb to the surface of the rocks. A *cationic* surfactant, for instance, has a positively charged head group and negatively charged counterion. This one cannot be used in a sandstone formation as the positively charged head would attract towards the negatively charged sandstone surface. It could, however, be used in a carbonate formation as the surfaces have a positive charge. For sandstone, it is common to use *anionic*, *nonionic* and *amphoteric* surfactants. Several surfactants have been tested in the lab and deemed as viable candidates for foam generation. The “Chaser CD 1045” has been implemented by several field pilot tests. It has been evaluated by many sources which describe it as an excellent foaming agent for CO₂ SAG processes (NETL, 2011).

Another important aspect is the surfactant concentration needed in order to successfully reduce the mobility of the gas. Figure 2.7.3 (a) illustrates mobility reduction of gas in Berea sandstone. At concentrations around 0.001 wt%, lamellae is not stable enough and foam cannot be generated. At 0.01 wt%, mobility is reduced by 75% and a further reduction is seen at 0.03-0.04 wt%. From 0.1-0.5 wt% there is almost no change (NETL, 2011).

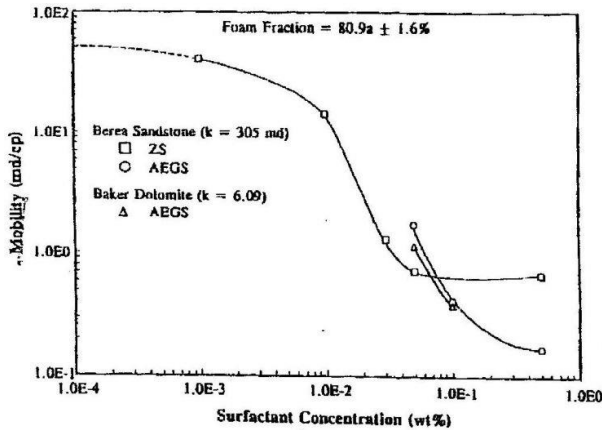


Figure 2.7.3 (a): CO_2 -in-brine foam with 80% quality. The surfactant is called Varion CAS. Mobility reduction as surfactant concentration increases (NETL, 2011).

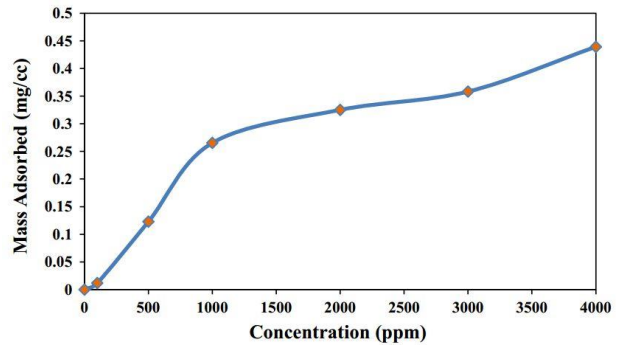


Figure 2.7.3 (b): Adsorption isotherm for a surfactant on silica at $70^\circ C$ and $144.74 \times 10^5 Pa$ (Salehi, et al., 2014).

The surfactant concentration also has importance in relation to mass adsorbed when injected into a reservoir. Figure 2.7.3 (b) shows how mass of adsorbed surfactant (mg/cc) increases with concentration (ppm). From 100 to 1000 ppm, the adsorbed mass increases steeply. However, in the range of 1000 to 3000 ppm, the value of adsorbed mass is relatively constant. At around 3000 ppm, it starts increasing again. This is because surfactant becomes insoluble in water at this point (Salehi, et al., 2014). The concentration of 1500 ppm was considered optimal for a specific SAG injection process, conducted by Salehi et al. (2014), because no drastic changes occurred in this area.

SAG Ratio: The amount of oil recovered in a SAG process is highly related to the surfactant-to-gas ratio. The, already mentioned, study done by Salehi et al. (2014) explains why this is the case. A SAG injection was conducted in the lab on a conventional sand pack core at fixed injection rate of 0.2 cc/min. Increasing the surfactant volume could, for instance, mean ratios of 2:1, 3:1 or 4:1. The oil recovery factor has been observed to decrease with increasing surfactant slugs. This is attributed to early breakthrough of surfactant solution. Increasing surfactant volume and reducing the fraction of gas in the injection fluid would mean that there will be less gas to contact the surfactant, and generate foam. In this case, oil recovery is affected directly by the earlier breakthrough time, like Figure 2.7.3 (c) and (d) illustrates (Salehi, et al., 2014).

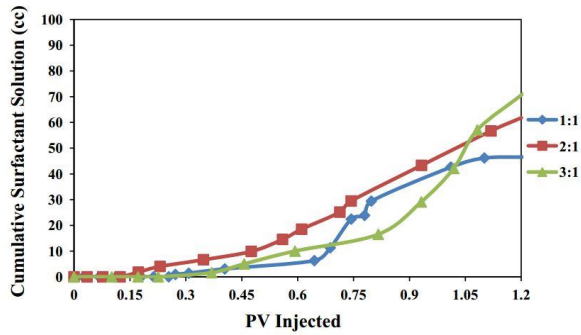


Figure 2.7.3 (c): Increasing surfactant volume. Cumulative surfactant produced vs. PV injected for SAG ratios 1:1, 2:1 and 3:1 (Salehi, et al., 2014).

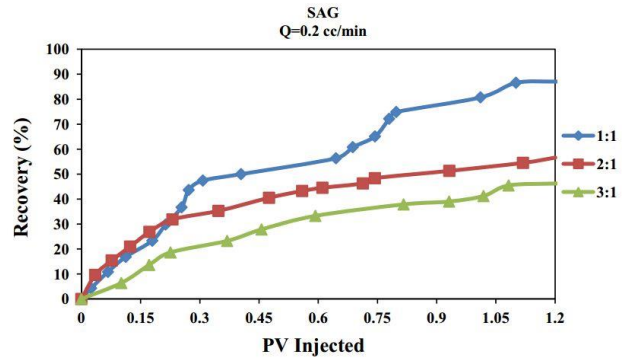


Figure 2.7.3 (d): Increasing surfactant volume. Recovery factor vs. PV injected for SAG ratios 1:1, 2:1 and 3:1.

Figure 2.7.3 (c) shows how a higher cumulative surfactant needed per pore volume injected for both ratios 3:1 and 2:1 compared to 1:1, which is more balanced. Figure 2.7.3 (d) shows that ratios 3:1 and 2:1 have earlier breakthrough of surfactant solution, as well as lower recovery efficiency compared to 1:1.

Increasing gas volume means that the SAG ratio could be 1:2, 1:3 or 1:4, for example. As the proportion of gas increases in the solution, it can disperse more of the solution phase in the gas, effectively reducing the macroscopic sweep efficiency. With early breakthrough of gas, as seen in Figure 2.7.3 (e) and (f), oil recovery will decrease as a consequence. Maximum efficiency was achieved at a ratio of 1:1 as both the macroscopic and microscopic efficiencies are high (Salehi, et al., 2014).

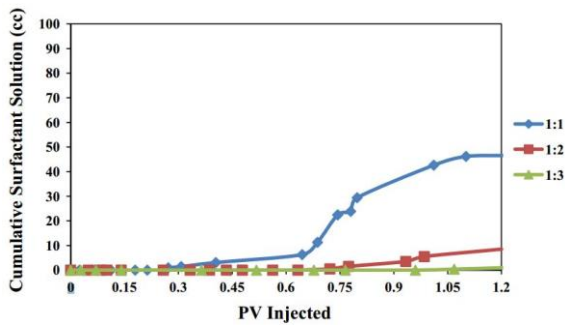


Figure 2.7.3 (e): Increasing gas fraction. Cumulative surfactant produced vs. PV injected for SAG ratios 1:1, 1:2 and 1:3 (Salehi, et al., 2014).

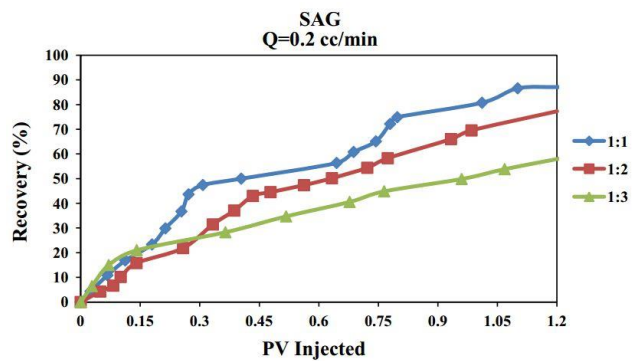


Figure 2.7.3 (f): Increasing gas fraction. Recovery factor vs. PV injected for SAG ratios 1:1, 1:2, 1:3 (Salehi, et al., 2014).

Fixed-Rate or Fixed-Pressure: Fluids can be injected at fixed injection rates or fixed injection pressure. It has been reported by Shan & Rossen (2002) that SAG injection is optimized at fixed maximum-allowable injection pressure for a homogeneous reservoir. This is to minimize both gravity override, injection time, and keep the increase in injection well pressure at a minimum. Injecting gas at maximum pressure allows for effects of *gravity slumping* for surfactant to partially reverse. Because of density differences in surfactant and gas, gravity may pull the surfactant solution downwards, causing gas to override it. The process of fixed injection pressure is also very insensitive to foam properties (Shan & Rossen, 2002). For heterogeneous reservoirs, Renkema & Rossen (2007) concluded that a maximum-fixed-pressure also renders the best results. However, different slug injection strategies were recommended.

It has been concluded that foam processes using SAG at fixed injection pressures are not affected by gravity override as much as continuous foam injection or SAG at fixed injection rates. Rather, gravity override can be overcome without reaching excessive injection pressures (Shan & Rossen, 2002).

Single- or Multi-Cycle: Slug sizes and the number of slugs are important design considerations for SAG field application. The term *single-cycle SAG* refers to a process where one slug of surfactant is injected, followed by one large slug of gas. In this case, an extra volume of surfactant must be injected to account of adsorption and to keep the surfactant slug ahead of the gas front. The other process is called *multi-cycle SAG* or simply just SAG. This is where slugs of surfactant are alternated with slugs of gas in two or more cycles (Renkema & Rossen, 2007).

Simulation results, based on fractional flow theory from (Shan & Rossen, 2002), suggests that SAG with fewer, larger slugs gives a somewhat better sweep efficiency compared to many smaller slugs. In a two-SAG-cycle process, surfactant would fill the lower portion of the reservoir where water saturation was 100 %, and unswept by gas. This essentially becomes an underdrive zone for the surfactant, promoting gravity segregation between surfactant and gas. The result is that a large portion of the injected surfactant may end up unused in the underdrive zone. In the single-cycle SAG, the piston-like sweep helps to push surfactant ahead, optimizing surfactant propagation in the reservoir. These cases were concluded for a homogeneous reservoir model (Shan & Rossen, 2002).

In simulations done by Renkema & Rossen (2007), single cycle SAG with maximum-fixed pressure has also proven to outperform multi-cycle SAG for a heterogeneous reservoir. They suggest injecting one big slug of surfactant followed by one big slug of gas. Field experience also suggest that SAG injection in both CO₂ and hydrocarbon miscible flooding yields better results when using smaller duration of the injection cycles in a multi-cycle SAG (Turta & Singhal, 2002).

2.7.4 | FOAM SELECTION AND RESERVOIR CONDITIONS

So far, it is clear that the selection of the appropriate foam injection strategy largely depends on the reservoir conditions. In order for SAG to be a natural choice as mobility control foam, several factors need to be considered. The desired distance of foam propagation must be longer than 20 meters. In addition, reservoir pressure should be higher than 30 bars. If the reservoir pressure is lower than 30 bars, permeability should also be low, preferentially under 200 mD. If these conditions deviate, then co-injection might be a better option (Turta & Singhal, 2002).

3 | LITERATURE SURVEY

This chapter will focus on previous laboratory investigations and field scale experiences within WAG and foam processes.

3.1 | EOR ON FIELD SCALE

3.1.1 | MISCIBLE CO₂-FLOODING

CO₂ injection has been the leading EOR process applied in carbonate reservoirs in the United States since the 1980s. In the U.S. 105 active CO₂ floods have been reported and 63 are in carbonates (Manrique, et al., 2010). CO₂ flooding has been successful in both *mature fields*, meaning fields where peak production has been reached (Halliburton, 2015), and waterflooded reservoirs. The utilization of CO₂ in EOR processes has steadily gained popularity in the United States (especially the Permian Basin) due to its abundant availability (Manrique, et al., 2007). Another contributor is the economic viability of CO₂ compared to other recovery alternatives. Figure 3.1.1 shows how oil production increases over the years while miscible CO₂ becomes more prevalent.

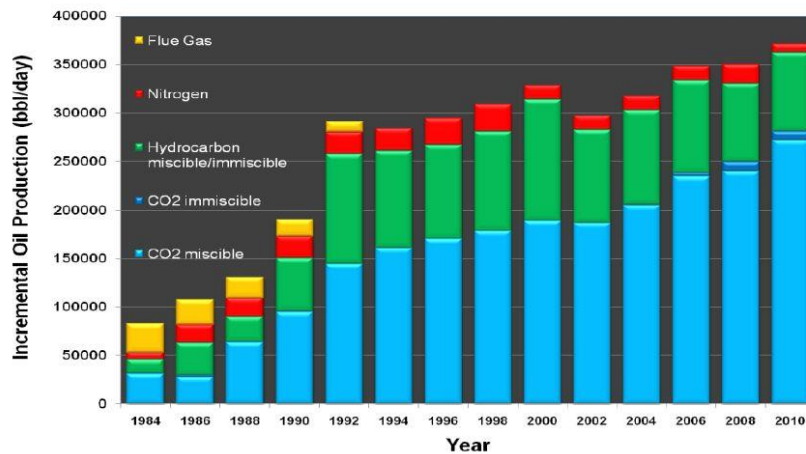


Figure 3.1.1: Increase in oil production over the years by use of gases in enhanced oil recovery in the U.S. (Koottungal, 2010).

The first large scale projects, which used tertiary miscible CO₂-flooding, were conducted in 1972 at two locations in the Permian Basin in West Texas. These were the SACROC field in Scurry and the North Crosset field in Crane and Upton (Melzer, 2012). For the SACROC field, recovery was estimated at 5.75 % of OOIP, which was not considered economic with the oil price at the time (Graue & Blevins, 1978). A number of successful CO₂ EOR field tests were completed in 1972-

1987 (Brock & Bryan, 1989). Among these, some were pure CO₂ miscible floods and others were CO₂-WAG. Incremental recoveries ranged from about 7-22% of OOIP (Brock & Bryan, 1989). The rest were re-cycling of injected CO₂, referred to as immiscible *huff-n’puff*. This recovery method was not as effective as miscible CO₂ or WAG, but was considered a cheap alternative for companies that could not handle large up-front investments.

As long as CO₂ is available it will continue to remain the most sound recovery choice for carbonate reservoirs. Recoveries from immiscible and miscible gas flooding vary between 5–20 % OOIP, with an average of 10 % and 6 % incremental recovery, respectively. Although recovery by gas flooding is economical, 55 % of the oil is left after a miscible gas flood (Manrique, et al., 2007). The large amount of oil left behind is caused by phenomena such as gas channeling, reservoir heterogeneity, dispersion and gravity effects (Johns & Dindoruk, 2013). In more recent years, most fields do not use gas injection alone, but rather water-alternating-gas in their field processes (Manrique, et al., 2007).

3.1.2 | WAG INJECTION

WAG injection has been widely applied since the late 1950s. The first field application was initiated by Mobil in 1957, in the *North Pembian field* in Alberta, Canada. They reported no injectivity abnormalities (Rogers & Grigg, 2001). A study was done on WAG field projects in the period of 1957-1994 (Christensen, et al., 2001), and included a total of 60 cases. The findings are summarized in Figure 3.1.2. Of the projects included in the survey, 79% were miscible WAG treatments, using either hydrocarbon gases or CO₂ (Figure 3.1.2, A). In 38 % of the cases, the reservoir rock was limestone, dolomite or other carbonate types (Figure 3.1.2, B). As much as 88 % of the projects were conducted in onshore fields, as these are mainly in the U.S. (Figure 3.1.2, C). Very few of the reviewed cases were considered unsuccessful, with recoveries ranging between 5-20% (Christensen, et al., 2001).

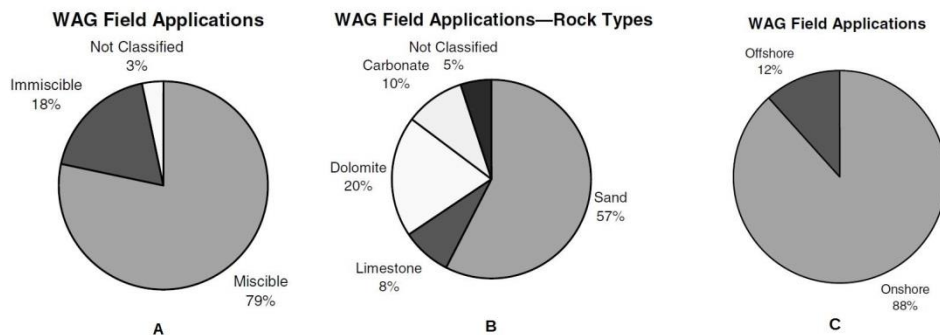


Figure 3.1.2: WAG field applications for (A) number of gas displacement mechanisms, (B) reservoir rock types and (C) number of onshore/offshore fields (Christensen, et al., 2001).

The miscible flood pilot in West Texas, San Andres dolomite is an example of a successful WAG treatment. A recovery of about 50 % by water injection was obtained during the 1970s. WAG was then implemented at a later time with an incremental recovery of 20 %, and a total recovery of around 70 % OOIP for this pilot. This is above average for most fields (Johns & Dindoruk, 2013).

WAG has been applied to several fields on the Norwegian Continental Shelf: Statfjord, Gullfaks, Snorre and Brage are a few examples (Statoil, 2008). Pilots were initiated in 1994 on both Snorre and Brage, which have proven that WAG is both technically and economically successful (Utseth, 1996).

It has been reported that 90 % of domestic tertiary CO₂ field projects in the United States implement WAG (Manrique, et al., 2007). The remaining fields employ gravity drainage, *double displacement*, *gas cycling* and *huff-and-puff* processes. WAG is less effective in tight reservoirs and water-sensitive reservoirs. In such cases, continuous CO₂ injection is more favorable. In West Texas, gas injection is sometimes tapered (TWAG), which means that a large slug of CO₂ is delivered initially and once gas breaks through the production well, it is changed to water-alternating-gas with a ratio that increases incrementally. This variable WAG has since been used by most operators.

The typical potential for WAG injection compared to water injection is at 5-10 % increase in recovery (Manrique, et al., 2007). From experience, WAG renders better recovery than continuous CO₂ injection, but still leaves behind 1/3 to 2/3 of the oil from the waterflooding that preceded it (NETL, 2011).

3.1.3 | FOAM: CO-INJECTION AND SAG

Foam, as an EOR technique, was first applied in the *Siggins field* in Illinois, USA in 1964 (Holm, 1970). Air was used as the injection gas together with “O.K Liquid” as the surfactant. Both co-injection and SAG was tried in this field. During the SAG process, mobility of air was reduced by more than 50 %, stopping the channeling of air towards the producing well. Although an improvement was observed in the injection profile, no incremental oil was produced.

The first use of CO₂-foam was in a SAG process in the *Willmington field* in California, USA in 1984 (Turta & Singhal, 2002). A mixture of CO₂ and N₂ was injected together with an “Alipal CD-128” foaming agent. Eight cycles of gas and surfactant were injected. Results showed that gas

reaching the top high-permeable layer was significantly reduced. The overall goal for this project was achieved as channeling of injected fluids was effectively mitigated.

Five field tests were conducted by ExxonMobil in two reservoirs (Turta & Singhal, 2002), using foam: *McElmo Creek*, Utah and *East Mallet Unit*, Texas. Both co- and SAG injections were tried in these fields as the main problem was related to thief zones. The McElmo Creek field had a wide range of permeabilities (0.01-1000 mD) with 19 layers. During co-injection, excessive reduction in injectivity was experienced. SAG injection performed better as the reduction in CO₂ mobility was significantly larger.

A field application survey done by Sheng (2013) included 60 projects around the world that involved foam. More than half of the fields were applying steam-foam, while the rest implemented CO₂-foam. Steam-foam was mostly used in California and Venezuela, predominantly in sandstone with only a few in carbonates. CO₂ was present in more than 50 % of the projects. From the previously mentioned survey, about 2/3 were SAG injection and 1/3 were co-injection of gas and water.

In the North Sea, the Snorre field underwent foam-assisted water-alternating-gas (FAWAG), This became the largest instance of foam application in the oil industry, and a breakthrough for foam as an EOR method. Results showed a delay in gas breakthrough and that the gas-oil-ratio was reduced significantly compared to the preceding gas cycles without foam. The cost of this recovery process was 1M USD while the value of oil recovery was 25-40M USD with oil prices from 2002 (Arra, et al., 2002).

3.2 | EOR ON CORE SCALE

3.2.1 | WAG

In 1958, Caudle and Dyes proposed that injecting water and gas simultaneously would result in greater recovery compared to waterflooding or a pure miscible flood. This was the first WAG-related experimental work, according to Arra et al. (2002).

Optimization of the CO₂-WAG process has been studied on carbonate cores under reservoir conditions (Amin, et al., 2012). A series of tertiary WAG injections were conducted at various ratios, where 1:1 was considered most efficient. The effect of miscible CO₂-WAG injection on three phase relative permeability has also been investigated for carbonate cores (Duchenne, et al., 2014). With an injection ratio of 1:1, high recovery efficiency was estimated.

3.2.2 | FOAM

Many gas injection projects are facing problems that involve inefficient utilization of gas, poor sweep efficiency and low increased oil recovery. This is mainly caused by channeling, fingering and gravity segregation. These phenomena are often attributed to low viscosity and density of the injected fluid, as well as heterogeneity of the reservoir. By use of *in situ* foam generation, achieved through co-injection of gas and surfactant, or surfactant-alternating-gas, these drawbacks can be mitigated (Farajzadeh, et al., 2012).

In 1958, Bound and Holbrook patented the gas-drive process, using surfactant to improve sweep efficiency by generation of foam (Bound & Holbrook, 1958). Foam mechanisms and flow behavior has been studied extensively since then.

In situ foam propagation was studied for co-injection in carbonate cores (Wassmuth, et al., 2001). In both the foam-generation and foam-propagation regions, water saturation was found to decrease with increasing foam quality. Co-injection by use of CO₂ and surfactant has been found to improve the sweep efficiency in carbonate cores (Zuta & Fjelde, 2010). Simjoo et al. (2012) examined foam stability in the presence of oil for selected commercial surfactants. This displayed a rapid decay at first, followed by stable foam and then a second decay over a relatively long period.

Foam flow and mobility control, for increased sweep efficiency, has been studied in fractured carbonate networks (Fernø, et al., 2014). Co-injection of surfactant and gas reduced mobility of gas more effectively than SAG. With increasing gas fractions, shear-thinning behavior occurred during co-injection. Flooding experiments in heterogeneous and naturally fractured rocks have shown that foam can block gas flow effectively in the fracture pathways of the sample (Yan, et al., 2006), (Ocampo, et al., 2014).

Comparisons have been made between both immiscible and miscible CO₂-foam injections as tertiary recovery methods (Eide, et al., 2012), (Haugen, et al., 2014). Miscible injections were much more efficient than immiscible ones at oil-wet conditions, in fractured carbonates. CO₂-foam performed best after a waterflood as opposed to after a pure CO₂ flood.

SAG injection into carbonate rocks have been studied (Gandomkar, et al., 2012), demonstrating an increase in microscopic sweep efficiency, which is caused by *in situ* foam generation. Gas displacement efficiency has been reported by others to improve during a SAG injection (Albrecht & Marsden, 1970), (Yaghoobi, et al., 1998), (Salehi, et al., 2014).

The success of gas diversion in a SAG process has been shown to depend on steady-state (constant saturation) foam behavior at very high foam quality (Xu. & Rossen, 2003).

Salehi, et al. (2014) showed the importance of optimization of surfactant type and concentration as well as SAG ratio to get optimal recovery results. SAG, with no previous injections, recovered more oil than waterflooding, gas injection and WAG.

The experimental work within this thesis will focus on comparison of co-injection of CO₂ and surfactant, WAG and SAG in fractured carbonate core plugs, as tertiary recovery methods. It is a continued investigation of previous foam experiments in fractured carbonate (Svenningsen, 2011), (Haugen, et al., 2012), (Opdal, 2014), (Steinsbø, et al., 2015) at the Department of Physics and Technology at UiB.

4 | EXPERIMENTAL SETUP AND PROCEDURES

4.1 | FLUID PROPERTIES AND ROCK MATERIAL

This section presents an overview of properties of fluids and rock material that has been used to conduct experiments.

4.1.1 | FLUIDS

Table 4.1 - Fluids used in experimental work. These include brine, gas, alkane and surfactants. Sources from (NIST, 2011).

Fluid	Composition	Density (g/ml)	Viscosity (cP)	Condition
Chalk Brine	Distilled water 50 g/cm ³ - NaCl 50 g/cm ³ - CaCl ₂ · 2H ₂ O 0.05 cm ³ - NaN ₃	1.05	1.09	20 °C
ES Brine (Brine C)	Distilled water 22.80 g/cm ³ - NaCl 2.76 g/cm ³ - MgCl ₂ · 6H ₂ O 5.83 g/cm ³ - CaCl ₂ · 2H ₂ O 0.46 g/cm ³ - KCl	0.94 * ± 0.01	n/a	
CO ₂	> 99.999 % CO ₂	0.662	0.051	35 °C, 90 bar
n-Decane	C ₁₀ H ₂₂ Purity ≥ 99 %	0.730	0.913	20 °C, 1 bar
		0.723	0.818	35 °C, 1 bar
		0.726	0.818	35 °C, 90 bar
Petrostep C-1 (AOS C ₁₄₋₁₆)	Chalk Brine 1.29 wt% Petrostep C1	1.01 * ± 0.01	n/a	
Surfonic L24-22	ES Brine 1 wt% Surfonic L24-22	0.95 * ± 0.01	n/a	

* These values were measured in the lab.

4.1.2 | EDWARD LIMESTONE

All experiments have been done using 1.5" diameter Edward limestone core plugs. These outcrop rocks are a sub-group of carbonate and are considered to be strongly water-wet. Because the limestone has trimodal pore sizes, vugs and microporosity, the porosity and permeability distribution becomes quite heterogeneous (Eide, et al., 2012). This is illustrated by Figure 4.1.2 (A). Porosities and permeabilities that were prepared for this thesis were in the range 21-26 % and 13–30 mD, respectively. Porosities and permeabilities from Haugen et al. (2014) were in the range $\phi = 19\text{-}26\%$ and $K = 5\text{-}32$ mD, respectively.

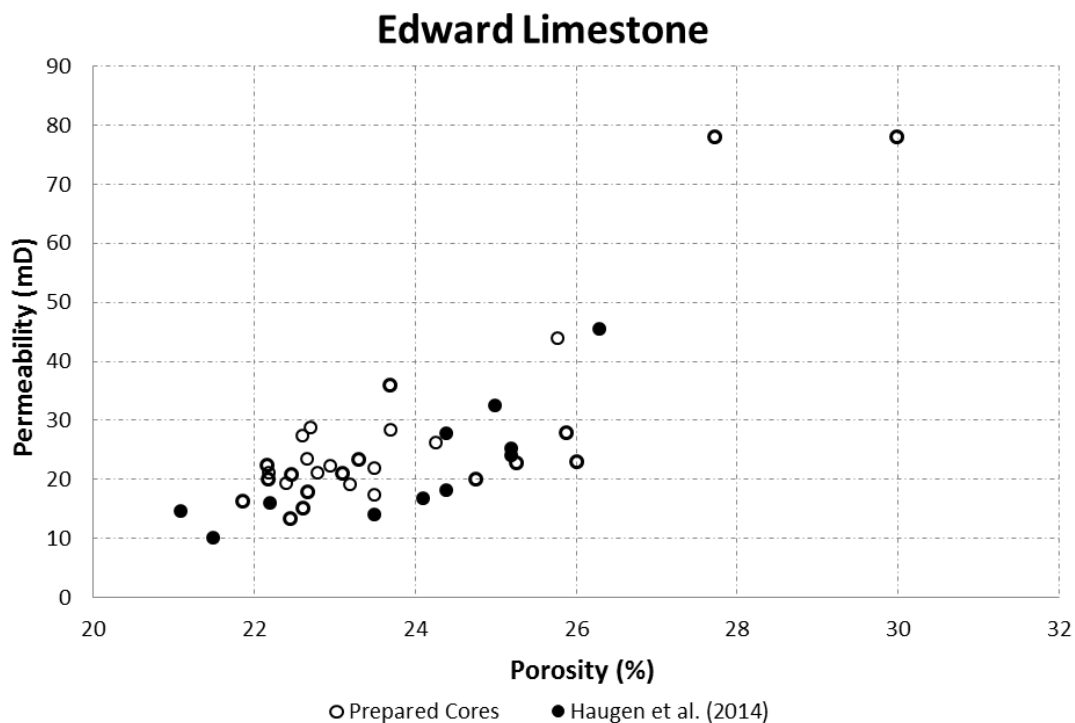


Figure 4.1.2 (A): Permeability vs. porosity for a set of prepared Edward limestones. These are matched with data are taken from Haugen et al. (2014).

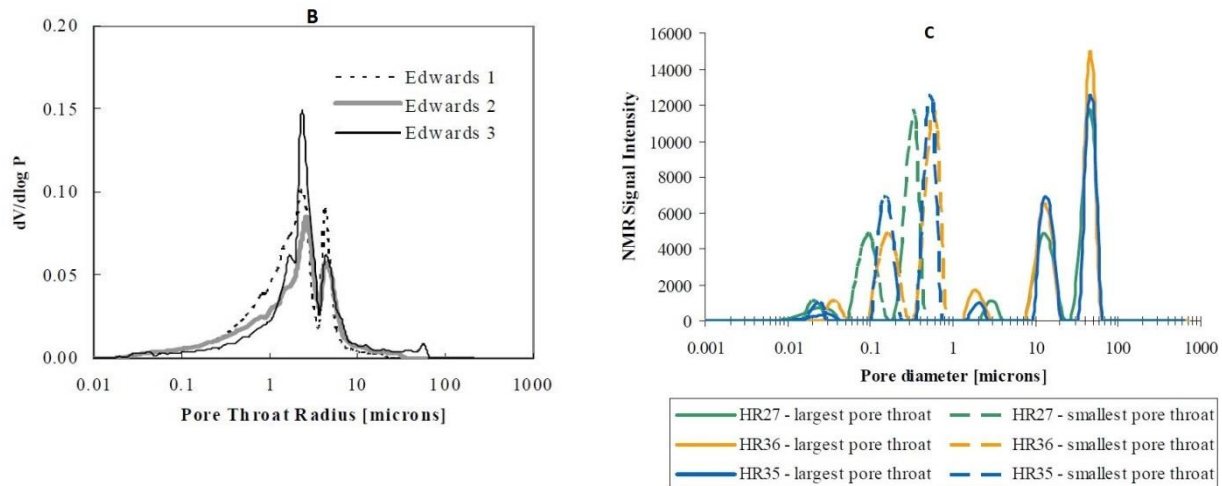


Figure 4.1.2 (B): Pore throat distribution of three Edwards limestone samples (Tipura, 2008). (C): Pore size distribution by correlation of NMR T2 relaxation time distribution to pore diameter. Dashed curves show pore diameter distribution for three core samples when relaxivity constant is defined by small pore throat (short T2). The solid line presents the same cores scaled with largest pore throats (long T2). (Tipura, 2008). Results were achieved by mercury injection into pores.

In Figure 4.1.2 (B) and (C), data from pore throat distribution and pore diameter distribution, respectively, in limestone samples are presented by Tipura (2008). Figure 4.1.2 (C), illustrates the trimodal pore size distributions found in limestone (Eide, 2014). Based on thin sections from a limestone core, pore radii and diameter distributions, porosity and permeability measurements, the Edwards limestone was characterized as a highly heterogeneous, bioclastic grain stone Tipura (2008). Data were obtained from mercury injection methods and MRI measurements.

4.1.3 | PREPARATION AND FRACTURING OF CORES

Sample preparation methods have great influence on the generated data; therefore it is vitally important to document detailed procedures.

The coreflooding experiments are a representation of the field. Therefore, the core must be saturated with oil, and porosity and absolute permeability must be measured. The cores are then cut in half to simulate the presence of a fracture. This section will explain further details.

Limestone cores were cut to a certain length using a circular saw with a diamond coated blade. These were then washed to remove smaller particles left on the sample. Next, the cores were set to dry in room temperature for 24 hours before being placed in a heating cabinet of 60 °C for 2-5 days. Once the cores are dry, they were taken out and weighed. Accurate length and diameter were measured with a caliper.

Porosity Measurement: By saturating the cores under vacuum, weight difference before and after saturation could be used to calculate porosity. The cores were placed inside a glass bulb, which is connected to another spherical glass bulb on top, separated by a valve. This contains a fluid that was used to saturate the core. Both glass bulbs were separately connected to a condensing chamber that was connected to a vacuum pump. If brine is the saturating fluid, both the sample and the brine would be vacuumed, but if decane is the saturating fluid, only the sample would be vacuumed.

The condensing chamber was cooled using liquid nitrogen so that any brine sucked in by the pump became trapped there. The pressure transducer indicates (in *torr*) how close the system is to vacuum. About 200 *mtorr* was sufficient, and the valve underneath the fluid was opened to let the fluid down to the sample. The fluid would then spontaneously imbibe into the core. The setup is displayed in Figure 4.1.3.

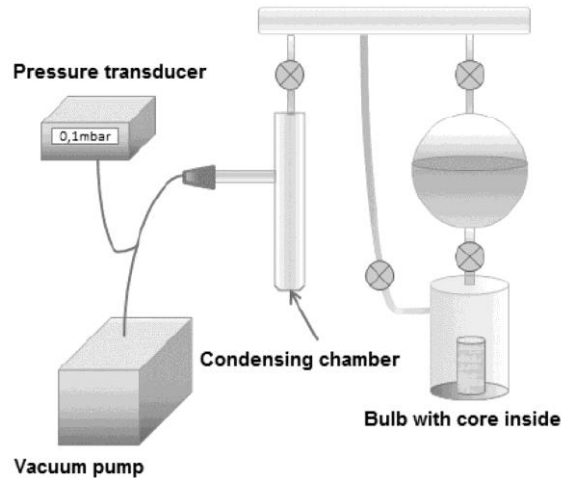


Figure 4.1.3: Experimental setup used for porosity measurements (Opdal, 2014).

After the core was saturated, it was weighed again. Porosity (ϕ) was then calculated using the following equation:

$$\phi = \frac{W_s - W_d}{\rho V_b} \quad 4.1.1$$

where W_s = weight of saturated sample, W_d = weight of dry sample, ρ = density of the fluid and V_b = bulk volume of the sample.

Permeability Measurement: With constant flow of brine or decane through the core, permeability could be calculated by Darcy's law. The core was mounted in a coreholder and a confining pressure was applied. A pump, controlled by a computer, was connected to the

coreholder so that fluid could be pumped through the core. Differential pressure across the core was recorded by a pressure transducer. Figure 4.1.4 gives an overview of the setup.

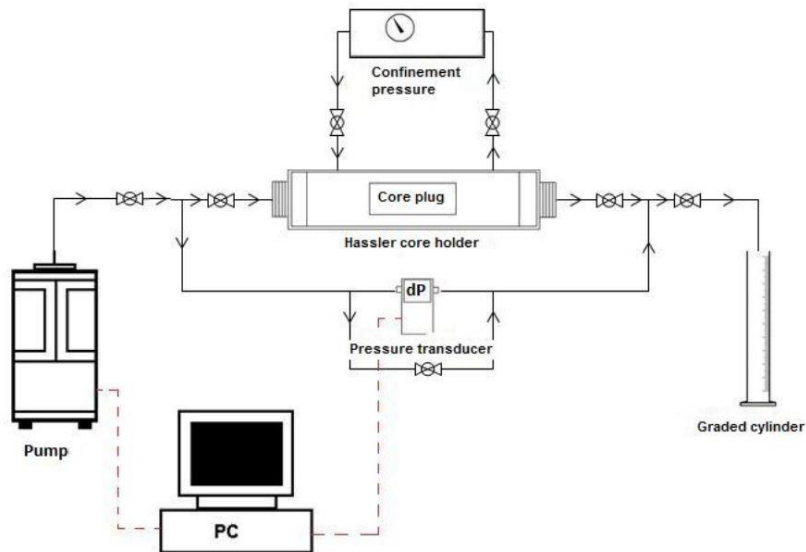


Figure 4.1.4: Illustration of the setup used for permeability measurements (Opdal, 2014).

Darcy's law is given by:

$$Q = \frac{K \cdot A}{\mu} \cdot \frac{\Delta P}{L} \quad 4.1.2$$

where Q = flow rate (cm^3/s), K = absolute permeability (Darcy), A = cross section of core (cm^2), μ = viscosity of fluid (cP), ΔP = pressure difference across core (atm) and L = length of core (cm).

A few different flow rates (Q) were used to induce different pressures (ΔP). These were then plotted as Q vs. ΔP , using Equation 4.1.2, and a trend line could be fit through the data points.

Some cores were initially saturated with brine and then drained until irreducible water saturation (S_{wi}), using n-Decane. Drainage was conducted with a constant pressure drop equal to 2 bar/cm to avoid capillary end effects and to reach sufficiently low saturations. 5 pore volumes of n-Decane were injected in both directions of the core to achieve uniform saturation distribution.

Fracturing: In core and at field scale, injected fluids have a higher flow velocity in fractures than in the matrix (Haugen, et al., 2014). The cores are fractured to investigate how well foam reduces mobility and divert the injected fluids from fractures and into the matrix blocks. The cores were split in two longitudinally. It was necessary to weigh the cores again because the saw

removed a small portion of the volume. The weight difference before and after cutting was used to find a new fractured pore volume (PV_{frac}):

$$PV_{frac} = PV \cdot \frac{W_{frac}}{W_s} \quad 4.1.3$$

where PV is the initial pore volume, W_{frac} is the weight of the core after fracturing and W_s is the initial weight of the core.

Core Assembly (With Spacer): All fractured cores that were drained to irreducible water saturation contained a spacer. Figure 4.1.5 illustrates the final process before the core can be placed in the coreholder, and an experiment can start. (A)-(B): The two halves of the core were separated by a plastic spacer, of 1 mm thickness, to create a fracture space. (C)-(D): Aluminum was wrapped around the core to isolate it so that injected CO_2 would not come in contact with the sleeve inside the coreholder. Since CO_2 is acidic in contact with water, the rubber sleeve will dissolve without the aluminum foil. (E): The inlet and outlet of the coreholder were attached to the core using aluminum tape. It was important to keep the seal tight so that no gas escaped.

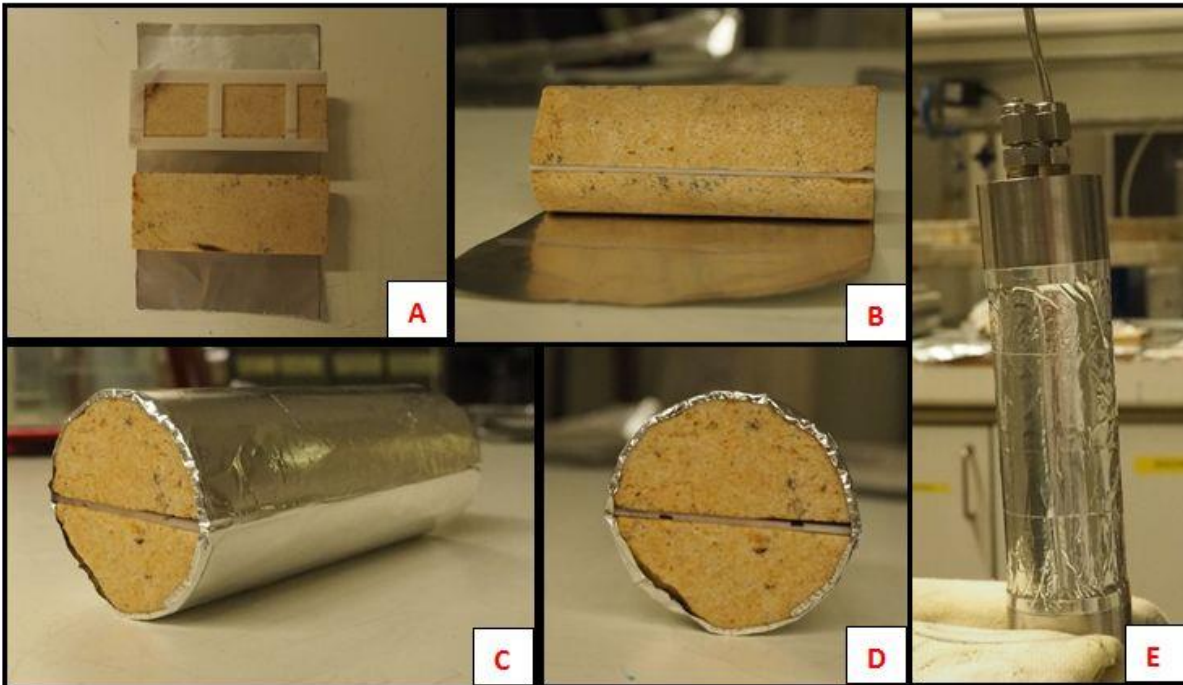


Figure 4.1.5: (A)-(B) Spacer is placed between the core pieces. (C)-(D) Aluminum foil is used to wrap the core and keep the pieces in place. (E) Aluminum tape is used to attach the core to the inlet and outlet before placing it in the coreholder.

Core Assembly (No Spacer): All cores that were saturated with 100 % n-Decane contained no spacer. These cores were also an alignment of two stacked cores. Figure 4.1.6 shows a procedure of how the cores were assembled before each experiment. (A) After the cores had been cut by a circular diamond coated saw, (B)-(C) they were filed to make the surfaces in the fracture rougher. This was done because smooth surfaces in a fracture are not realistic. Next, (D)-(F) two cores were stacked as one core, with one fracture aligned vertically and one fracture aligned horizontally to achieve a non-uniform fracture system.

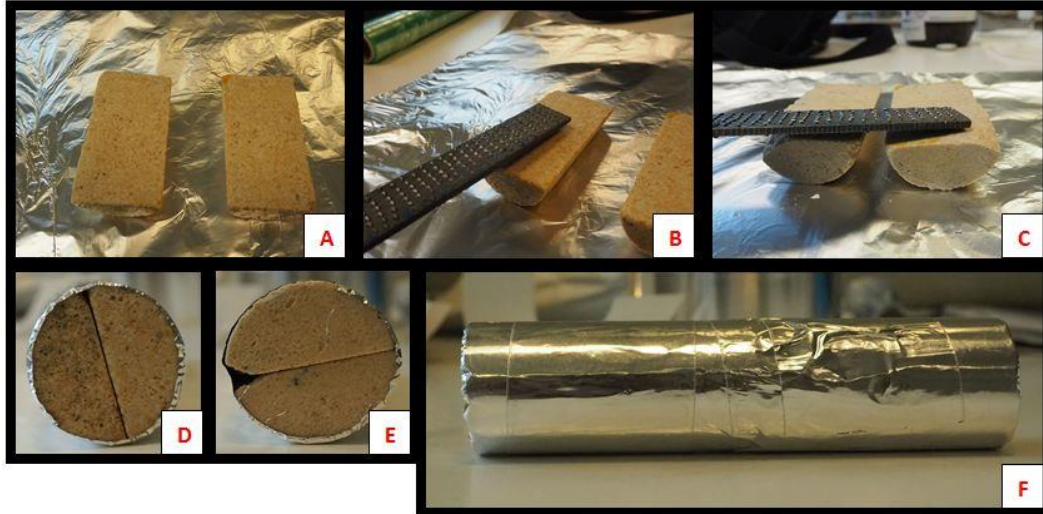


Figure 4.1.6: (A) the core has been separated longitudinally. (B)-(C) fracture surfaces of the core are filed down to make them rougher. (D)-(E) two cores are stacked with one fracture aligned vertically, and one fracture aligned horizontally. (F) the two cores are completely wrapped in aluminum foil.

4.2 | SETUP AND PROCEDURES

This section provides a detailed overview of equipment, experimental design and procedures used for co-injection, WAG and SAG in carbonate core plugs. All injection methods were performed as a tertiary recovery scheme.

4.2.1 | SETUP

The setup shown in figure 4.2.1 is from the laboratory at the Department of Physics and Technology at UiB.

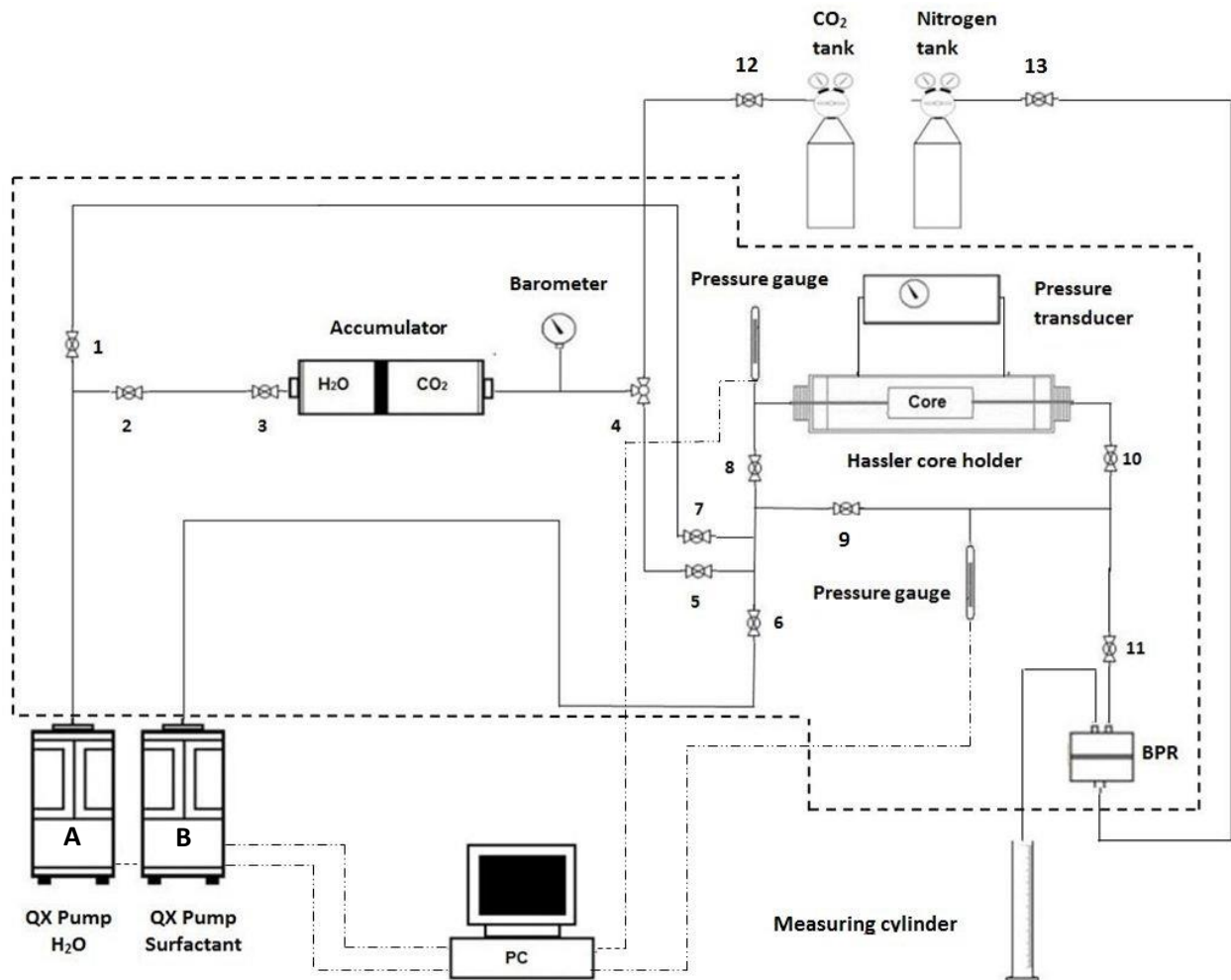


Figure 4.2.1: Illustration apparatus used in the experimental setup. The apparatus inside the heating cabinet is marked by the strong dotted lines. Modified from Opdal (2014).

4.2.2 | EQUIPMENT

- *Heating cabinet* to conduct the experiment in.
- *Accumulator* for pressurization of CO₂ by water.
- *Quizix QX-1500 pump (A)* for injecting water into the accumulator and pressurizing CO₂.
- *Quizix QX-1500 pump (B)* for injecting surfactant or decane.
- *Manometer* for measurement of pressure in the accumulator.
- *Hassler core holder*
- 2 x *ESI 250* pressure gauges for measurement of differential pressure between inlet and outlet of the core.
- *Pressure transducer* for application of confinement pressure to the core holder by injection of pump oil into the sleeve.
- *CO₂ tank* to supply the accumulator.
- *Back pressure regulator (BPR)*, pressurized by nitrogen, to maintain a high pressure in the system.
- *Swagelock tubings, fittings and valves*.
- *Computer* to control Quizix pumps and for pressure readings.

4.2.3 | PROCEDURES

This section will refer to the experimental setup in Figure 4.2.1.

CO₂ was pressurized to approximately 92 bar in a heating cabinet of 35 °C to get the CO₂ to a supercritical state. Pressurization was done by injection of distilled water at the bottom of the accumulator. Once the desired pressure was achieved, the quizix pump was set to constant pressure of 92 bar to stabilize the supercritical CO₂ for 24-48 hours. A syringe was used to fill the pressure gauges with distilled water. The fluid in the pump was exchanged with decane, which was injected into the tubings. The inlet of the core holder had to be flooded with decane before mounting the core inside the core holder. Fractured cores had to be mounted with the fracture aligned vertically to eliminate gravity effects during the experiments.

When the experiment is conducted at high pressures, the fluid becomes compressed. This means that the amount of injected fluid (at high pressure) does not match the produced fluid at ambient pressure, downstream of the BPR. To account for this, a pressurization factor (F_p) is estimated. Decane was injected through the core and bypass, using pump B. First, valve 6 and 9 were open while all other valves were closed. Then decane was pressurized to 90 bar through the bypass, until valve 11. The amount of decane used to pressurize the bypass is denoted $V_{o,bypass}$. Second, valve 8 and 10 were opened while valve 9 was closed. The system was then

pressurized to 90 bar again. A confinement pressure of 110 bar was applied to the core, mounted with a pressure transducer. The amount of decane used to pressurize the coreholder is denoted as $V_{o,core}$. Since $V_{o,bypass}$ is part of $V_{o,core}$, this must be subtracted to get the final pressurized volume ($V_{o,system}$):

$$V_{o,system} = V_{o,core} - V_{o,bypass} \quad 4.2.1$$

The volumes between valve 8 to the core and valve 10 to the core, are referred to as dead volumes ($V_{o,dead}$). These contain oil before the experiment starts and must be excluded from the final production volume.

The spacer between the two core pieces, in a fractured core, contains a volume (V_{frac}) which will be filled with decane, and should also be excluded from production.

The pressurization factor (F_p) can be calculated as:

$$F_p = \frac{S_o + V_{o,dead} + V_{frac}}{S_o + V_{o,dead} + V_{frac} + V_{o,system}} \quad 4.2.1$$

where S_o is the volume of oil which the core was saturated with, initially. The pressurization factor is multiplied with the produced volume. Generally, F_p is calculated to 0.95 for these experiments.

Waterflooding:

The fluid in pump B was changed from decane to brine. This was then injected through the bypass, displacing the oil, to prepare for a waterflooding. By opening valve 13, nitrogen was let into the BPR and pressurized to around 90 bar. Valve 9 was then closed and valves 8 and 10 were opened. Starting time of the experiment was noted at the moment brine was let through valve 8.

WAG and Foam:

Both WAG and foam floodings were conducted using CO_2 at miscible conditions. In these experiments, the core holder was mounted vertically and cores contained no spacer. After a completed waterflood, a sequence of gas and water slugs was injected into the core. A WAG ratio of 1:1 was used for all experiments. The rate varied in a few different experiments: 5, 10 and 25 ml/h, but was kept constant throughout each one. CO_2 was injected by use of pump A,

while brine was injected using pump B. First, a gasflooding was started by closing valve 6 and opening valve 5. When a certain fraction of the pore volume (0.15 PV) had been injected, valve 6 was closed and valve 5 was opened. Then the same amount of brine was injected before switching back to CO₂, and so on. The injection of alternating slugs continued until oil production from the core stopped.

Production from the core continued by use of alternating slugs of surfactant (pump B) and gas (pump A) with a ratio of 1:1. SAG was accomplished operationally in the same way as the WAG.

Co-injection experiments were completed in co-operation with fellow master student, Henriette Horjen. Co-injection was also conducted after a waterflooding. Surfactant and brine were injected simultaneously with both valves 5 and 6 open. A foam quality of 80 % was used for all co-injections. Petrostep C-1 was used as the surfactant together with chalk brine. Injection rate was 5 ml/h in total to keep the velocity of the displacement front low. The separate injection rates were 4 ml/h for CO₂ and 1 ml/h for the surfactant.

5 | RESULTS AND DISCUSSION

Results from experimental work will be presented and discussed in this chapter. A total of 27 1.5” Edward limestone cores were prepared. Of the 13 experiments conducted, 6 were tertiary CO₂/co-injections. These were carried out together with fellow master student, Henriette Horjen. The other 7 were tertiary WAG/SAG injections.

5.1 | CORE PROPERTIES

This section lists all cores with their respective core properties (Table 5.1).

Permeability was plotted against porosity in an earlier section (see Figure 4.1.2). This provides a good illustration of the wide range of properties that exist for the Edwards limestone rock, provided in Table 5.1. These data suggest that the Edward limestone is relatively heterogeneous, and one reason is that this rock contains macropores (5-10 μm), transitional pores (0.01-0.02 μm) and micropores (0.8-2 nm). Hence, the typical pore size distribution of an Edward limestone is trimodal (Dullien, 1979). Another reason is that pore spaces mainly consist of moldic pores, and have interparticle porosity that has been reduced by recrystallization of calcite (Haugen, et al., 2014). Vugs in the limestone can provide more permeable paths for fluid to flow through (Eide, 2014), causing permeability measurements to vary.

A variety of core assemblies have been prepared for experiments: *whole*, *fractured* and *stacked* cores (see Table 5.1). *Whole* cores have been used as a reference to observe differences in oil production and differential pressure from fractured cores. It is more likely that a limestone reservoir contains fractures; therefore experiments are mainly conducted on *fractured* cores. By *stacking* cores, a larger system can be created, which might provide results that are more representative of the field. Shorter cores mean that there are higher risks of having capillary end effects distort experimental data by delaying production of fluids. Additionally, the smaller the sample, the faster the breakthrough of fluids will occur (Chou, 1991).

Table 5.1 – Properties of all the Edward limestone core plugs that were prepared. The cores are either whole, fractured or stacked.

Core	State	Length (cm)	Dia. (cm)	PV/PV _{frac} (ml)	Porosity (%)	K/K _{frac} (mD)	S _o
#2	Whole	7.10	3.75	18.6	23.7	28.32	0.77
#3	Whole	7.00	3.75	17.3	22.4	19.31	0.76
#4	Frac.	7.20	3.75	17.4	23.5	17.30	0.76
#5	Frac.	7.20	3.80	18.6	22.7	28.60	1.00
#6	Frac.	7.10	3.75	18.0	23.2	19.10	1.00
#7	Frac.	6.70	3.75	16.8	22.7	23.40	1.00
#8	Frac.	6.70	3.80	16.9	22.2	21.10	1.00
#9	Frac.	6.80	3.80	18.1	23.5	21.85	0.72
#10	Frac.	6.70	3.75	16.7	24.3	26.21	0.79
#11	Frac.	7.10	3.80	17.7	22.6	27.24	0.83
#12	Frac.	7.20	3.75	16.8	22.8	21.01	0.70
#13	Frac.	9.00	3.80	23.4	22.9	22.16	0.76
#14	Frac.	9.35	3.80	27.3	25.8	43.81	0.75
L5	Whole	6.80	3.85	18.4	23.0	26.00	1.00
L6	Whole	6.70	3.80	15.8	21.0	23.10	1.00
LS2	Whole	10.0	3.75	25.0	22.6	15.21	1.00
LS3	Whole	10.0	3.75	24.5	22.2	20.01	1.00
LS4	Frac.	9.90	3.75	29.9	30.0	78.00	1.00
LS6	Frac.	7.60	3.85	16.2	22.4	13.44	1.00
LS8	--	7.45	3.80	--	23.7	36.02	1.00
LS9	Frac.	7.60	3.85	22.2	22.7	78.00	1.00
LS10	--	7.10	3.80	--	22.5	22.17	1.00
LS14	--	7.20	3.80	--	23.3	23.48	1.00
ST1	Stacked	14.60	3.80	31.8	20.5	729.67	1.00
ST2	Stacked	14.95	3.85	37.5	23.7	112.91	1.00
ST3	Stacked	14.95	3.90	41.7	25.9	676.25	1.00
ST4	Stacked	14.95	3.80	33.4	21.9	--	1.00

Stacked cores are an alignment of two fractured cores that have been assigned average porosity and permeability values. Length and PV_{frac} are also added up.

5.2 | INJECTION METHODS

The objective of the experimental work in this chapter is to test the performance of different injection strategies in limestone cores, with emphasis on those that are fractured. Methods, shown in Table 5.2, will then be compared and contrasted to each other to evaluate its prospects and drawbacks. All tertiary methods involve the use of supercritical CO₂ above minimum miscibility pressure to achieve first-contact miscibility between CO₂ and n-Decane. Fosse (2012) simulated MMP at 37.8 °C to 77.4 bar, which means that all experiments in this thesis, at 35 °C and 89-95 bar, are well above the MMP.

A pure CO₂ injection is expected to perform well in terms of microscopic sweep efficiency, compared to a waterflood (Kokal & Al-Kaabi, 2010). However, this method has been proven to have disadvantages for heterogeneous and fractured reservoirs as the CO₂ is likely to channel through fracture pathways because of its low viscosity (Uleberg & Høier, 2002). Therefore, brine was injected together with CO₂ in a WAG process to test if the mobility of CO₂ would be reduced, and macroscopic sweep improved.

WAG injection is also a cost-efficient way to achieve similar or better ultimate recovery as pure CO₂ injection while cutting back on CO₂ utilization. Since brine has a limited effect on CO₂ mobility reduction, experiments were conducted using foam. Several field pilots have proven that replacing brine with surfactant, in a co-injection or SAG process, reduces mobility of CO₂ more effectively than WAG (Ocampo, et al., 2014). Most experiments listed in Table 5.2 are a combination of two tertiary injection methods: CO₂ and co-injection or WAG and SAG.

Table 5.2 – Experimental conditions for each core is summarized in this table. All cores were waterflooded before implementing tertiary recovery methods. Cores #2-#14 were flooded horizontally, while the rest were flooded vertically.

Core	State	EOR method	P (bar)	T(°C)	Rate (ml/h)	Injection direction
<i>EOR by miscible CO₂ and co-injection</i>						<i>Horizontal</i>
#2	Whole	Pure CO ₂	92	35	5	
#3	Whole	CO ₂ -foam	91	35	5	
#4	Frac.	CO ₂ -foam	93	35	5	
#10	Frac.	Pure CO ₂	95	35	5	
#12	Frac.	Pure CO ₂ + CO ₂ -foam	92	35	5	
#14	Frac.	CO ₂ -foam	95	35	5	
<i>EOR by miscible WAG and SAG</i>						<i>Vertical</i>
L5	Whole	WAG+SAG	92	35	5	Top-bot.
L6	Whole	WAG+SAG	92	35	5	Top-bot.
LS2	Whole	WAG+SAG	89	35	25	Top-bot.
LS3	Whole	WAG+SAG	90	35	10	Top-bot.
ST1	Stacked	WAG+SAG	89	35	10	Top-bot.
ST2	Stacked	WAG+SAG	90	35	10	Bot.-top
ST3	Stacked	SAG	95	35	10	Bot.-top

A schematic overview of the flooding sequences is shown in Figure 5.2.1. Four branches of experiments have been conducted: WF + CO₂ + Co-injection, WF + Co-injection, WF + WAG + WAG and, WF + SAG.

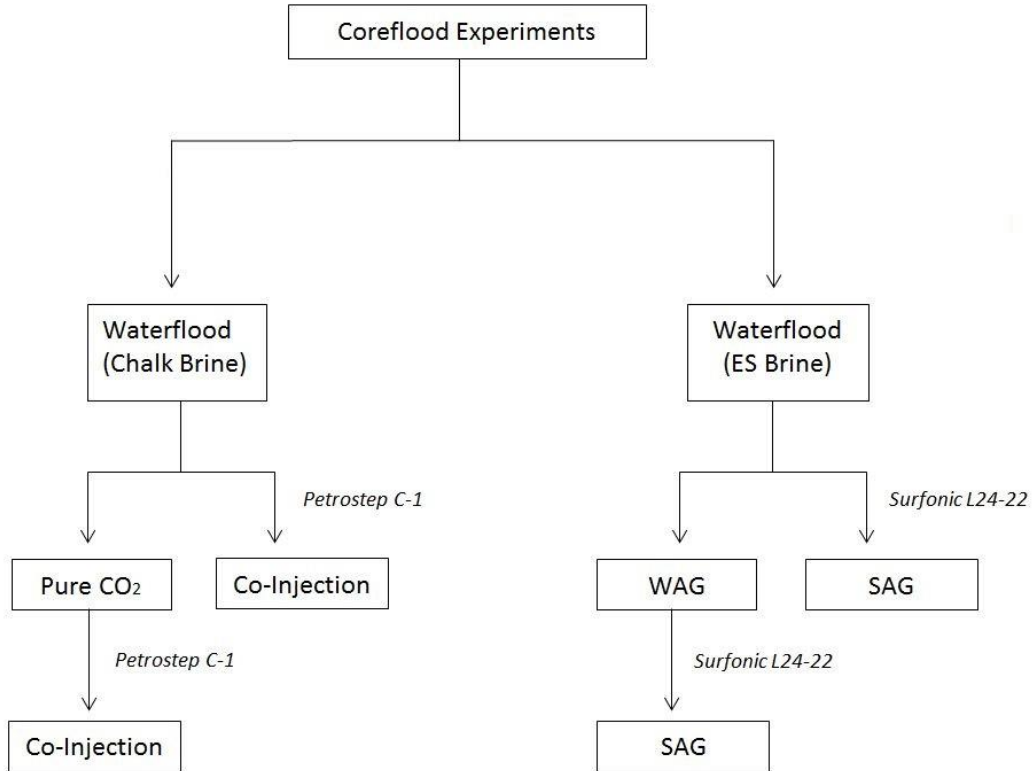


Figure 5.2.1: Overview of the flooding sequence in the different coreflood experiments. These branch out into the two main groups: CO₂/co-injection and WAG/SAG.

A summary of parameters that differ between the two types of experiments can be seen in Table 5.3. A spacer has initially been used in co-injection experiments to see how foam performs in high permeable fractures with very low pressure drops. In other experiments, utilization of spacers were abandoned because large fracture volumes may not be representative of the field, as overburden pressure is likely to severely compact it. In co-injection experiments, cores were flooded to irreducible water saturations, since this can be found in most water-wet fields. For WAG/SAG, initial saturations were kept at 100 % oil saturated to be able to better observe production trends and evaluate the performance of these injection strategies.

Surfactants have been changed from Petrostep C-1, in co-injections, to Surfonic L24-L22 as well as an increase of injection rates from 5 to 10 ml/h. Although 5 ml/h was initially selected because the velocity of the displacement front would be more stable, it was changed to 10 ml/h in the later experiments to achieve experimental results faster. Co-injections were accomplished horizontally, because gravity needed not be accounted for. As for WAG and SAG, a larger coreholder was needed to fit stacked cores, and this would only fit in the heating cabinet if mounted vertically. Hence, gravity became a factor that has to be discussed for the results that have been obtained during these experiments.

Table 5.3 – Parametrical differences summarized for experiments.

Experiments Type	Injection Rate	Spacer	Stacked	Initial Saturation	Inj. Direction	Surfactant
CO ₂ /co-injection	5	Yes	No	Irreducible water	Horiz.	AOS C ₁₄₋₁₆ (anionic)
WAG/SAG	10 & 25	No	Yes	100% oil	Vertical	Surfonic L24-22 (non-ionic)

5.3 | TERTIARY WAG AND SAG INJECTION WITH SUPERCRITICAL CO₂

Fluids were injected alternately in these experiments. Surfonic L24-22 (in Table 4.1), a non-ionic surfactant, was used for SAG injections. A fluid injection ratio of 1:1, meaning equal volumes of injected fluids, and slug sizes of 0.15 pore volumes were applied in both WAG and SAG. Injection ratio for SAG was chosen based on the experiments done by Salehi et al. (2014), where 1:1 was shown to be optimal. WAG injection ratio has also been proven to be optimal at 1:1, as concluded by Amin et al. (2012). In addition, 1:1 is commonly used in most fields that apply WAG (Amin, et al., 2012).

A waterflooding, WAG and SAG has been completed in the same core for both whole and fractured ones. The WAG process is a popular injection strategy in the field, and has almost always been applied as a tertiary recovery method (Aarra, et al., 2002). For this reason, it is conducted in these experiments before completing a SAG injection. One tertiary SAG experiment was carried out to directly compare with WAG. All fractured cores in this section consisted of two stacked cores (see Figure 4.1.6). All experiments were run at 90-95 bars with 35 °C, making CO₂ first-contact miscible with the oil (n-decane). Different injection rates of 5, 10 and 25 ml/h were used (Table 5.2), with no spacer volume in the fractures. Confining pressures of 140 bars were applied.

5.3.1 | BASELINE: WAG AND SAG COMBINED IN WHOLE CORES

Fluids are injected from the top of the vertically positioned core to the bottom. Two different injection rates have been used: 25 ml/h for core LS2 and 10 ml/h for LS3. This was to see how injection rates would affect differential pressure and ultimate recovery. Results of these experiments are plotted in Figure 5.3.1. The last point of the WAG in LS2 has been extrapolated to match the last point of the WAG in LS3.

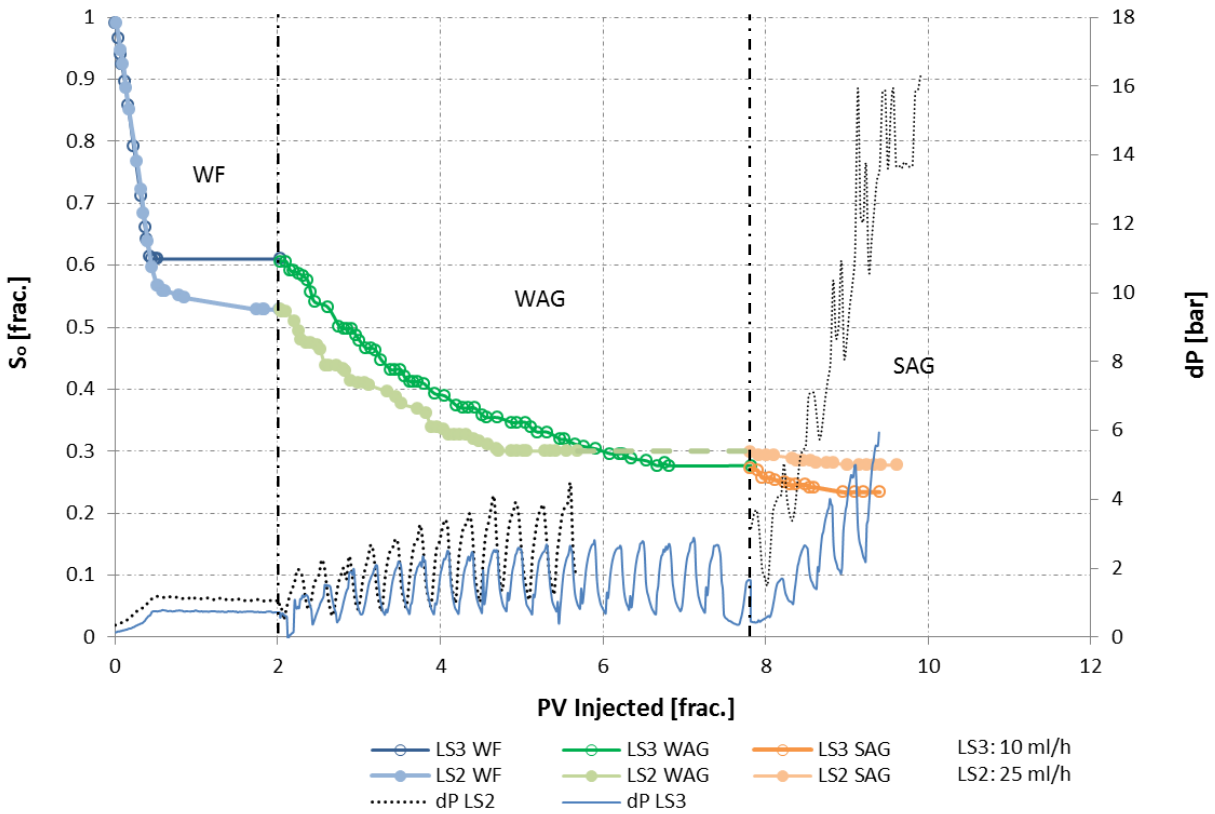


Figure 5.3.1 (a): Waterflood, WAG and SAG have been performed on two whole cores (LS2 and LS3). Residual oil saturation vs. pore volumes injected has been plotted; with their respective differential pressures shown beneath.

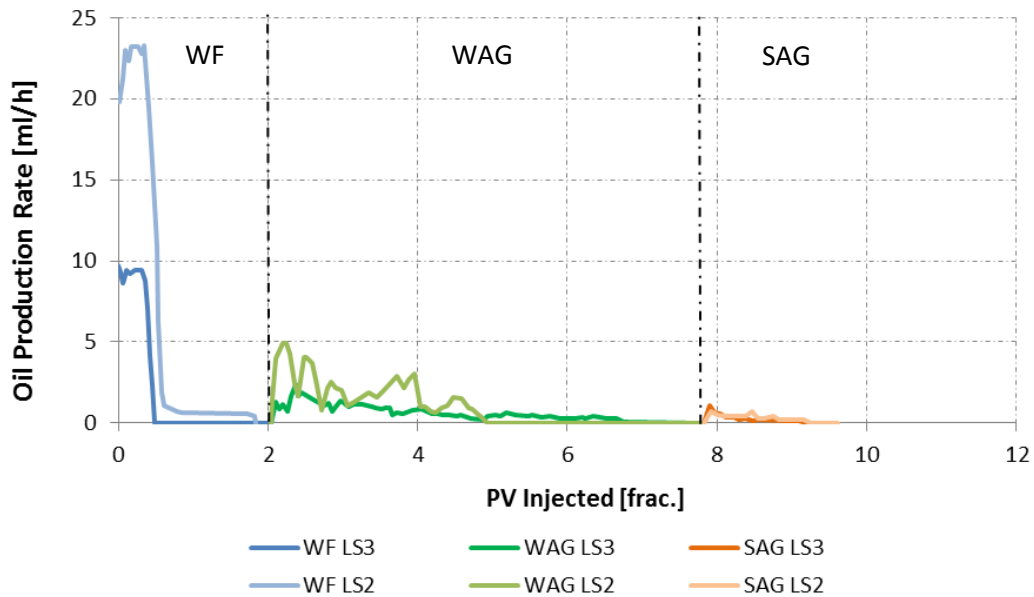


Figure 5.3.1 (b): Oil production rate (ml/h) vs. PV injected (frac.) for waterflood, WAG and SAG in cores LS2 and LS3.

Table 5.4 – Production data for cores from figure 5.2.1. Oil saturation and recovery factor after each method is listed as well as total recovery.

Core	$S_{o,initial}$ [frac.]	$S_{o,WF}$ [frac.]	$R_{F,WF}$ [%OOIP]	$S_{o,WAG}$ [frac.]	$R_{F,WAG}$ [%OOIP]	$S_{o,SAG}$ [frac.]	$R_{F,SAG}$ [%OOIP]	$R_{F,total}$ [%OOIP]
LS2	1.00	0.53	47.1	0.30	22.8	0.28	2.3	72.2
LS3	1.00	0.61	39.4	0.28	33.4	0.23	4.3	76.6

Because the Edwards limestone is strongly water-wet, a sharp decrease in oil saturation can be seen during waterflooding in Figure 5.3.1 (a)-(b) as water spontaneously imbibes into the cores and produces oil from the smaller pores. This means that most of the residual oil is trapped in the center of the small pores. A higher capillary entry pressure is required to mobilize these oil droplet compared to the larger pores, with lower water saturation and lower capillary pressure (Chatzis, 1983). As a result, LS2 and LS3 end up with recoveries of 47.1% and 39.4% of OOIP during waterflooding, respectively. WAG further increases recovery by 22.8% and 33.4% of OOIP for LS2 and LS3, respectively.

From these results (Table 5.4) it is apparent that the injection rate of 25 ml/h in core LS2 produced oil more efficiently during WAG as it takes less time for the production curve to even out. However, a lower recovery than core LS3 can be observed, which has 10 ml/h. The higher WAG injection rate did not lead to a higher ultimate recovery in this case, although a larger differential pressure can be observed, as flow rate and pressure are directly proportional. It is a possibility that WAG mostly produces residual oil from the large pores, while oil in the small pores, shielded by water, is held back by stronger capillary forces. This effect would be higher for LS2 since the water saturation is higher after waterflood.

Previous experimental observations of flow rate and core length effects on WAG have been done (Rogers & Grigg, 2001). These imply that a decrease in recovery with increased flow rate indicates that dispersive bypassing or fingering is dominant. If the rate is lowered the velocity of the WAG front may be more stable and have better sweep efficiency since occurrence bypassing is lowered, leaving more time for diffusive mixing between CO₂ and oil. The pressure difference between the two cores is not as significant as for the SAG process.

Continuing with a SAG, viscous forces are increased (since pressure increases), but it does not seem to have a significant effect on displacement efficiency in the core since very limited oil is recovered. There could be a high degree of water-shielding, leading to a low potential for the successive SAG flood. Laboratory SAG floods often show a late peak in apparent viscosity reduction. An example is found in experiments conducted by Ma et al. (2013) where the maximum pressure drop occurs significantly later than the gas breakthrough. So a slow

generation of strong foam is a considerable option as to why the SAG injection, in both cores LS2 and L3, shows a general lack of effectiveness.

The pressure difference is much larger for a SAG process than for WAG in core LS2. A rapid pressure rise can be observed when CO₂ becomes more discontinuous as surfactant saturation increases within the core. The pressure increase could also become slightly delayed if surfactant adsorbs to the limestone surface within the pore spaces. The increased flow rate in LS2 shows a higher degree of foam generation. Because this foam generation happens quickly due to a high flow rate, a large amount of lamella creation as well as rupturing may occur as it could take time for the foam to stabilize. LS3 has a more linear and steady increase in pressure, which could indicate stabilized foam and might also explain why recovery is slightly higher in this case.

Capillary end effects can lead to pressure drops that maintain wet foam conditions at the core outlet, while parts of the core, closer to the inlet, contain dry conditions (Kapetas, et al., 2014). The macroscopic sweep efficiency seems to remain the same as during the WAG, but a lowering of interfacial tension between injection fluids and the oil can lead to slight improvements in microscopic sweep in LS2 and LS3 during SAG (Farajzadeh, et al., 2012). Since reduction of residual oil saturation in cores LS2 and LS3 are similar, uncertainties in production readings could mean that their performances are virtually identical.

5.3.2 | WAG AND SAG COMBINED IN FRACTURED CORES

Fluids are injected from the top of vertical core ST1 to the bottom. In core ST2, direction is reversed: fluids are injected from the bottom to the top. The rate for both cores is 10 ml/h (Table 5.2). Results are plotted in Figure 5.3.2 (a), showing a clear difference in recovery during WAG, depending on direction of injected fluids. The measured fracture permeability before each of the experiments showed that ST1 had $K_{frac} = 729$ mD, while ST2 had $K_{frac} = 112$ mD (Table 5.1). When a core is re-assembled and stacked together with another core, the fractures can have slightly different volumes and orientations. Some cores might have small pieces missing from when it was cut by the circular saw. This permeability contrast can also reflect the degree of capillary continuity between the stacked core plugs. So it is natural that permeability can vary significantly, although changes in parameters are small.

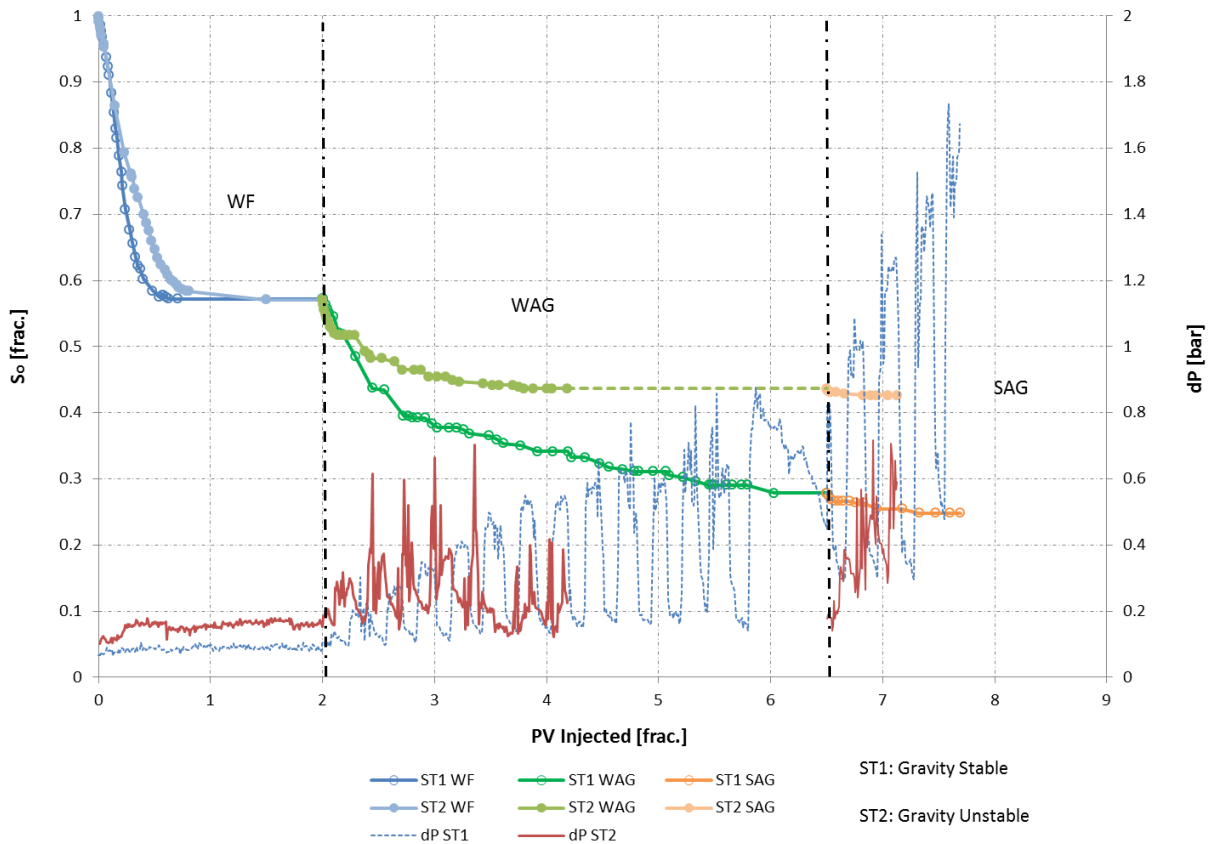


Figure 5.3.2 (a): Waterflood, WAG and SAG have been performed on fractured cores (ST1 and ST2). Residual oil saturation vs. injected pore volume has been plotted; with their respective differential pressures shown beneath. The last point in the WAG curve of ST2 has been extrapolated to match the last point in the WAG curve for ST1. No pressure curves are available for ST2 in this region.

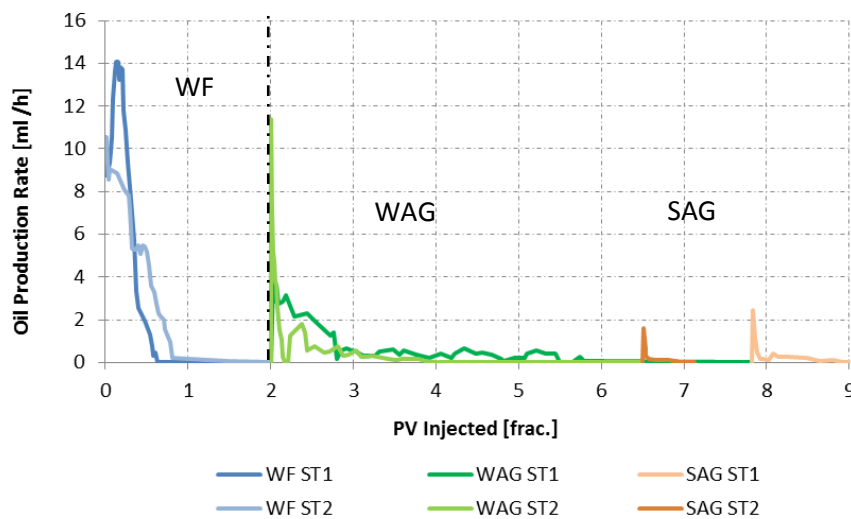


Figure 5.3.2 (b): Oil production rate (ml/h) vs. pore volumes injected (frac.) for cores ST1 and ST2.

Table 5.5 – Production data for cores from figure 5.2.1. Oil saturation and recovery factor after each method is listed as well as total recovery.

Core	$S_{o,initial}$ [frac.]	$S_{o,WF}$ [frac.]	$S_{o,WAG}$ [frac.]	$S_{o,SAG}$ [frac.]	$R_{F,total}$ [% OOIP]
ST1	1.00	0.43	0.29	0.03	75.1
ST2	1.00	0.43	0.13	0.01	57.3

Table 5.5 shows the reduction in oil saturation units for each core. Recoveries in ST2 proved to be lower in both WAG and SAG compared to ST1. This leads to a large difference in ultimate recovery.

The recovery process in core ST2 is possibly a display of poor macroscopic displacement efficiency. During the WAG, the density difference between CO₂ and brine could promote gravity segregation (Grigg & Schechter, 1998). This is controlled by the mobility ratio between gas-water and gas-oil, which depends on relative permeability of the gas. Breakthrough occurs shortly after production start in core ST2 in Figure 5.3.2 (a). Since the displacement process in ST2 is not gravity stable, matrix intrusion from the fracture becomes restricted by the unstable displacement front and viscous bypassing could occur. In the experiment with core ST1, the WAG front seems to become stabilized by gravity. The later breakthrough of the displacement front at 2.5 PV confirms this, and a much higher recovery can be observed.

Significant differences can be observed between the two pressure curves in ST1 and ST2. Differential pressure in core ST2 is lower than ST1 during the waterflood, and there is no clear indication that a gravity unstable front affects the imbibition process, since oil recovered is about the same. As the WAG injection starts, the differential pressure in ST1 surpasses that of ST2 and stays higher in general, which means that CO₂ and water is intruding into the matrix of the core to a larger extent than in ST2. This would mean that fluids are mostly flowing through the fractures in core ST2, rather than into the matrix. This is the case for both the WAG and the SAG injections.

The lower fracture permeability in ST2 is expected to induce a higher differential pressure than in core ST3. This occurs for the first 1.5 PV injected after production start, but a decrease in pressure can be observed as end point production is reached in ST2. This confirms that mobility reduction of CO₂ during WAG is ineffective for a gravity unstable injection. Grigg & Schechter (1998) achieved excellent displacement efficiency by gravity drainage of CO₂ (from top-bottom) in a vertical limestone core. This shows the importance of having gravity stable CO₂, even in WAG injections.

The subsequent SAG injection in core ST2 has a relatively unstable pressure curve compared to in core ST1. Here too, a higher differential pressure should occur in ST2 because of its much lower fracture permeability. This implies that, although foam is generated in ST2 because of the sudden increase in pressure, it does not stabilize enough to sweep the core evenly. It is likely that both water-shielding as well as viscous fingering occurs, significantly lowering the potential for oil mobilization.

5.3.3 | COMPARISON: WHOLE AND FRACTURED CORES

The aim of this section is to compare fractured cores to the baseline experiments previously shown, both in terms of oil production and pressure responses. The whole core, LS3 (Figure 5.3.1), has been plotted together with the fractured core, ST1 (Figure 5.3.2), for comparison in Figure 5.3.3 (a).

Table 5.6 shows reductions in oil saturation after each injection method. The waterfloods in whole and fractured cores are very similar, and are within range of previous recovery rates in limestone (Haugen, et al., 2014). More oil is recovered during the WAG in whole core, LS3, with a lowered oil saturation of 0.33, compared to fractured core, ST1, with 0.29. By studying Figure 5.3.3 (b), oil production rate can be observed as higher at the start of ST1 than for LS3, which means that WAG in the fractured core is more efficient than in the whole core at the beginning of production, as less pore volumes are required to mobilize oil. After approximately 2.8 PV injected, production rate drops down from 1.5 ml/h to less than 0.5 ml/h for ST1. This high production rate could be coupled with the fact that CO₂, flowing in the fracture, has a higher degree of contact with the oil along the fracture walls, which could lead to more diffusive mixing between CO₂ and oil.

Another possibility is as to why oil production is accelerated in the fractured core, could be related to the entrapment of gas, which diverts water into the matrix from the fracture. Improvement from the waterflood happens when CO₂ (non-wetting phase) is being bypassed by the water (wetting phase). This will lead to entrapment of CO₂ in a discontinuous, immobile state. With increasing volume of trapped CO₂, injected fluids will have lower relative mobility (Surguchev, et al., 1992). This can lead to diversion of water into the matrix, and could be what is observed in Figure 5.3.3 (b) for the first period of the WAG injection in core ST1.

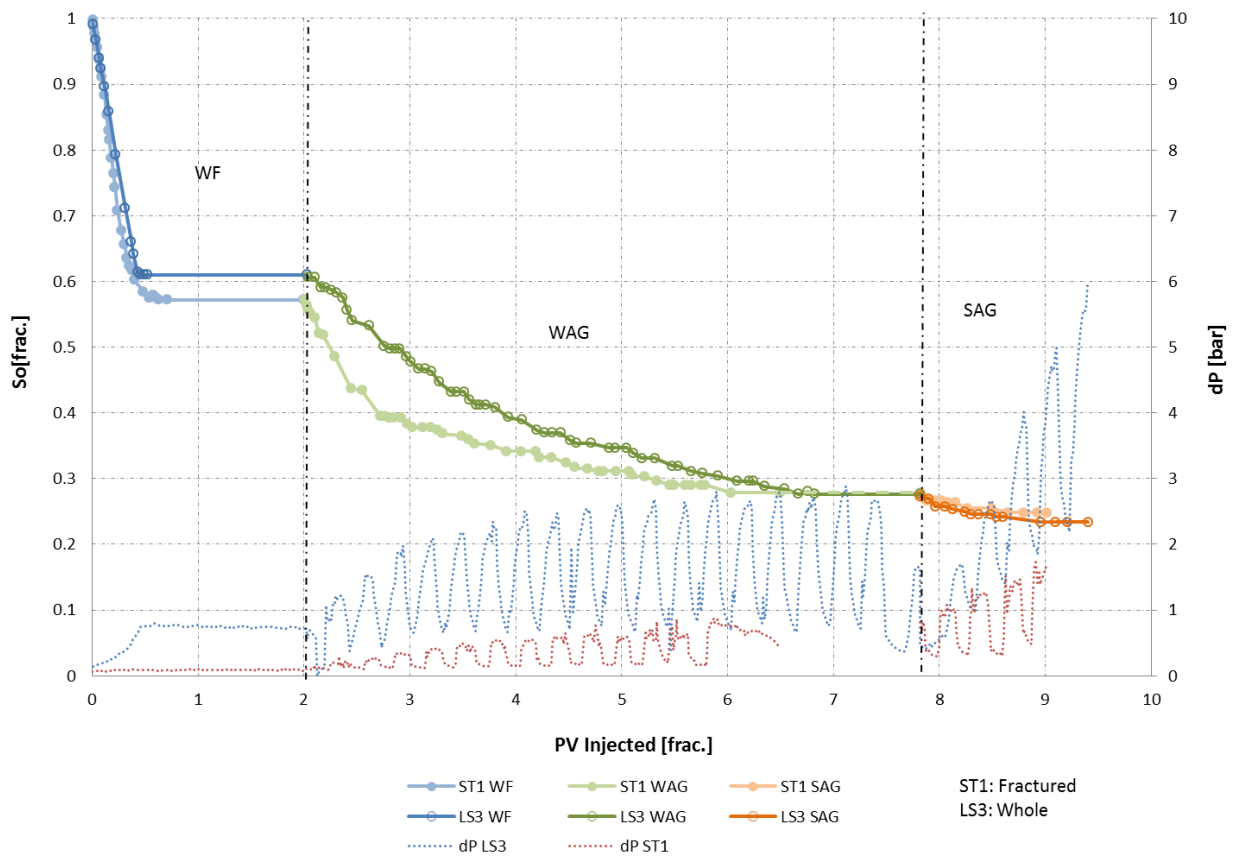


Figure 5.3.3 (a): Residual oil saturation vs. pore volumes injected for fractured (ST1) and whole (LS3) cores for comparison. Differential pressures are shown in blue (LS3) and red (ST1).

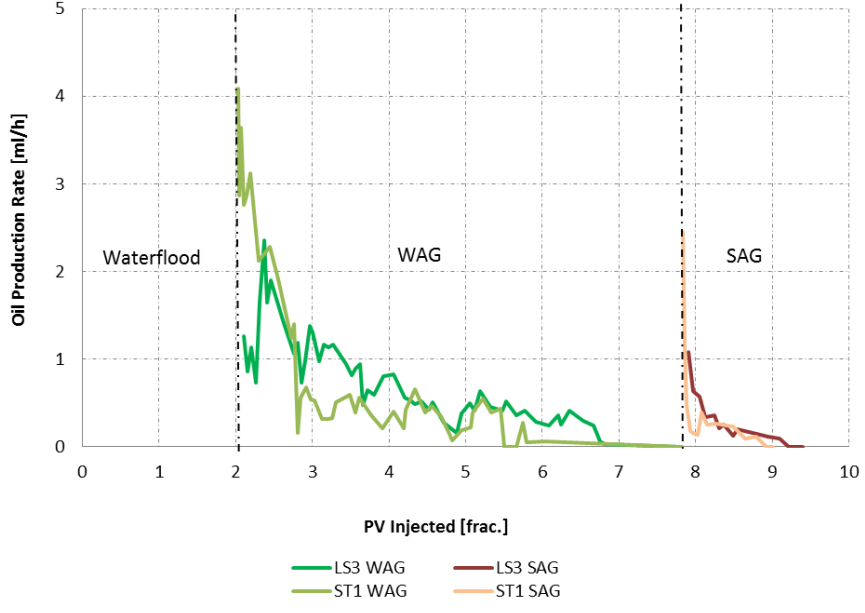


Figure 5.3.3 (b): Oil production rate vs. PV injected for core LS3 and ST1 during WAG and SAG. Waterfloods are not shown.

Table 5.6 – Production data for cores from figure 5.3.3 (a). Delta residual oil saturation for each core is presented after waterflooding, WAG and SAG, as well as the total oil saturation reduction.

Core	$S_{o,initial}$ [frac.]	$\Delta S_{o,WF}$ [frac.]	$\Delta S_{o,WAG}$ [frac.]	$\Delta S_{o,SAG}$ [frac.]	$\Delta S_{o, total}$ [frac.]
ST1	1.000	0.428	0.294	0.030	0.751
LS3	1.000	0.390	0.330	0.039	0.766

The high production rate could also be a result of equal velocity for gas and water for a short period of time in a gas-water mixture zone, which typically occurs in a WAG process at the early production stage in the field, leading to optimum conditions for oil displacement by WAG in heterogeneous reservoirs (Surguchev, et al., 1992). However, this may not be as likely to happen in at core scale due to the constricted time span of the experiment. After breakthrough of CO₂, the following slugs will propagate where CO₂ has already contacted the oil, propagating along the path where capillary pressure is lowest. The sharp drop in production rate in fractured core, ST1, can be explained by segregation of CO₂ and brine in the fracture, as discussed in Section 2.6.3.

SAG recovery appears to be the same for both cores, since there are uncertainties in reading production off the imbibition cell. At production start of SAG, for both cores, there is a spike in the oil production rate, followed by a steep decline. This reflects the low potential for recovery after a WAG.

Gas entrapment is a phenomenon that can possibly explain why differential pressure behaves a certain way during WAG in Figure 5.3.3 (a). The WAG displacement mechanism is a combination of imbibition and drainage, caused by the cyclic nature of the process (Rogers & Grigg, 2001). It combines imbibition from the waterflood and the drainage from the continuous CO₂ injection, which is why it is able to significantly improve on the secondary waterflood and the reason why differential pressure is observed to fluctuate. Since the viscosity of CO₂ is lower than water, differential pressure is expected to peak as the slug of CO₂ exits the core and the slug of water behind it has entered the core. A slug of CO₂ followed by a slug of water will likely prevent the next slug of CO₂ to follow the same path as the first slug of CO₂, thereby contacting more of the porous media and resulting in a steady increase of fluctuating differential pressure. This is more pronounced in the whole core, LS3, than in the fractured core, ST1, but still observable in both cases.

5.3.4 | TERTIARY WAG VS. TERTIARY SAG IN FRACTURED CORES

This section will focus on direct comparison between WAG and SAG as tertiary recovery methods. Fluids were injected as gravity unstable (upwards) through both cores ST2 and ST3 at 10 ml/h. These experiments can be used to investigate if foam generation counteracts fluid segregation under conditions where an unstable front is likely to occur.

Tertiary WAG gives a slightly higher incremental recovery compared to tertiary SAG. WAG recovers 13.4 % of OOIP while SAG recovers 12.5 % of OOIP, as listed in Table 5.7. The most noticeable observation in this case, compared SAG in previous sections, is how low the pressure is from the start of production until breakthrough. It is approximately the same differential pressure as for the preceding waterflood, which indicates that foam has not been effectively generated to decrease CO₂ mobility. This explains the reason why early breakthrough occurs and why almost no additional oil is recovered thereafter.

It is possible that the injected slug volumes are too small so that the first surfactant slug does not sufficiently pre-saturate the core before CO₂ is injected. If gas mobility is not reduced during gas injection, the entire SAG process is likely to fail as the gas could end up in the override zone before the next surfactant slug is injected (Zaganeh, et al., 2009), which may very well be what is seen in core ST3. As more surfactant is injected, large differential pressures occur in ST3 as CO₂ disperse in the surfactant solution, generating in situ foam. This is, however, not sufficient to mobilize the oil. Capillary end effects, as discussed in Section 5.3.1, for LS2 and LS3, may also be a considerable factor for low recovery in this case as well. With wet foam conditions maintained at the outlet of the core, it would be possible to explain why the differential pressure keeps increasing even after oil production from ST3 ceases. The waterflooding of ST3 is significantly higher than for ST2, which will affect the SAG process by form of water-shielding effects. This is a possible explanation as to why WAG recovers slightly more oil in ST2.

The differential pressure is lower for the WAG compared to SAG throughout the experiment. This arises as a direct result of flow resistance in the core, which appears to be very small in the WAG process. The ratio of viscous to gravity forces is one of the primary factors that influence a WAG. And since the gravity forces will dominate in a tertiary WAG flood of a strongly water-wet system, macroscopic sweep becomes worsened by viscous bypassing occurring between CO₂ and the oil (see Section 2.6.3). Water-shielding effects are present throughout the WAG, so that CO₂ has to displace water before contacting oil, which could cause capillary-induced bypassing in core ST2.

Knowing that the displacement processes in both WAG and SAG are gravity unstable, this may very well be the most significant factor, causing early breakthrough of fluids and inefficient ultimate recoveries.

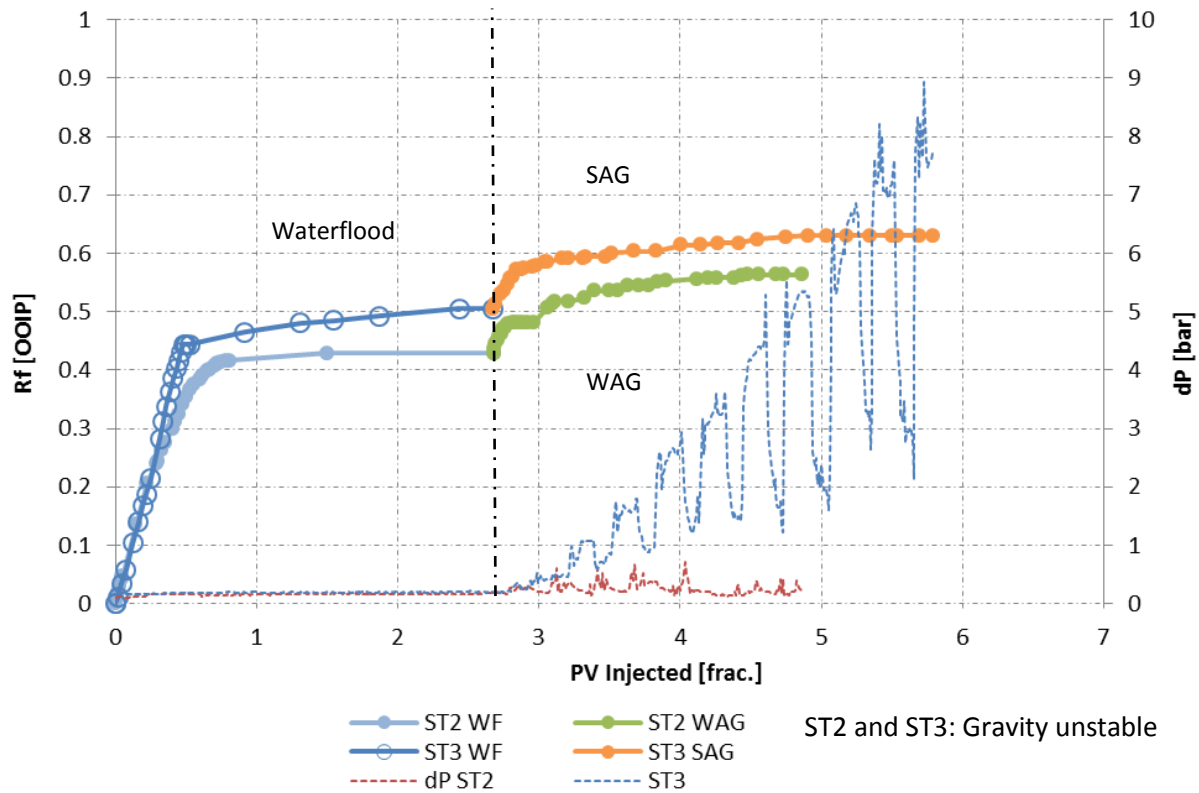


Figure 5.3.4: Recovery factor vs. PV injected for tertiary WAG and tertiary SAG processes. Differential pressure is plotted for ST2 (red) and ST3 (blue).

Table 5.7 – Recovery factors after waterflood, tertiary WAG (ST2) and tertiary SAG (ST3). Total recovery for each core is also shown.				
Core	$R_{f,WF}$ [%OOIP]	$R_{f,WAG}$ [%OOIP]	$R_{f,SAG}$ [%OOIP]	$R_{f,total}$ [%OOIP]
ST2	42.9	13.4	---	56.3
ST3	50.6	---	12.5	63.1

5.4 | TERTIARY CO-INJECTION OF SUPERCRITICAL CO₂ AND SURFACTANT

The experimental data analyzed in this section were obtained in co-operation with fellow master student, Henriette Horjen.

These experiments were conducted by injecting surfactant and CO₂ simultaneously into the core. Petrostep C-1, listed in Table 4.1, was selected as the surfactant, based on previous successful foam experiments (Haugen, et al., 2012). It has also been used in field pilots for diversion in fractured reservoirs (Ocampo, et al., 2014). This AOS surfactant exhibited high longevity in the presence of oil in experiments by Simjoo et al. (2013). Core properties from Table 5.1 show that these cores were all drained to irreducible water saturation. Pressures of 90-95 bars with a temperature of 35 °C were applied, achieving a first-contact miscible displacement process. These experiments were performed horizontally to eliminate gravity effects; this is also why the fractures in the cores were aligned vertically. All fractured cores contained a plastic spacer with a certain spacer volume. Injections were run at 5 ml/h and an overburden pressure of 100-105 bars was applied.

5.4.1 | BASELINE: CO₂ AND CO₂-FOAM IN WHOLE CORES

Pure CO₂ (#2) and CO₂-foam (#3) were injected into two whole cores to establish baseline experiments. Next, three experiments (#4, #10 and #12) were run on fractured cores to investigate foam effects on oil production and compare them to whole cores. Figure 5.4.1 (a) shows the resulting oil production from cores #2 and #3.

During the water injection, the brine imbibes spontaneously into the strongly water-wet core (Alotaibi, et al., 2010). A high, constant oil production rate can be observed (5.4.1 (b)), eventually leading to clean water cut (Figure 5.4.1 (a)) after water breaks through at the core outlet. Initial oil saturation in cores #2 and #3 was reduced by around 0.28 and 0.25 saturation units, respectively. For pure CO₂ injection, a steep decrease in oil saturation could be observed as production began. Core #2 had its oil saturation lowered by 0.13 saturation units, all of which was recovered after 1 PV. CO₂ is believed to achieve first-contact miscibility with the decane within the core. The oil is displaced by viscous forces, with gravity drainage as the main driving mechanism. Diffusion is also believed to be an important factor to determine displacement efficiency at core scale.

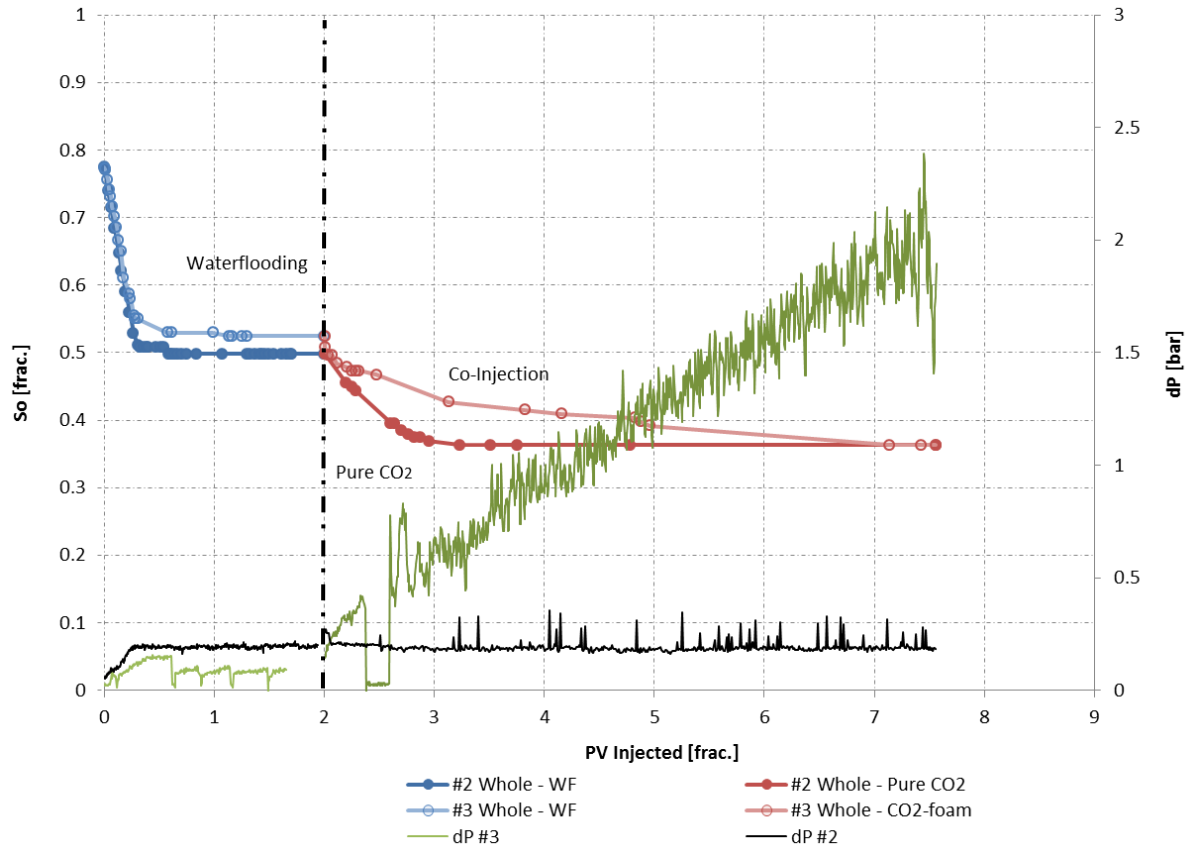


Figure 5.4.1 (a): Oil saturation vs. pore volumes for pure CO₂ injection and co-injection into whole limestone core plugs after waterfloods. Pure CO₂ in core #2 has been extrapolated to match the last point of CO₂-foam in core #3.

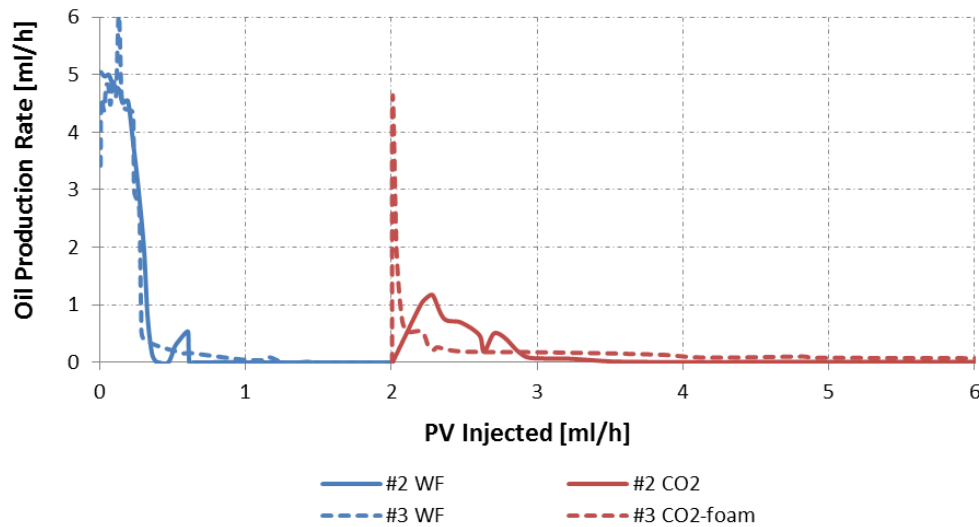


Figure 5.4.1 (b): Oil production rate vs. PV injected for #2 (CO₂) and #3 (CO₂-foam).

Table 5.8 – Production data for whole cores from figure 5.3.1. Delta residual oil saturation for each core is presented after waterflooding, CO₂ and CO₂-foam, as well as the total oil saturation reduction.

Core	S _{o,initial} [frac.]	ΔS _{o,WF} [frac.]	ΔS _{o,CO2} [frac.]	ΔS _{o,Co-inj.} [frac.]	ΔS _{o, total} [frac.]
#2	1.00	0.28	0.13	---	0.41
#3	1.00	0.25	---	0.16	0.41

Once CO₂ has reached the outlet of the core, continuous injection will likely not recover more oil in core #2 as it will follow the least resistant path already containing CO₂. This is why production in core #2 completely evens out at breakthrough after 1 PV. During co-injection, oil production was observed to be slower than for pure CO₂ injection, in terms of PV injected required to recover the same amount of oil.

Results from Haugen et al. (2014):

When comparing these results with Haugen et al. (2014), incremental recovery of pure CO₂ injection is higher, with residual oil saturation of 0.19. Haugen injected for 10 pore volumes to achieve this final recovery, and there was a long period of time with very little extra oil produced. In figure 5.4.1 (a), CO₂ injection was stopped between 4-5 pore volumes, and then extrapolated to match the last point of CO₂-foam. It is possible that the same amount of oil could have been recovered here if injection had continued.

Results from Svenningsen (2011):

Reductions in residual oil saturation units by Svenningsen (2011), in two whole cores, were around 0.20 by supercritical tertiary CO₂ injection. This does not match well with core #2. However, another core had a reduction of 0.12 residual oil saturation units, which is in the same for area for Svenningsen as core #2, although connate water saturation was 0.40. During tertiary supercritical foam experiments, reduction of oil saturation in one of the cores was 0.13, which is less than core #3. So for Svenningsen, pure tertiary CO₂ injection performed better than CO₂-foam in whole cores. This is the same result obtained for whole cores #2 and #3.

When CO₂ has a lower mobility, as in CO₂-foam, it is expected to perform better than a pure CO₂ injection, where mobility is higher and likely to reach breakthrough earlier. Therefore, it is not straight forward to explain the trend seen in Figure 5.4.1 (a), where the opposite occurs: CO₂ injection performs better than CO₂-foam. This could mean that the generated foam does not have time to reach steady state, as the length of the core is rather short. Differential pressure can be observed to increase steadily throughout the co-injection process as foam is being

generated. As mentioned in previous sections, this could mean that the texture of the foam is becoming finer with a greater amount of lamellae per unit length (Yan, et al., 2006). Oil is being produced throughout the pressure increase because viscous forces become stronger and able to sweep more of the oil.

Observations made in experiments by Chou (1991) indicated that foam reduction factor in the last section of the core continued to increase over time, with constant injection rate. This is seen as common in weak CO₂-foam with low flow rates, even if surfactant concentration is as high as 1 wt %. High differential pressures can be generated even for weak foams, according to Chou (1991). This could be the case for foam in core #3, in addition to the nature of the water-wet limestone that can cause capillary end-effects to hold surfactant solution back, meaning that the oil being displaced by foam has to displace the surfactant solution before leaving the core.

Both the efficiency of the waterflood and the pure CO₂ injection was found, by Eide (2014), to depend on the exact pore size distribution (see Section 4.1.2), ranging significantly between limestone samples. Therefore, the efficiency of a CO₂ injection may show better recovery than a CO₂-foam injection in a whole core, depending on the effect of small scale heterogeneities within the sample.

After the waterflood, core #3 has higher initial oil saturation than core #2. Oil has been proven to be detrimental to foam as it spreads on the film until it ruptures (Simjoo, et al., 2013). This is a factor that can delay generation and stabilization of foam, and can also be a contributing explanation as to why recovery is slower than during CO₂ injection. Because of a constant injection of surfactant solution, the CO₂ has to go through water films in order to contact oil. This water-shielding effect can slow down the recovery process in early production stages.

As the surfactant propagates through core #3, it is adsorbed on the limestone surface. Layers of adsorbed surfactant can influence relative permeability of water by transitioning to a more water-wet system. Since co-injection is performed at constant water fractional flow of 0.2 (80% foam quality), a build-up of water saturation can occur within the core between foam fronts and delay foam propagation (Wassmuth, et al., 2001), which could be related to the slow production in core #3.

The low overburden pressure in these experiments could have made fluid bypass the core along the sleeve, as the aluminum foil wrapped around it causes less resistance to fluid flow. This may also explain why more pore volumes are required for co-injection to reach the same end point recovery as CO₂ injection.

5.4.2 | CO₂ AND CO₂-FOAM IN FRACTURED CORES

This section compares reduction in residual oil saturation of pure CO₂ injection (#10) with co-injection (#4 and #13) in fractured cores. Results are presented in Figure 5.4.2 (a) and 5.4.2 (b).

From Figure 5.4.2 (a), it is apparent that CO₂-foam, by co-injection in core #4, has slightly better oil recovery compared to that of continuous CO₂ injection in core #10. As listed in Table 5.9, co-injections in cores #4 and #13 have reductions of 0.24 and 0.21 oil saturation units, respectively. This is a higher production by foam in #4 compared to pure CO₂ in core #10, with a reduction of 0.21 oil saturation units, which is the same as in core #13. After breakthrough in during pure CO₂ injection, no significant additional oil production takes place. At around 3.8 PV in Figure 5.4.2 (a), slightly more oil is produced for core #10 by CO₂, which is unexpected because it is unlikely that CO₂ will contact additional oil after breakthrough. This could be explained by uncertainties in measurements.

The displacement process in pure CO₂ injection is likely to have very little contribution from viscous forces, as gas channels through the high permeable fracture in the center of the core. This has been confirmed by Eide (2014) through CT-imaging and MRI-imaging of oil production of a fractured core. It can also be observed from the low differential pressure, which indicates limited flow resistance. For an Edward limestone rock, that has low matrix permeability and high fracture permeability, molecular diffusion tends to become a dominating oil recovery mechanism during the pure CO₂ injection (Shojaei & Jessen, 2015).

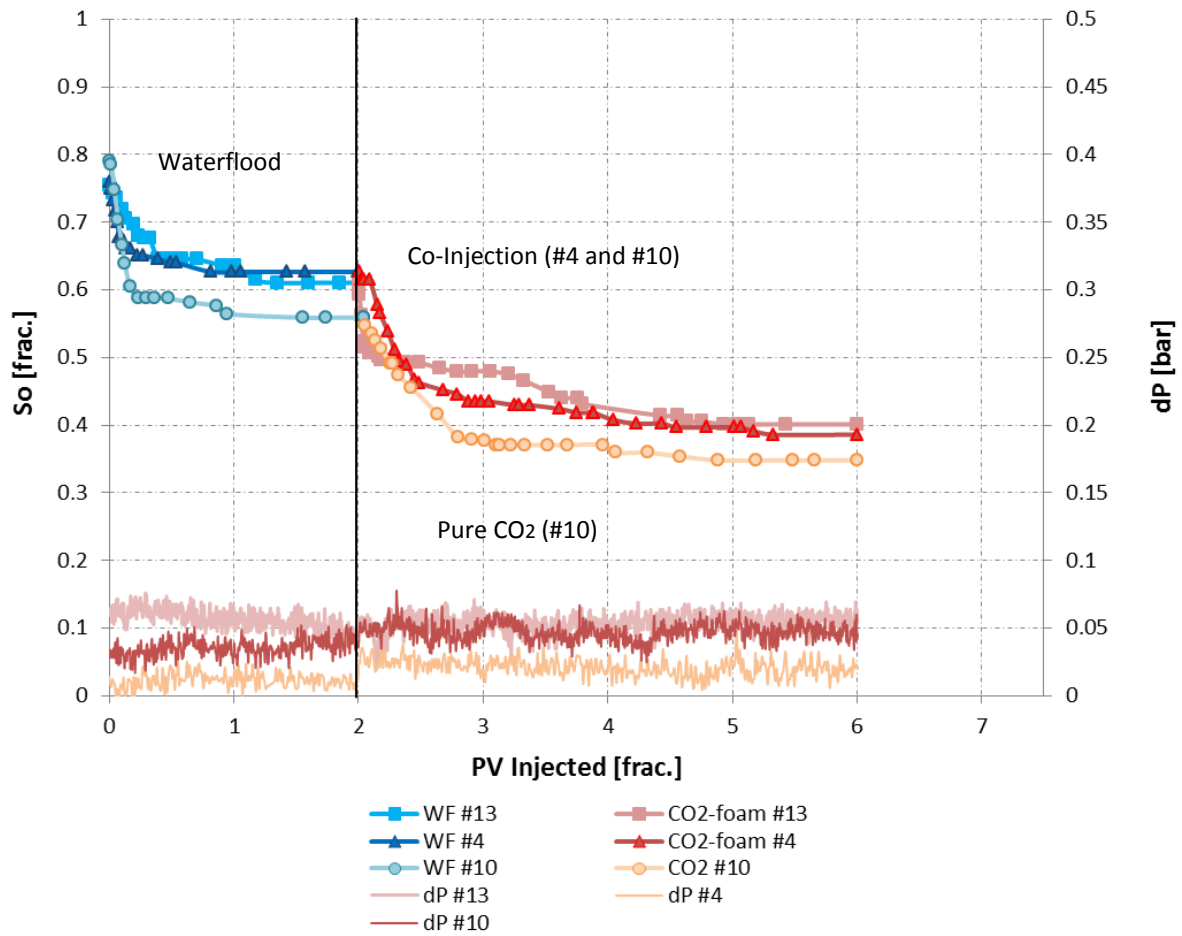


Figure 5.4.2 (a): Residual oil saturation vs. PV injected for pure CO₂ injection (#10) and co-injection (#4 and #13) in fractured cores. Differential pressure is shown for CO₂ (black) and CO₂-foam (green).

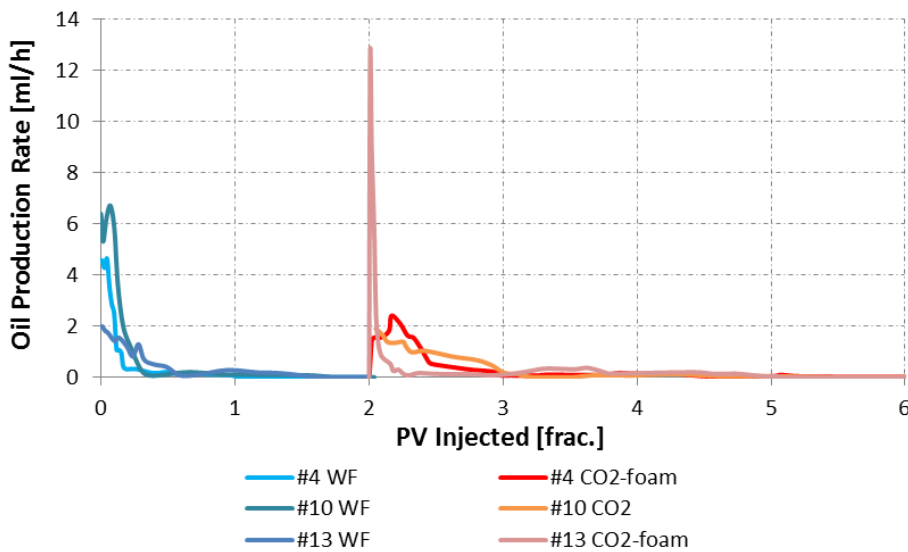


Figure 5.4.2 (b): Oil production rate (ml/h) vs. PV injected (frac.) for cores #10 (CO₂-foam) and #4 (CO₂).

Table 5.9 – Production data for fractured cores from figure 5.4.2 (a). Delta residual oil saturation for each core is presented after waterflooding, CO₂ and CO₂-foam, as well as the total oil saturation reduction.

Core	S _{o,initial} [frac.]	ΔS _{o,WF} [frac.]	ΔS _{o,CO2} [frac.]	ΔS _{o,Co-inj.} [frac.]	ΔS _{o, total} [frac.]
#4	0.76	0.13	---	0.24	0.37
#13	0.76	0.14	---	0.21	0.36
#10	0.79	0.23	0.21	---	0.44

Oil production rate in Figure 5.4.2 (b) becomes accelerated when CO₂-foam is introduced to core #4 and #13. This rate eventually evens out and overlaps with production rate for pure CO₂ in core #10. The fracture permeability within core #4 could be as high as two orders of magnitude larger than the matrix permeability. It is clear that entrapment of CO₂ within water film occurs at the early stage of production, which is why the oil rate peak in CO₂-foam is higher than for pure CO₂. After breakthrough of CO₂, diversion of fluid from the fracture and into the matrix occurs to a more limited extent and the rate can be observed to level out in Figure 5.4.2 (b).

Co-injection in core #4 showed slightly better potential than pure CO₂ injection, but since the same recovery was observed for co-injection in core #13, this difference could be attributed uncertainty as well as to the heterogeneous nature of limestone. However, the oil production was slightly accelerated in both core #4 and #13 in the early production phase compared to core #10.

5.4.3 | COMPARISON: WHOLE AND FRACTURED CORES

In section 5.4.1 observations were made that pure CO₂ and CO₂-foam performed similarly in whole cores, while in section 5.4.2 there was an observable difference between oil production in pure CO₂ and CO₂-foam for fractured cores. This section will compare and contrast CO₂ and CO₂-foam as recovery methods in whole and fractured cores. Combined plots of the earlier figures have been made in Figures 5.4.3 (a) and 5.4.3 (b).

There is slight difference in oil production between fractured and whole cores for both pure CO₂ and CO₂-foam. This difference is more pronounced in the recovery efficiency of CO₂-foam in the whole and fractured cores (Figure 5.4.3 (b)), contrary to CO₂ in whole and fractured cores (Figure 5.4.3 (a)). Because the core plugs are relatively short, diffusion becomes an important factor that determines recovery during CO₂ injection at laboratory scale.

Both cores have a short transient period of production after CO₂ breakthrough in Figure 5.4.3 (a). However, after 2 PV, additional oil is recovered for the fractured core. This is normally not expected to happen, and could be a matter of uncertainty in measurements.

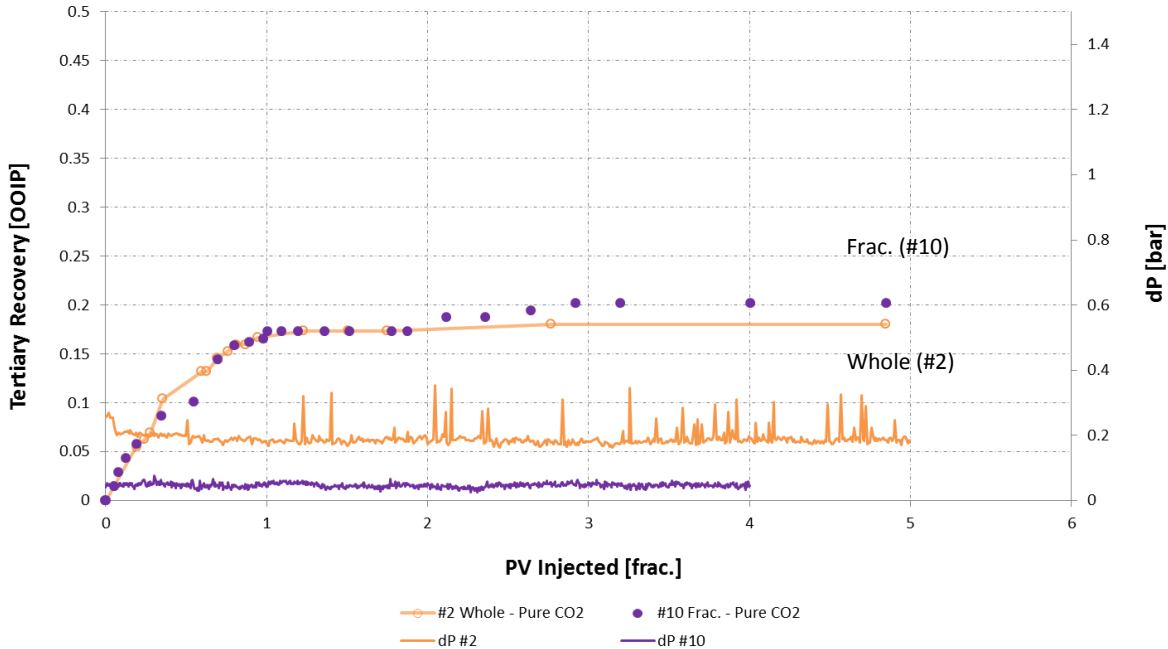


Figure 5.4.3 (a): Comparison of tertiary CO₂ injection in whole (#2) and fractured (#10) core. This plot shows tertiary recovery (OOIP) vs. PV injected (frac.). Waterfloods have been omitted so that the curves start from zero.

According to Figure 5.4.3 (a), there is no difference in the efficiency at which oil is recovered by CO₂ injection in the presence of fractures. During the first PV injected, data points completely overlap for the two cores. Since recovery mechanisms in whole cores are dominated by viscous displacement through gravity drainage as well as diffusion, a higher displacement is expected compared to fractured cores. Pressure drop induced in the whole core, by viscous forces, is higher than in the fractured core. In section 5.4.1, various reasons for the low displacement in the whole were discussed.

Figure 5.4.3 (b) has a more pronounced difference in tertiary recovery for whole and fractured cores. Viscous displacement occurs in porous media by co-injection, generating in situ foam which lowers apparent viscosity of CO₂. Differential pressures between the whole (#3) and fractured (#4) cores indicate that viscous forces are strong in the whole core, while weak in the fractured core. Investigations conducted on foam generation by Chou (1991) showed that strong foam can be generated at low pressure gradients. The same observation can be made in figure 5.4.3 (b), where differential pressure in the whole core rises up to around 2 bars, compared to a much lower differential pressure in the fractured core. Yet, the

amount of recovered oil is significantly higher and more efficient for the fractured one. In addition to the given explanation, it could also be that either fluid has bypassed core #3 or the steadily increasing pressure could indicate that steady state has yet to be reached. The trend in Figure 5.4.3 (b) suggests that foam is favorable in fractured cores, since a larger contact area is available, as opposed to a whole core where foam will sweep the core along the cross-section only.

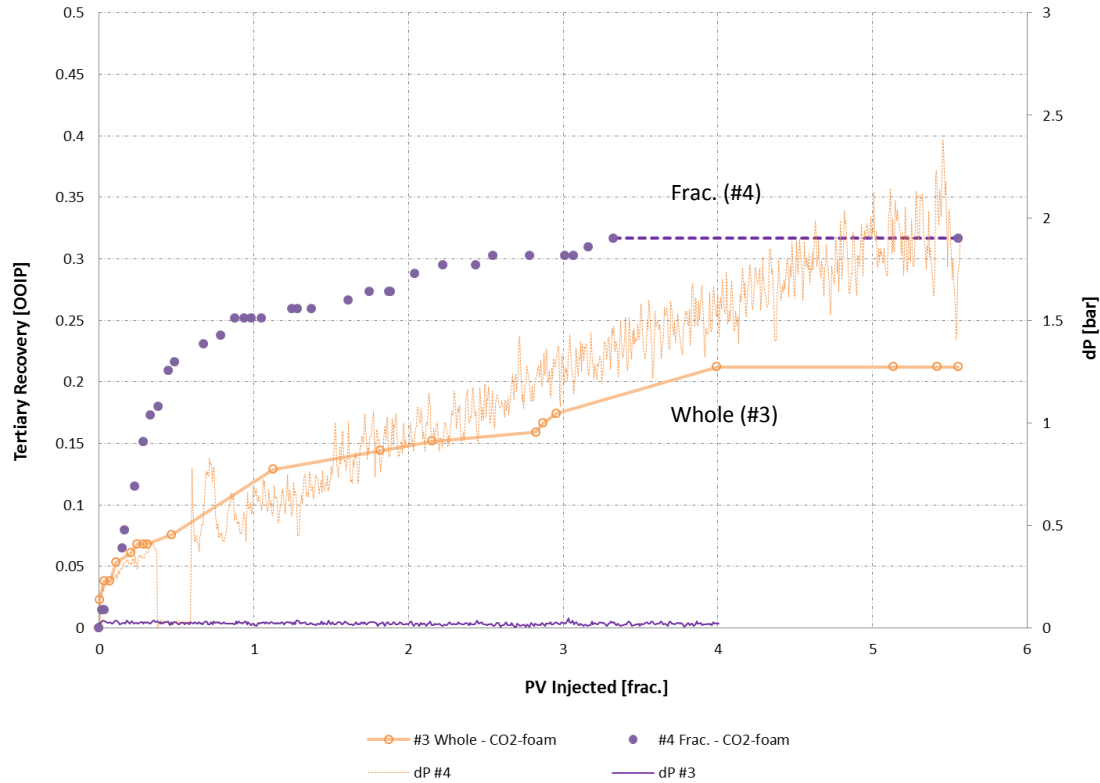


Figure 5.4.3 (b): Comparison of tertiary CO_2 -foam co-injection in whole (#3) and fractured core (#4). This plot shows tertiary recovery (OOIP) vs. PV injected (frac.). Waterfloods have been omitted so that the curves start from zero.

5.4.4 | INTEGRATED EOR: CO_2 AND CO_2 -FOAM IN FRACTURED CORES

Experiments with CO_2 and CO_2 -foam have been discussed separately in the previous sections. This section will expand on the utilization of these two techniques by combining them in a fractured core (#12) to investigate whether or not this strategy can improve recovery even further. The experiment conducted on core #12, at a rate of 5 ml/h, has been plotted together with a previous experiment by Opdal (2014) on core AC_1, which had an injection rate of 10 ml/h. Foam was generated in both cores by using Petrostep C-1 as the surfactant. Pure CO_2 injection in core #10 has been added to better observe the effect of switching to foam. Properties of the cores are compared in Table 5.10 and this shows their

similarity. The main difference between the two lies in injection rate, oil type and slightly different sizes. AC_1 is also a multi-fracture system of two different fractured cores, with no spacer volume, which leads to lower fracture permeability. Results are plotted in Figure 5.4.4 (a) and Figure 5.4.4 (b).

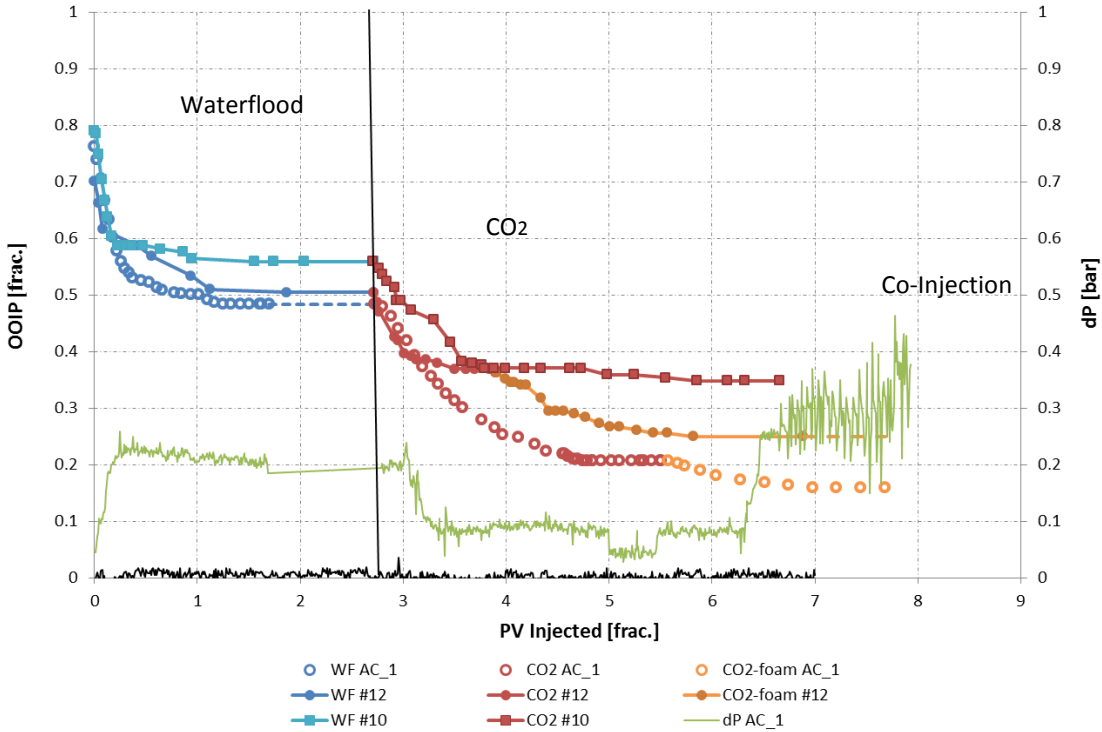


Figure 5.4.4 (a): Oil recovery as a fraction of OOIP vs. pore volumes injected for a waterflood, CO₂ and CO₂-foam in fractured cores. Core #12 is plotted together with core AC_1 from Opdal (2014) for comparison. Pure CO₂ in Core #10 has been plotted to directly see the effect of switching to foam.

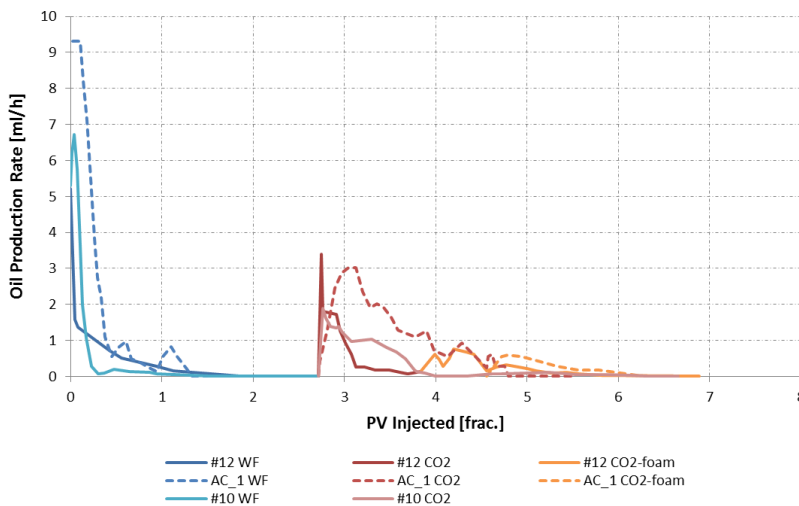


Figure 5.4.4 (b): Oil production rate vs. pore volumes injected during waterflood, CO₂ and CO₂-foam in cores #10, #12 and AC_1. A production spike occurs once CO₂ hits the core. The same spike happens when CO₂ and surfactant are introduced to generate in situ foam.

Table 5.10 – Core properties and oil types are given for fractured cores #10, #12 and AC_1.

Core	Rock	Length [cm]	PV _{frac} [ml]	Porosity [%]	K _{frac} [mD]	Swi [frac.]	Oil Type
#10	Limestone	6.70	16.67	24.26	---	0.21	Decane
#12	Limestone	7.20	16.80	22.80	---	0.30	Decane
AC_1	Limestone	9.70	21.40	21.90	85 ± 57	0.237	Paraffin

Table 5.11 – Production data for fractured cores from figure 5.4.4 (a). Delta residual oil saturation for each core is presented after waterflooding, CO₂ and CO₂-foam, as well as the total oil saturation reduction.

Core	S _{o,initial} [frac.]	ΔS _{o,WF} [frac.]	ΔS _{o,CO₂} [frac.]	ΔS _{o,CO₂-inj.} [frac.]	ΔS _{o,total} [frac.]
#10	0.79	0.23	0.21	---	0.44
#12	0.70	0.20	0.14	0.11	0.45
AC_1	0.76	0.28	0.28	0.05	0.60

A waterflood was completed for core #12, which reduced oil saturation with 0.196 units. AC_1 had its oil saturation reduced by 0.28. Then a subsequent CO₂ injection was initiated, producing 0.14 saturation units for #12, while 0.8 units were produced for AC_1. CO₂ injection lasted longer in core AC_1 than #12, since an early transition was made in core to foam in core #12. The CO₂ injection is over a very short time span compared to the earlier CO₂ experiments, and it is not likely that CO₂ would have been able to produce more oil if the process continued. This can be observed from pure CO₂ injection in core #10, where very limited additional oil is produced after breakthrough.

Several parameters were different, and it is not clear which one contributes the most to AC_1 achieving higher oil production. It could be because of a higher differential pressure than for #12, induced by lower fracture permeability. This is a significant factor since CO₂ breakthrough will be slower than in core #12. At the inlet part of core of AC_1, CO₂ will produce oil by viscous forces at the beginning, until breakthrough of CO₂. Then the main displacement mechanism turns to molecular diffusion, causing production of the rest of the oil. On the contrary, diffusion is likely the only displacement mechanism in core #12 because nothing prevents CO₂ from channeling through the fracture.

Figure 5.4.4 (b) displays oil production rate in core #12. CO₂ injection and CO₂-foam can both be observed as peaks once injection fluids hit the core, continuing oil production where

waterflooding left off. CO₂-foam has a decline in production rate at 4.3 PV before its maximum oil production rate at 4.5 PV. A similar observation can be made from the recovery curve in Figure 5.4.4 (a), where oil production starts to even out at 4.2-4.3 PV before speeding up and starts to even out again at 4.5 PV. This could be attributed to effects of surfactant adsorption and detrimental effects of oil on foam stability. Experiments have confirmed the instability of foam in the presence of oil (Simjoo, et al., 2013). The decrease in oil saturation as more fluid is injected, as well as surfactant saturation, could be the reason for the small increase in oil production at the start, before the curve flattens out again.

Viscous-induced forces are created in the system as foam generation takes place inside the core. This is an important additional mechanism to diffusion. There are also effects of swelling of oil and reduction of interfacial tension of gas-oil and water-oil by surfactant. Because of these processes, oil recovery increases further in core #12 than what can be seen for core #10. Although core AC_1 has a higher ultimate recovery than core #12 by running the CO₂ injection for a longer period of time, before switching to foam, it is also a different fracture system with a higher degree of viscous displacement. The sequence that was conducted in core #12, with no viscous displacement during CO₂ injection, seems to be an efficient way to produce the oil in terms of CO₂ usage and maximizing the ultimate recovery.

5.5 | COMPARISON OF SUPERCRITICAL CO₂ EOR INJECTION STRATEGIES

Several different injection strategies have been studied and discussed in this thesis. While certain recovery methods clearly out-perform others, some of the techniques that have been looked at have inconclusive recovery potential due to gravity effects and uncertainties in the way some experiments were conducted. In this section, the main focus will be to compare every method that has been shown so far. Figure 5.5 contains all the recovery curves from previous figures, but modifications have been made so that all curves start from zero by subtracting pore volumes and recovery of the waterfloods. Only tertiary plots are included and dotted lines are drawn to mark the recovery plateau and to match the end points of every curve.

It is important to note that parameters are varying between experiments related to CO₂/co-injection and WAG/SAG experiments (Table 5.3). The main differences are: flow rate, use of spacer, single and stacked cores, core length, initial oil saturations, and surfactant types. These parameters could all influence oil production.

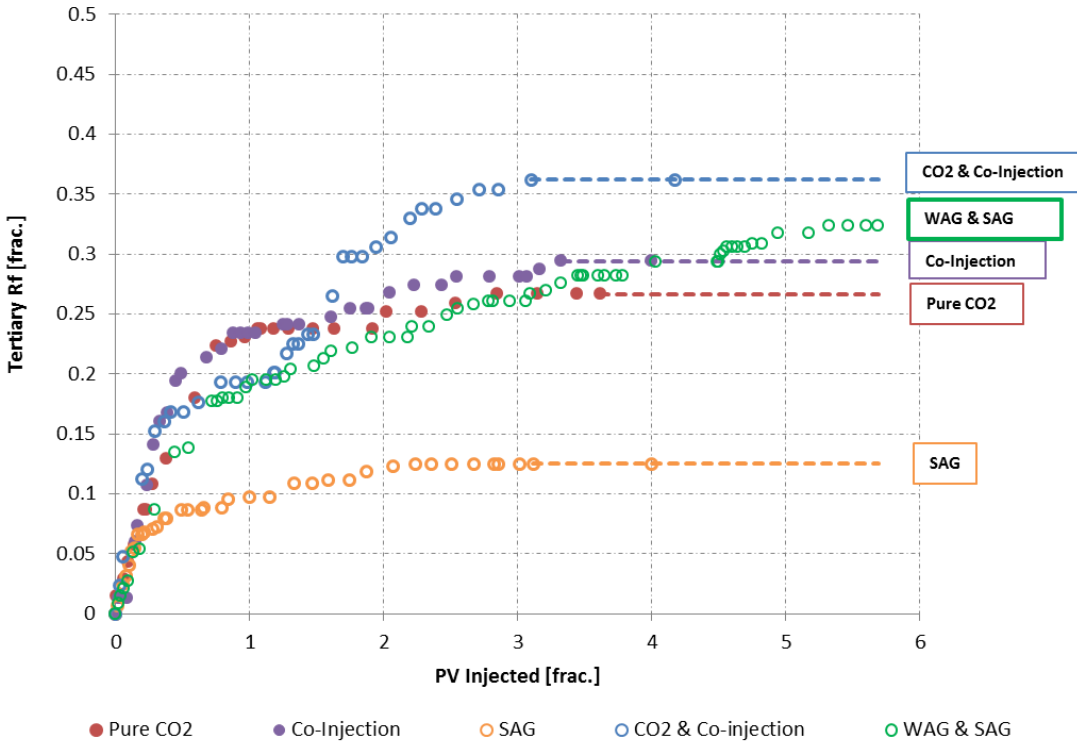


Figure 5.5: Tertiary recovery factor vs. pore volumes injected. Previously shown recovery methods have been plotted together: SAG, pure CO₂, WAG, co-injection and combined CO₂ + co-injection. All curves have been modified to start from zero and dotted lines are drawn to matching end points.

Table 5.12 – Recovery factors for each tertiary method shown in Figure 5.5.

Injection Method	Core	R _{f,WF} [% OOIP]	Tertiary Recovery [% OOIP]
CO ₂ +Co-Injection	#12	41.3	36.2
WAG+SAG	ST1	42.8	32.4
Co-Injection	#4	36.2	29.4
Pure CO ₂	#10	29.4	26.7
SAG	ST3	50.6	12.5

The weakest tertiary recovery method appears to be the SAG, with the earliest breakthrough and the lowest total recovery of 12.5 % of OOIP. As stated in previous sections, the direction of injection in this experiment proved disadvantageous since gravity forces as well as capillary forces inhibited fluid from intruding into pores. In addition, the density differences between CO₂

and surfactant possibly lead to CO₂ disappearing in an over-ride zone, causing the production to cease after breakthrough. Because gravity has to be accounted for, this result may not be representative of an actual SAG injection, which makes realistic comparisons with other strategies difficult. There are different surfactant types in the two foaming strategies of SAG and co-injection. Perhaps the anionic surfactant, used in co-injection, is more compatible with the core size as well as experimental conditions.

Second lowest in terms of total recovery was the pure CO₂ injection, although an improvement can be seen when compared with SAG. This method was governed by diffusion as its main production mechanism, which seems effective to a certain extent because it improves microscopic sweep. However, it falls short in light of co-injection and WAG. With injection of WAG and SAG on the same core, pure CO₂ injection is exceeded in terms of efficiency at early stages of production, as well as in the final recovery process. Co-injection has a higher oil production rate after breakthrough occurs compared to that of WAG, and at no point does the recovery curve of WAG surpass the co-injection recovery curve. This poses the question whether or not it is worth implementing combined WAG and SAG since co-injection arguably out-performs this strategy in terms of overall efficiency. It could be considerable if WAG/SAG is less costly overall.

Lastly, tertiary CO₂ followed by co-injection extracts the highest oil volume, with a total of 36.2 % of OOIP recovered. That is 3.8% OOIP more than WAG/SAG and 6.8% OOIP more than co-injection, which are the only two strategies that are able to compete with it. CO₂ injection, before initiating co-injection, shows a slightly more efficient recovery curve than the WAG process, but less efficient than co-injection.

5.6 | UNCERTAINTIES AND CALCULATIONS

Every instrument that has been used throughout the experiments contains an uncertainty, and by combining these in calculations, the magnitude of uncertainty can be assigned to important values obtained from raw data.

Instrumental Uncertainties:

Pressure gauge (max 250 bar):	± 0.1% of full scale.
Pressure gauge (max 40 bar):	± 0.1% of full scale.
QX Pump, injection rate:	± 5% ml/h
QX Pump, PV injected:	± 0.5 ml
Caliper:	± 0.01 mm
Core Weight:	± 0.01 g
Imbibition cell measurements:	± 0.05 ml

Uncertainty Equations:

The uncertainty, σ_y , of a value, y , is given by the equation:

$$\sigma_y = \sqrt{\sum_{i=1}^n \left(\frac{\partial y}{\partial x_i} * \sigma_{x_i} \right)^2} \quad 5.6.1$$

Where $i = 1, \dots, n$, $y = f(x_1, x_2, x_3, \dots, x_n)$ and x_i is an independent variable with independent uncertainty, σ_{x_i} .

Calculating Porosity Uncertainty:

Porosity is calculated by Equation 4.1.1, which also can be written as pore volume divided by bulk volume: $\varphi = V_p/V_b$. Bulk volume is written as: $V_b = \pi \cdot r^2 \cdot L$, where r is the radius of the core and L is the length of the core. Pore volume is written as $V_p = \frac{m}{\rho}$, where m is the weight difference between saturated core and dry core, ρ is the density of the saturating fluid.

In order to calculate the uncertainty of porosity, bulk volume and pore volume uncertainties must be calculated separately.

Bulk volume uncertainty, $\sigma_{V_{b,core}}$, is calculated by input of variable into Equation 5.6.1 and deriving it:

$$\sigma_{V_{b,core}} = \sqrt{\left(\frac{\pi * D * L}{2} * \sigma_D\right)^2 + \left(\frac{\pi * D^2}{4} * \sigma_L\right)^2} \quad 5.6.2$$

where D is the diameter of the core and L is the length.

Pore volume uncertainty, σ_{V_p} , is given by equation:

$$\sigma_{V_p} = \sqrt{\left(\frac{1}{\rho_{fluid}} * \sigma_{m_{sat}}\right)^2 + \left(\frac{-1}{\rho_{fluid}} * \sigma_{m_{dry}}\right)^2 + \left(-\frac{m_{sat} - m_{dry}}{\rho_{fluid}^2} * \sigma_{\rho_{fluid}}\right)^2} \quad 5.6.3$$

Where $\sigma_{m_{sat}}$ is the uncertainty in weight of saturated core, $\sigma_{m_{dry}}$ is the uncertainty in weight of dry core and ρ_{fluid} is the density of saturating fluid.

Finally, combining these two gives the uncertainty of porosity:

$$\sigma_{\phi} = \sqrt{\left(\frac{\partial \phi}{\partial V_p} * \sigma_{V_p}\right)^2 + \left(\frac{\partial \phi}{\partial V_b} * \sigma_{V_b}\right)^2} \quad 5.6.4$$

Calculating Permeability Uncertainty:

Permeability is calculated using Darcys law, given in Equation 4.1.2. The uncertainty, σ_K is calculated using the following equation:

$$\sigma_K = \sqrt{\left(\frac{\mu * L}{A * \Delta p} * \sigma_Q\right)^2 + \left(\frac{Q * L}{A * \Delta p} * \sigma_{\mu}\right)^2 + \left(\frac{Q * \mu}{A * \Delta p} * \sigma_L\right)^2 + \left(-\frac{Q * \mu * L}{A^2 * \Delta p} * \sigma_A\right)^2 + \left(-\frac{Q * \mu * L}{A * (\Delta p)^2} * \sigma_{\Delta p}\right)^2} \quad 5.6.5$$

where is uncertainties of the Darcy equation are given as: flow rate, σ_Q , viscosity of fluid, σ_{μ} , length of core, σ_L , cross-section of core, σ_A , differential pressure, Δp .

Calculating Oil Saturation Uncertainty:

Uncertainty of oil saturation, σ_{S_o} , is calculated using the following equation:

$$\sigma_{S_o} = \sqrt{(\sigma_{S_{oi}})^2 + \left(-\frac{1}{V_p} * \sigma_{V_{o,p}}\right)^2 + \left(\frac{V_{o,p}}{V_p^2} * \sigma_{V_p}\right)^2} \quad 5.6.6$$

where uncertainties are given as: initial oil saturation, $\sigma_{S_{oi}}$, and displaced volume of oil, $\sigma_{V_{o,p}}$.

Example Values:

An example will be given where core properties of core #10 has been used, where uncertainties of bulk volume, pore volume, porosity, permeability and irreducible water saturation has been calculated using the equations above. These uncertainties are assumed to be representative of other cores as well.

<i>Table 5.11 – Example properties from core #10 with uncertainties.</i>	
Parameter	Value
Length (cm)	6.70 ± 0.01
Diam. (cm)	3.75 ± 0.01
V _b (g)	74.0 ± 0.4
V _p (ml)	18.60 ± 0.01
Porosity (%)	23.7 ± 0.4
Perm. (mD)	28.32 ± 0.07
S _{wi} (frac.)	0.21 ± 0.01

Source of Experimental Errors

All experimental work has uncertainties that can affect the accuracy of measurements. The most significant factors will be mentioned here.

Laminated Fractures: All cores that were used in CO₂ and co-injection experiments were flooded to irreducible water saturation and then cut in half by a circular saw (see Section 4.1.3). After

being cut, very small grains of the limestone were coating the fracture areas of the core. The limestones were washed with decane, which may have led these small grains filling pore spaces, resulting in laminated fracture walls. This may have made it harder for fluids to intrude into the matrix along the fracture.

Back Pressure Regulator: After each waterflooding, some of the produced oil would get trapped in the BPR. This varied from 0.5 - 1 ml, which could significantly affect the ultimate recovery. Therefore, oil had to be added to the production curves afterwards.

Cylinder Readings: Reading the menisci between the oil-water interfaces was sometimes difficult, especially if emulsions occurred in the cylinder.

Core Properties: There are uncertainties in measurements such as porosity and permeability, which depend on other factors that contain uncertainties.

ESI Measurements: There were fluctuations in the ESI gauges during permeability measurements and during ongoing experiments. Because of this, uncertainties occur in the actual pressure measurement.

QX Pump: Pressures shown by the QX pump did not always correlate with ESI pressures, amounting to a certain pressure difference between the two.

Tubing Leakages: When pressurizing the system, different pressurization factors would be measured, meaning that there were leakages in the connections between tubings.

Correlating ESI to Production: Delay between the production measurement and the pressure readings, meant that pressures had to be moved forward in time to match production curves. Therefore, it was necessary to know the length travelled by the fluids from the core to the cylinder. Uncertainties in these values would affect correlation between time of pressures and production.

6 | CONCLUSION AND FUTURE WORK

6.1 | CONCLUSION

The experimental work within this thesis was a continued investigation of tertiary recovery by injection of supercritical CO₂ and CO₂-foam under miscible conditions for enhanced oil recovery in fractured limestone.

Pure CO₂ injection showed a significant improvement from a waterflood, with recovery of 26.7% OOIP as a tertiary injection method in fractured limestone cores.

Water-alternating-gas (WAG) injection proved to be a useful way to reduce mobility of CO₂ and improve recovery compared to pure CO₂ injection. Reduction of CO₂ usage in combination with storage of CO₂, within the core, makes WAG an economical choice.

Co-injection of surfactant and CO₂ accelerated oil production, compared with both pure CO₂ and WAG injections, by foam generation to reduce the mobility of the injected gaseous phase. A higher tertiary recovery was also achieved, with 29.4% OOIP. This shows that foam delays CO₂ breakthrough more effectively than WAG.

Integrated EOR by initiating SAG, after WAG end point production, increased total oil recovery compared to tertiary co-injection. The pressure difference shows that foam was generated in situ throughout the SAG injection, which shows that mobility of CO₂ was further reduced by SAG.

More residual oil can become mobilized through integrated EOR of CO₂ and CO₂-foam that may not have been possible through utilization of each method individually. The timing of switching from CO₂ to CO₂-foam proved to be effective at CO₂ breakthrough to maximize ultimate recovery. This method had the overall best performance compared to all the others, producing 36.2 % OOIP. This was higher than integrated WAG and SAG, which produced 32.4% OOIP.

SAG mobilized some additional oil when integrated with WAG, recovering slightly more than co-injection. However, early breakthrough of surfactant occurred. This could be a result of an insufficiently large pre-injected slug of surfactant and water-shielding effect of high water saturation. Gravity stable CO₂ injections in both WAG and SAG were important to avoid viscous fingering and achieve a high as possible ultimate recovery. Oil production did not prove to be more efficient or higher in whole cores compared to fractured cores.

6.2 | FUTURE WORK

- Additional experiments needs to be conducted to verify tertiary SAG as a viable injection strategy.
- Performing SAG and co-injection on longer cores, preferably of 2” diameter, could yield results more representative of the field.
- Screening of surfactants, to find the one that is best suited for certain experimental conditions, can help optimize the recovery efficiency of SAG and co-injection.
- Using larger slugs in WAG and SAG might perform better than injection of small slugs.
- It could be worth testing other ways to generate foam in situ, such as single-cycle SAG to see if one large slug of pre-injected surfactant is better.
- Visualize complicated injection strategies such as WAG and SAG by use of MRI or PET/CT.

7 | ABBREVIATIONS AND NOMENCLATURE

OOIP	Oil Originally in Place
EOR	Enhanced Oil Recovery
IEOR	Integrated Enhanced Oil Recovery
WF	Waterflood
SAG	Surfactant-Alternating-Gas
WAG	Water-Alternating-Gas
BPR	Back Pressure Regulator
MMP	Minimum Miscibility Pressure
MRI	Magnetic Resonance Imaging
PV	Pore volume
M_{rf}	Mobility Reduction Factor
$wt\%$	Weight percent of surfactant
A	Cross section area of core [cm^2]
L	Length of core [cm]
K	Absolute permeability of matrix in sample [mD]
K_{frac}	Fracture permeability of sample [mD]
K_{rf}	Foam relative permeability
m_{dry}	Weight of dry core
m_{sat}	Weight of saturated core
M	Mobility Ratio
Δp	Pressure drop
Q	Flow rate [cm^3/s]

R_f	Recovery factor [OOIP]
E_v, E_h, E_m	Vertical, horizontal and microscopic sweep efficiency, respectively
S_{iw}	Irreducible water saturation
S_{or}	Residual oil saturation
S_{of}	Foam saturation
Π	Disjoining pressure [N/m ²]
μ_f	Apparent viscosity [cP]
μ_i	Viscosity of fluid i (water, oil, gas)
ϕ	Effective porosity of sample
μ	Fluid viscosity [cP]
ρ	Fluid density [g/ml]
V_b, V_p	Bulk and pore volume, respectively
M	Mobility ratio
$k_{r,i}$	Relative permeability of fluid i (water, oil or gas)
u	Velocity of displacing fluid
$R_{v/g}$	Viscous to gravity force ratio
F_p	Pressurization factor
σ_y	Uncertainty of value, y
N_{vc}	Capillary number
$R_{f,I}$	Recovery factor after injection method, I
$S_{or,I}$	Residual oil saturation after injection method, I

8 | REFERENCES

- Aarra, M. G., Skauge, A., & Martinsen, H. A. (2002). FAWAG: A Breakthrough for EOR in the North Sea. San Antonio, Texas: Paper SPE-77695-MS presented at the SPE Annual Technical Conference and Exhibition, September 29-October 2.
- Ahr, M. M. (2008). *Geology of Carbonate Reservoirs*. Hoboken, New Jersey: John Wiley & Sons, Inc.
- Albrecht, R. A., & Marsden, S. S. (1970). Foams as Blocking Agents in Porous Media. *Society of Petroleum Engineers*, 10(01), 51 - 55.
- Allan, J., & Sun, S. Q. (2003). Controls on Recovery Factor in Fractured Reservoirs: Lessons Learned from 100 Fractured Fields. Denver, Colorado: Paper SPE-84590-MS presented at the Annual Technical Conference and Exhibition, October 5-8.
- Alotaibi, M., Nasralla, R. A., & Nasr-El-Din, H. A. (2010). Wettability Challenges in Carbonate Reservoirs. Tulsa, Oklahoma: Paper SPE129972 presented at the Improved Oil Recovery Symposium, 24 - 28 April.
- Al-Shuraiqi, H. S., Muggeridge, A. H., & Grattoni, C. A. (2003). Laboratory Investigations of First Contact Miscible WAG Displacement: The Effects of WAG Ratio and Flow Rate. Kuala Lumpur, Malaysia: Society of Petroleum Engineers.
- Amin, M. E., Zekri, A. Y., Almehaideb, R. A., & Al-Attar, H. H. (2012). Optimization of CO₂ WAG Processes in Carbonate Reservoirs-An Experimental Approach. Abu Dhabi: Society of Petroleum Engineers.
- Basu, S., & Sharma, M. M. (1996). Measurement of Critical Disjoining Pressure for Dewetting Solid Surfaces. *Journal of Colloid and Interface Science*(181), 443-455.
- Bertin, H., Quintard, M., & Castanier, L. (1998). Development of a Bubble-Population Correlation for Foam-Flow Modeling in Porous Media. *Society of Petroleum Engineers ,SPE-52596-PA*, 3(04), 356 - 362.
- Boud, D. C., & Holbrook, O. C. (1958). *Patent No. US2866507 A*. U. S.
- Brock, W., & Bryan, L. (1989). Summary Results of CO₂ EOR Field Tests, 1972-1987. Denver, Colorado: Paper SPE 18977 presented at Joint Rocky Mountain Regional/Low Permeability Reservoirs Symposium and Exhibition, March 6-8.

- Brown, C. E. (2002). Ph.D. Director, IGER INSTITUTE INC. In *World energy resources* (pp. 149-150). Berlin and New York: Springer-Verlag.
- Caudle, B., & Dyes, A. (1958). Improving Miscible Displacement by Gas-Water Injection. Dallas, Texas: Paper SPE-911-G presented at 32nd Annual Fall Meeting of Society of Petroleum Engineers, October 6-9.
- Chatzis, I. (1983). Magnitude and Detailed Structure of Residual Oil Saturation. *Society of Petroleum Engineers Journal, Paper SPE-10681-PA, 23(02)*, 311 - 326.
- Chordia, M., & Trivedi, J. J. (2010). Diffusion in Naturally Fractured Reservoirs - A Review. Brisbane, Australia: Society of Petroleum Engineers.
- Chou, S. (1991). Conditions for Generating Foam in Porous Media. Dallas, Texas: Paper SPE-22628-MS presented at the SPE Annual Technical Conference and Exhibition.
- Christensen, J. R., Stenby, E. H., & Skauge, A. (2001). Review of WAG Field Experience. *Society of Petroleum Engineers, 4(02)*, 97-106.
- Crussler, E. (2009). *Diffusion: Mass Transfer in Fluid Systems* (Third Edition ed.). Cambridge: Cambridge University Press.
- Dai, Z., Middleton, R., Viswanathan, H., Fressen-rahm, J., Bauman, J., Pawar, R., et al. (2013). An Integrated Framework for Optimizing CO₂ Sequestration and Enhanced Oil Recovery. *Environmental Science & Technology Letters*.
- Donaldson, E., Chilingarian, G., & T.F, Y. (1989). *Enhanced oil recovery II, processes and operations* (Vol. 17B ed.). Amsterdam: Elsevier science publishers B. V.
- Duchenne, S., Puyou, G., Cordelier, P., Hy-Billiot, J., & Hamon, G. (2014). Efficient Experimental Data Acquisition for Miscible CO₂ WAG Injection Corefloods in Carbonate. Tulsa, Oklahoma: Paper SPE-169045-MS presented at SPE Improved Oil Recovery Symposium, April 12-16.
- Dullien, F. A. (1979). *Porous Media: Fluid Transport and Pore Structure*. London, UK: Academic Press, Inc.
- Eide, Ø. (2014). *Co₂ Injection for Enhanced Oil Recovery: Production Mechanisms in Fractured Reservoirs*. Bergen, Norway: Institute of Physics and Technology. University of Bergen. PhD Dissertation.
- Eide, Ø., Haugen, Å., Svenningsen, S., Hoff, K., Erslund, G., Fernø, M., et al. (2012). Tertiary Liquid and Supercritical CO₂ Injection in Chalk and Limestone at Strongly Water-Wet and

Near Neutral-Wet Conditions. Aberdeen, Scotland: Paper presented at the International Symposium of the Society of Core Analysis, August 27-30.

Eson, R. L., & Cooke, R. W. (1989). A Comprehensive Analysis of Steam Foam Diverters and Application Methods. Paper SPE18785 presented at the SPE California Regional Meeting, Bakersfield, California, April 5-7.

Farajzadeh, R., Andrianov, A., Hirasaki, G. J., & Rossen, W. R. (2012). Foam-Oil Interaction in Porous Media: Implications for Foam Assisted Enhanced Oil Recovery. Muscat, Oman: Paper SPE 154197 presented at the EOR Conference at Oil and Gas West Asia, 16-18 April.

Farajzadeh, R., Risjwijk, Eftekhari, A., Hajibeygi, H., Meer, J. v., Vincent-Bonnieu, S., et al. (2015). Simulation of Instabilities and Fingering in Surfactant Alternating Gas (SAG) Foam Enhanced Oil Recovery. *SPE Reservoir Simulation Symposium*. Houston: Society of Petroleum Engineers.

Fernø, M. A., Gauteplass, J., Pancharoen, M., Haugen, Å., Graue, A., Kovscek, A. R., et al. (2014). Experimental Study of Foam Generation, Sweep Efficiency and Flow in a Fracture Network. Amsterdam, Netherlands: Paper SPE-170840-MS presented at the SPE Annual Technical Conference and Exhibition, October 27-29.

Fosse, E. (2012). An Experimental Study of CO₂ Injection for Oil Recovery in Chalk. Bergen: Department of Physics and Technology, University of Bergen, Master Thesis.

Frampton, A. (2014). Chapter 9: Fracture Transmissivity Estimation Using Natural Gradient Flow Measurements in Sparsely Fractured Rock. In J. M. Sharp (Ed.), *Fractured Rock Hydrogeology* (pp. 147-165). London, UK: Taylor & Francis Group.

Fulcher, R., Ertekin, T., & Stahl, C. (1985). Effect of Capillary Number and Its Constituents on Two-Phase Relative Permeability Curves. *Journal of Petroleum Technology, SPE-12170-PA*, 37(02), 249-260.

Gandomkar, A., Kharrat, R., Motealleh, M., Khanamiri, H. H., Nematzadeh, M., & Ghazanfari, M. H. (2012). An Experimental Investigation of Foam for Gas. *Petroleum Science and Technology*, 30, 976-985.

Graue, D. J., & Blevins, T. R. (1978). SACROC Tertiary CO₂ Pilot Project. Tulsa, Oklahoma: Paper SPE7090 presented at the 5th Symposium on Improved Methods for Oil Recovery, April 16-19.

Grigg, R. B., & Schechter, D. S. (1998). *Improved Efficiency of Miscible CO₂ Floods and Enhanced Prospects for CO₂ Flooding Heterogeneous Reservoirs*. Socorro, New Mexico: New

Mexico Petroleum Recovery Research Center and New Mexico Institute of Mining and Technology.

- Halliburton. (2015). *Halliburton.com*. Retrieved 03 18, 2015, from <http://www.halliburton.com/en-US/ps/solutions/mature-fields/default.page?node-id=hgjyd46l>
- Haugen, Å., Fernø, M., Graue, A., & Bertin, J. (2012). Experimental Study of Foam Flow in Fractured Oil-Wet Limestone for Enhanced Oil Recovery. *SPE Reservoir Evaluation & Engineering*, 15(02), 218 - 228.
- Haugen, Å., Mani, N., Svenningsen, S., Brattekkås, B., Graue, A., Ersland, G., et al. (2014). Miscible and Immiscible Foam Injection for Mobility Control and EOR in Fractured Oil-Wet Carbonate Rocks. *Transport in Porous Media*, 104(1), 109-131.
- Hoiteit, H., & Firoozabadi, A. (2006). Numerical Modeling of Diffusion in Fractured Media for Gas Injection and Recycling Schemes. San Antonio, Texas: Society of Petroleum Engineers.
- Holm, L. W. (1970). Foam Injection Test in the Siggins Field, Illinois. *Journal of Petroleum Technology, paper SPE-2750-PA*, 22(12), 1499-1506.
- Holm, L. W. (1974). Mechanisms of Oil Displacement by Carbon Dioxide. *Journal of Petroleum Technology, Journal Paper SPE-4736-PA*, 26(12), 1,427 - 1,438.
- Holm, L. W. (1986). Miscibility and Miscible Displacement. *Journal of Petroleum Technology, Journal Paper SPE-15794-PA*, 38(08), 817 - 818.
- IPCC. (2005). *Intergovernmental Panel on Climate Change: Special Report on Carbon Dioxide Capture and Storage*. Working Group III. Cambridge and New York: Cambridge University Press.
- Jackson, D. D., & Andrews, G. L. (1985). Optimum WAG Ratio vs. Rock Wettability in CO₂ Flooding. Las Vegas, Nevada: Paper SPE-14303-MS presented at the 60th Annual Technical Conference and Exhibition, September 22-25.
- Johns, R. T., & Dindoruk, B. (2013). Ch. 1: Gas Flooding. In J. J. Sheng (Ed.), *Enhanced Oil Recovery: Field Case Studies*. Waltham, Massachusetts: Gulf Professional Publishing.
- Kamalipour, M., Shahrabadi, A., Sabzkouhi, G. A., Ali, S. M., & Jamialahmadi, M. (2014). The Role of Diffusion and Dispersion in Miscible CO₂. *Petroleum Science and Technology*, 32(2), 158-161.

- Kapetas, L., El, W. A., & Rossen, W. R. (2014). Representing Slow Foam Dynamics in Laboratory Corefloods for Foam Enhanced Oil Recovery. Tulsa, Oklahoma: Paper SPE-169059-MS presented at the SPE Improved Oil Recovery Symposium, April 12-16.
- Kokal, S., & Al-Kaabi, A. (2010). *Enhanced oil recovery: challenges & opportunities*. Retrieved December 19, 2014, from http://www.world-petroleum.org/docs/docs/publications/2010yearbook/P64-69_Kokal-Al_Kaabi.pdf
- Koottungal, L. (2010). 2010 Worldwide EOR Survey. *Oil and Gas Journal*, 108(14), 45-60.
- Kovscek, A. R. (1998). Reservoir Simulation of Foam Displacement Processes. Beijing, China: Paper presented at the 7th UNITAR International Conference on Heavy Crude and Tar Sands, October 27-31.
- Kovscek, A., Patzek, T., & Radke, C. (1995). *A Population Balance Model for Transient and Steady-State Foam Flow in Boise Sandstone*. Berkeley, CA: Lawrence Berkely Laboratory, University of California.
- Lake, L. W. (1989). *Enhanced Oil Recovery*. Eaglewood Cliffs, New Jersey: Prentice Hall Incorporated.
- Lee, S., & Kam, S. (2013). Ch. 2: Enhanced Oil Recovery by Using CO₂ Foams: Fundamentals and Field Applications. In J. J. Sheng (Ed.), *Enhanced Oil Recovery: Field Case Studies*. Waltham, Massachusetts: Gulf Professional Publishing.
- Liontas, R., Ma, K., Hirasaki, G. J., & Biswal, L. (2013). Neighbor-induced bubble pinch-off: novel mechanisms of insitu foam generation in microfluidic channels. *Soft Matter*, 9(46), 10933-11144.
- Ma, K., Lopez-Salinas, J. L., Puerto, M. C., Miller, C. A., Biswal, S. L., & Hirasaki, G. J. (2013). Estimation of Parameters for the Simulation of Foam Flow through Porous Media. Part 1: The Dry-Out Effect. *Energy & Fuels*, 27(05), 2363-2375.
- Manrique, E. J., Muci, V. E., & Gurfinkel, M. E. (2007). EOR Field Experiences in Carbonate Reservoirs in the United States. *Society of Petroleum Engineers, Journal Paper SPE-100063-PA*, 10(06), 667 - 686.
- Manrique, E., Thomas, C., Ravikiran, R., Izadi, M., Lantz, M., Romero, J., et al. (2010). EOR: Current Status and Opportunities. Tulsa, Oklahoma: Paper SPE-130113-MS presented at the SPE Improved Oil Recovery Symposium, April 24-28.

- Mathiassen, O. M. (2003, May). CO₂ as Injection Gas for Enhanced Oil Recovery and Estimation of the Potential on the Norwegian Continental Shelf, Part I of II. 20. Trondheim: Norwegian University of Science and Technology, Master Thesis.
- Melzer, L. S. (2012). *Carbon Dioxide Enhanced Oil Recovery: Factors Involved in Adding Carbon Capture, Utilization and Storage (CCUS) to Enhanced Oil Recovery*. Midland, Texas: National Enhanced Oil Recovery Initiative.
- National Energy Technology Laboratory. (2010). *Storing CO₂ and Producing Domestic Crude Oil with Next Generation CO₂-EOR Technology: An Update*. United States: U.S. Department of Energy.
- NEORI. (2012). *The National Enhanced Oil Recovery Initiative: CARBON DIOXIDE ENHANCED OIL RECOVERY: A CRITICAL DOMESTIC ENERGY, ECONOMIC, AND ENVIRONMENTAL OPPORTUNITY*. Washington, D.C: The National Enhanced Oil Recovery Initiative (NEORI).
- NETL. (2010). *National Energy Technology Laboratory: Carbon Dioxide Enhanced Oil Recovery. Untapped Domestic Energy Supply and Long Term Carbon Storage Solution*. United States: U.S. Department of Energy.
- NETL. (2011). *National Energy Technology Laboratory: Mobility and Conformance Control for Carbon Dioxide Enhanced Oil Recovery (CO₂-EOR) via Thickeners, Foams and Gels - A Detailed Literature Review of 40 Years of Research*. United States: U.S. Department of Energy.
- NIST. (2011). *National Institute of Standards and Technology Chemistry WebBook*. Retrieved 12 05, 2014, from <http://webbook.nist.gov/chemistry/>
- Ocampo, A., Restrepo, A., Rendon, N., Coronado, J., Correa, J., D.ramirez, et al. (2014). Foams Prove Effectiveness for Gas Injection Conformance and Sweep Efficiency Improvement in a Low porosity Fractured Reservoir - Field Pilots. Kuala Lumpur, Malaysia: Paper IPTC-17950-MS presented at the International Petroleum Technology Conference, December 10-12.
- Opdal, I. (2014). *Mobility Control by CO₂-foam Injection for Integrated EOR*. Bergen: Department of Physics and Technology, University of Bergen, Master Thesis.
- Perkins, T., & Johnston, O. (1963). A Review of Diffusion and Dispersion in Porous Media. *Society of Petroleum Engineers Journal*, 3(01), 70 - 84.
- Ransohoff, T., & Radke, C. (1988). Mechanisms of Foam Generation in Glass-Bead Packs. *Society of Petroleum Engineers, SPE-15441-PA*, 3(02), 573-585.

- Renkema, W. J., & Rossen, W. R. (2007). Success of SAG Foam Processes in Heterogeneous Reservoirs. *SPE Annual Technical Conference and Exhibition*. Anaheim, California: Society of Petroleum Engineers.
- Rogers, J. D., & Grigg, R. B. (2001). A Literature Analysis of the WAG Injectivity Abnormalities in the CO₂ Process. *Society of Petroleum Engineers*, 4(05), 375-386.
- Sahimi, M., Rasaei, M. R., & Haghghi, M. (2006). Ch. 8: Gas Injection and Fingering in Porous Media. In C. K. Ho, & S. W. Webb (Eds.), *Gas Transport in Porous Media* (pp. 133-168). Dordrecht: Springer.
- Salehi, M. M., Safarzadeh, M. A., Sahraei, E., & Nejad, S. A. (2014). Comparison of oil removal in surfactant alternating gas with water alternating gas, water flooding and gas flooding in secondary oil recovery process. *Journal of Petroleum Science and Engineering*, 120, 86-93.
- Schlumberger. (2014). *Schlumberger*. Retrieved 01 13, 2014, from http://www.slb.com/services/technical_challenges/carbonates.aspx
- Schramm, L. L. (2005). *Emulsions, Foams and Suspensions: Fundamentals and Applications*. Weinheim, Germany: John Wiley & Sons.
- Shan, D., & Rossen, W. R. (2002). Optimal Injection Strategies for Foam IOR. *SPE/DOE Improved Oil Recovery Symposium*. Tulsa, Oklahoma: Society of Petroleum Engineers.
- Shehata, A. M., Alotaibi, M. B., & Nasr-El-Din, H. A. (2014). Waterflooding in Carbonate Reservoirs: Does the Salinity Matter? *Society of Petroleum Engineers, Paper SPE-170254-PA*, 17(03), 304 - 313.
- Sheng, J. J. (2013). Ch. 11: Foams and Their Applications in Enhancing Oil Recovery. In J. J. Sheng (Ed.), *Enhanced Oil Recovery: Field Case Studies*. Waltham, Massachusetts: Gulf Professional Publishing.
- Shi, J. X., & Rossen, W. R. (1998). Improved Surfactant-Alternating-Gas Foam Processes to Control Gravity Override. *SPE/DOE Improved Oil Recovery Symposium*. Tulsa, Oklahoma: Society of Petroleum Engineers.
- Shojaei, H., & Jessen, K. (2015). Diffusion and Matrix-fracture Interactions during Gas Injection in Fractured Reservoirs. Dresden, Germany: Paper SPE-169152-MS presented at the SPE IOR 2015 – 18th European Symposium on Improved Oil Recovery, April 14-16.
- Simjoo, M., Rezaei, T., Andrianov, A., & Zitha, P. (2013). Foam Stability in the Presence of Oil: Effect of Surfactant Concentration and Oil Type. *Colloids and Surfaces, A: Physicochemical and Engineering Aspects*, 438, 148-158.

- Skarestad, M. a. (2012). *Reservoarteknikk II: Fluid Properties and Recovery Methods*. Bergen: University of Bergen.
- Skauge, A. (2013). RE: PTEK312: Selected Topics in Petroleum Technology. Bergen: University of Bergen.
- Sorbie, K., & Dijke, M. v. (2007). *Fundamentals of Three-Phase Flow in Porous Media of Heterogeneous Wettability*. Edinburgh, Scotland, UK: Heriot-Watt university.
- Statoil. (2008). *Statoil*. Retrieved January 16, 2015, from [http://www.statoil.com/en/technologyinnovation/optimizingreservoirrecovery/recoverymethods/wateralternatinggaswag/pages/water-alternating-gas%20\(wag\).aspx](http://www.statoil.com/en/technologyinnovation/optimizingreservoirrecovery/recoverymethods/wateralternatinggaswag/pages/water-alternating-gas%20(wag).aspx)
- Steinsbø, M., Brattekkås, B., Ersland, G., Bø, K., Opdal, I., Tunli, R., et al. (2015). Foam as Mobility Control for Integrated CO₂-EOR in Fractured Carbonates. Dresden, Germany: Paper presented at the 18th European Symposium on Improved Oil Recovery, April 14-16.
- Stern, D. (1991). Mechanisms of Miscible Oil Recovery: Effects of Pore-Level Fluid Distribution. Dallas, Texas: Paper SPE 22652 presented at the SPE 66th Annual Technical Conference and Exhibition, October 6-9.
- Stosur, G. J., Hite, J. R., Carnahan, N. F., & Miller, K. (2003). The alphabet Soup of IOR, EOR and AOR: Effective Communication Requires a Definition of Terms. Kuala Lumpur, Malaysia: Paper SPE-84908-MS presented at the SPE International Improved Oil Recovery Conference in Asia Pacific, October 20-21.
- Suffridge, F., Raterman, K., & Russell, G. (1989). Foam Performance Under Reservoir Conditions. San Antonio, Texas: Paper SPE-19691-MS presented at the SPE Annual Technical Conference and Exhibition, October 8-11.
- Surguchev, L. M., Korbøl, R., Haugen, S., & Krakstad, O. S. (1992). Screening of WAG Injection Strategies for Heterogeneous Reservoirs. Cannes, France: Paper SPE25075 presented at the SPE European Petroleum Conference, November 16-18.
- Svenningsen, S. (2011). An Experimental Study of CO₂ Injection for Enhanced Oil Recovery in Chalk and Limestone. Bergen: University of Bergen, Master Thesis.
- Terry, R. E., & Rogers, J. B. (2014). Ch. 11: Enhanced Oil Recovery. In *Applied Petroleum Reservoir Engineering, Third Edition* (pp. 405-433). Westford, Massachusetts: Prentice Hall.
- Tipura, L. (2008). Wettability Characterization by NMR T₂ Measurements in Edwards Limestone. Bergen: Department of Physics and Technology, University of Bergen, Master Thesis.

- Turta, A., & Singhal, A. (2002). Field Foam Applications in Enhanced Oil Recovery Projects: Screening and Design Aspects. *Journal of Canadian Petroleum Technology*, 41(10).
- Uleberg, K., & Høier, L. (2002). Miscible Gas Injection in Fractured Reservoirs. Tulsa, Oklahoma: Paper SPE-75136-MS presented at SPE/DOE Improved Oil Recovery Symposium, April 13-17.
- Utseth, R. H. (1996). *RUTH 1992-1995. A Norwegian Research Program on Improved Oil Recovery*. Stavanger: Norwegian Petroleum Directorate.
- Wassmuth, F., Green, K., & Randall, L. (2001). Details of In-Situ Foam Propagation Exposed With Magnetic Resonance Imaging. *SPE Reservoir Evaluation & Engineering, Paper SPE-71300-PA*, 4(02), 135 - 145.
- Xu., Q., & Rossen, W. (2003). Experimental Study of Gas Injection in Surfactant-Alternating-Gas Foam Process. Denver, Colorado: Paper SPE-84183-MS presented at the SPE Annual Technical Conference and Exhibition, October 5-8.
- Yaghoobi, H., Tsau, J., & Grigg, R. (1998). Effect of Foam on CO Breakthrough: Is This Favorable to Oil Recovery? Midland, Texas: Paper SPE-39789-MS presented at the SPE Permian Basin Oil and Gas Recovery Conference, March 23-26.
- Yan, W., Miller, C. A., & Hirasaki, G. J. (2006). Foam sweep in fractures for enhanced oil recovery. *Colloids and Surfaces A: Physicochemical and Engineering Aspects*, 282-283, 348-359.
- Zaganeh, M. N., Kam, S. I., LaForce, T. C., & Rossen, W. R. (2009). The Method of Characteristics Applied to Oil Displacement by Foam. Amsterdam, Netherlands: Paper SPE-121580-MS presented at the SPE EUROPEC/EAGE Conference and Exhibition, June 8-11.
- Zahoor, M. K., Derahman, M. N., & Yunan, M. H. (2011). WAG Process Design - An Updated Review. *Brazilian Journal of Petroleum and Gas*, 5(02), 109-121.
- Zhou, D., Yan, M., & Calvin, W. M. (2012). Optimization of Mature CO₂ Flood - From Continuous Injections to WAG. Tulsa, Oklahoma: Paper SPE 154181 presented at the SPE IOR Symposium, April 14-18.
- Zolotukhin, A., & Ursin, B. (2000). *Introduction to Petroleum Reservoir Engineering*. Kristiansand: HøyskoleForlaget.
- Zuta, J., & Fjelde, I. (2010). Transport of CO₂-Foaming Agents During CO₂-Foam Processes in Fractured Chalk Rock. *SPE Reservoir Evaluation & Engineering, Paper SPE-121253-PA*, 13(04), 710 - 719.